N73-12935

CR
NAS 9-11722
LR 25387

DONALD E. PETTIT, DAVID W. HOEPPNER

SEPTEMBER 25, 1972

# FATIGUE FLAW GROWTH AND NDI EVALUATION FOR PREVENTING THROUGH CRACKS IN SPACECRAFT TANKAGE STRUCTURES

REPORT OF RESEARCH PERFORMED UNDER
CONTRACT NAS 9-11722

NASA
MANNED SPACECRAFT CENTER
HOUSTON, TEXAS 77058

NASA TECHNICAL MONITOR
MR. ROYCE FORMAN

LOCKHEED-CALIFORNIA COMPANY·BURBANK
A DIVISION OF LOCKHEED AIRCRAFT CORPORATION

DONALD E. PETTIT, DAVID W. HOEPPNER

SEPTEMBER 25, 1972

# FATIGUE FLAW GROWTH AND NDI EVALUATION FOR PREVENTING THROUGH CRACKS IN SPACECRAFT TANKAGE STRUCTURES

REPORT OF RESEARCH PERFORMED UNDER
CONTRACT NAS 9-11722

NASA
MANNED SPACECRAFT CENTER
HOUSTON, TEXAS 77058

NASA TECHNICAL MONITOR
MR. ROYCE FORMAN

**LOCKHEED-CALIFORNIA COMPANY • BURBANK**
A DIVISION OF LOCKHEED AIRCRAFT CORPORATION

# FATIGUE FLAW GROWTH AND NDI EVALUATION FOR
## PREVENTING THROUGH CRACKS IN SPACECRAFT TANKAGE STRUCTURES

Donald E. Pettit and David W. Hoeppner

The program reported herein was conducted to determine the fatigue-crack propagation behavior of parent and welded 2219-T87 aluminum alloy sheet tested under controlled cyclic stress conditions in room temperature air and 300°F air. Specimens possessing an initial surface defect of controlled dimensions were cycled under constant load amplitude until the propagating fatigue crack penetrated the back surface of the specimen. In actual hardware any leak in tankage could cause mission failure; thus, generation of a crack that could cause a leak (i.e., a through-the-thickness crack), represents a potential failure condition.

In addition to the fatigue-crack propagation study, a series of precracked specimens were prepared for a study to optimize penetrant, X-ray, ultrasonic, and eddy current nondestructive inspection procedures. A series of panels containing unknown flaws in parent and welded 2219-T87 aluminum then were inspected by three independent laboratories using their optimized procedures for the four NDI techniques. The panels then were proof tested by applying a stress value of 0.9 times yield strength and reinspected by each laboratory. The results of the fatigue flaw growth and NDI results are discussed in the framework of current fracture mechanics concepts.

FOREWORD

This report was prepared by the Lockheed-California Company under NASA contract NAS 9-11722. The study reported was initiated by the Manned Spacecraft Center of NASA to determine the fatigue-crack propagation behavior of surface flaws as they propagated to flaw breakthrough on the specimen's back surface and to determine the ability of current NDI techniques to detect surface flaws. The results of the program reported herein were completed between April 30, 1971, and July 15, 1972. The program was conducted under the technical cognizance of Mr. R.G. Forman of NAS/MSC. Mr. W.L. Castner, also of NASA/MSC, provided technical cognizance in the NDI area.

At the Lockheed-California Company, Dr. David Hoeppner, Senior Research Scientist, Fracture Mechanics and Materials Research Group, Rye Canyon Research Laboratory, provided technical direction and program leadership. Mr. Donald E. Pettit was Principal Investigator, Mr. Wendell Renslen and Mr. Bill Kerwin conducted the testing program, Mr. John Crocker conducted the NDI investigation, Mr. Hugh Pearson (Lockheed-Georgia Company) performed the NDI analysis work, and Mr. Donald Croke and Mr. John Rittenhouse assisted with the cycles-to-leak analysis. Ms. Sandra Johnson did the typing and aided in numerous aspects of the research. The efforts of all of those people listed is gratefully acknowledged.

TABLE OF CONTENTS

TABLE OF CONTENTS (CONT'D)

# LIST OF FIGURES

ix

LIST OF FIGURES (CONT'D)

LIST OF FIGURES (CONT'D)

xi

LIST OF FIGURES (CONT'D)

# LIST OF TABLES

# LIST OF SYMBOLS

A          Surface crack minor axis length

C          Surface crack major axis length

N          Number of fatigue cycles

$dA/dN$        Average rate of fatigue crack growth

B          Specimen thickness

S          Maximum gross stress

$S_y$         Material 0.2 percent yield stress

K          Stress intensity factor

R          Fatigue stress ratio, minimum stress/maximum stress

T          Temperature

$\phi$         Angle from major axis of a surface crack

$\phi_0$        Elliptic integral of the second kind

$\Delta K_C$       Alternating stress intensity at the major axis of a surface crack

$\Delta K_A$       Alternating stress intensity at the minor axis of a surface crack

$\Delta S$        Alternating stress

$K_c$         Critical stress intensity

$K_{Ic}$        Critical plane strain stress intensity

F          Front surface correction for crack growth in direction of minor axis

G          Front surface correction for crack growth in direction of major axis

M          Back surface correction for crack growth in direction of minor axis

Q          Modified Irwin plasticity corrected shape parameter

$C',n,P,m$    Constants

$S_o$         Arbitrary selected stress level

$\lambda$         $K_{min}/\Delta K$

$S_{tu}$        Ultimate tensile strength

$N_L$         Cycles-to-leak

$\bar{z}$         Arithmetic mean flaw size

$\sigma_z$         Normal standard deviation

$\sigma_y$         Log normal standard deviation

$\bar{Y}$         Log normal mean

$S_n$         Number of cracks detected in a sample of size n

p          Probability of crack detection

# Section 1

## INTRODUCTION

This program was initiated to assess the predictive capability of current
fracture mechanics/NDI analysis procedures as they apply to pressure vessels
where failure will occur by a leak-before-break design criteria. The
program was conducted in two phases; Phase I consisting of a fatigue-crack
propagation study, and Phase II consisting of a preliminary determination of
the fatigue crack size detection limits of current nondestructive inspection
procedures.

Phase I tests were conducted using precracked surface flaw specimens and
fatigue cycling at constant amplitude until the surface flaw penetrated the
back surface of the specimen. The variables examined included material
(parent, cross and longitudinal welds), thickness, stress ratio, initial
flaw shape, initial flaw depth, maximum stress, and temperature. During the
program it was found that insufficient constant amplitude fatigue crack
growth rate (dA/dN) data existed to allow a determination of the experimental
constants in the predictive equations to be examined. As a result, some of
the cycles-to-leak tests were modified to fatigue crack growth rate tests to
provide the required data. A matrix of the Phase I tests as modified during
the program to insure crack penetration of the back surface in less than
20,000 cycles is presented in Table 1.

The Phase II study consisted of fabricating a series of NDI calibration
blocks containing fatigue cracks for use in optimizing penetrant, X-ray,
eddy current, and ultrasonic inspection procedures. A series of 20 specimens
containing fatigue cracks in random locations then was inspected by Lockheed,
Magnaflux, and NASA/MSC personnel and the detected flaws and their estimated
size recorded. The specimens then were proof loaded to 90 percent of the
material yield strength and the inspection sequence repeated by the three

1

TABLE 1. PHASE I TEST PROGRAM

| Thickness, (B), (inch) | Number of Initial Flaw Depths per Condition (A/B) | Initial Flaw Shape $(A/2C)_i$ | $\left(\dfrac{\text{Maximum Stress}}{\text{Yield Stress}}\right)\ (S/S_y)$ | Fatigue Stress Ratio R | Temperature, T, °F |
|---|---|---|---|---|---|
| Parent Material, Cycles-To-Leak | | | | | |
| .040, .080, .160 | 3 | 0.15, 0.3, 0.5 | 0.8, 0.7, 0.5 | 0.05 | 75 |
| .040, .160 | 2 | 0.15, 0.5 | 0.8, 0.5 | 0.5 | 75 |
| .040, .160 | 2 | 0.15, 0.5 | 0.8, 0.5 | 0.05 | 300 |
| Cross Weld Material, Cycles-To-Leak | | | | | |
| .080, .160, .300 | 3 | 0.15, 0.3, 0.5 | 0.8, 0.7 | 0.05 | 75 |
| .080, .300 | 2 | 0.15, 0.5 | 0.8, 0.7 | 0.5 | 75 |
| .080, .300 | 2 | 0.15, 0.5 | 0.8, 0.7 | 0.05 | 300 |
| Longitudinal Weld Material, Cycles-To-Leak | | | | | |
| .080, .160, .300 Flaw at Weld $G_L$ | 2 | 0.15, 0.5 | 0.8, 0.7 | 0.05 | 75 |
| Flaw at Weld Edge | 2 | 0.15, 0.5 | 0.8, 0.7 | 0.05 | 75 |
| Cross Weld Material, dA/dN Test | | | | | |
| .16, .300 | 3 | Varied | Varied | 0.05 | 300 |

laboratories.  The flaw detection specimens containing unknown flaws are
listed in Table 2.

The results of this study are presented herein within the framework of
current fracture mechanics/NDI concepts.  When combined with the results from
other NASA programs, these data will form a basis for the assessment of the
structural reliability of leak critical 2219-T87 aluminum pressure vessels.
The following sections of this report present the technical framework and
results for each of the two phases of this study.

### TABLE 2.  FLAW DETECTION SPECIMEN ALLOCATION

| Specimen Type | Crack Aspect Ratio, A/2C | Relative Crack Depth, A/B | Thickness (B), inch | Number of Specimens |
|---|---|---|---|---|
| Base Metal | .1 to .5 | .1 to .5 | .040 | 2 |
|  | .1 to .5 | .1 to .5 | .080 | 2 |
|  | .1 to .5 | .1 to .5 | .160 | 2 |
| Cross Weld | .1 to .5 | .1 to .5 | .080 | 2 |
|  | .1 to .5 | .1 to .5 | .160 | 2 |
|  | .1 to .5 | .1 to .5 | .300 | 2 |
| Longitudinal Weld | .1 to .5 | .1 to .5 | .080 | 2 |
|  | .1 to .5 | .1 to .5 | .160 | 2 |
|  | .1 to .5 | .1 to .5 | .300 | 2 |
| Stiffened Panel | .1 to .5 | .1 to .5 | .080 | 1 |
|  | .1 to .5 | .1 to .5 | .160 | 1 |

3

Section 2

## TECHNICAL DISCUSSION

### 2.1 Background

The design of modern pressure vessels for aerospace application may be based
on one of several design criteria. Many early designs were based on basic
strength criteria such as yield and ultimate strength. However, the use of
higher strength materials and the realization that defects due to material
and fabrication procedure can occur has resulted in greater emphasis on the
"flawed" properties such as fracture toughness, fatigue-crack propagation,
and stress corrosion cracking. From these considerations emerged the current
fracture mechanics concept.

For certain pressure vessel designs failure will occur by plane strain
fracture of a surface crack and may be evaluated on the basis of classic
linear elastic fracture mechanics. For this case the initial flaw size may
be determined by NDI or more generally by proof testing to a stress higher
than the operating stress. For thinner thicknesses or designs using tougher
materials, failure may be defined as a surface crack penetrating the wall
thickness, thus resulting in a leak-before-break design criteria.

In the design of previous pressure vessels for space applications such as
those used in the Apollo program, a proof test philosophy based on fracture
mechanics concepts was successfully used. However, preliminary design
studies for future spacecraft tankage structure indicate that cryogenic fuel
tanks will in part be fabricated from 2219-T87 aluminum alloy. The walls for
the tanks will vary from 0.040-in. to 0.150-in. thick and the weld lands will
be at least twice the basic wall thickness. The design ultimate factor of
safety for the tanks will be 1.5. Assuming a proof stress of 90 percent of
the yield stress, the maximum proof test factor (proof stress/limit stress)
will be approximately 1.2.

The selection of 2219-T87 aluminum nsures that rapid fracture will not occur from a surface flaw at operating stress levels, the critical size crack for rapid fracture now being a crack approximately three (3) inches in length. In addition, some tanks will be designed to withstand significant head pressures during launch, and a 1.2 proof pressure factor covering all tank areas will not be possible with simple internal pressurization. Finally, if the tanks are integral with the primary structure, the tanks will sustain complicated flight loads in local areas. All of these factors make the use of the traditional proof test philosophy less applicable.

Since proof testing does not appear to be universally applicable, an alternate analysis method is required to insure the structural integrity of future spacecraft tankage. Current research indicates that the use of a combined fracture mechanics (FM) and nondestructive inspection (NDI) approach is applicable. For this analysis, a statistically based NDI minimum detectable flaw size limit is used to set the initial maximum size flaw that could exist in the structure. Fatigue-crack propagation behavior then is used to predict the life of the tank until crack penetration of the entire thickness i.e., until leakage, occurs.

Experience from the Saturn V program has shown that sharp flaws in tankage structures fabricated from 2219-T87 aluminum will occur, and the flaws must be found and repaired before they propagate to leak by fatigue loading. The Saturn V had flaws found during inspection in both parent and weld material, the flaws in parent material evidently developed during forming process but a greater number of flaws occurred in weld metal due to weld processing. One weld surface crack was 0.4-inch long and 0.15 to 0.17-inch deep, i.e., the crack depth was 70 percent of the 0.231-inch thickness. The Saturn V experience also has shown that cracks often go undetected during initial dye penetrant and radiographic inspections. However, after a proof pressure test, the cracks appeared to be much more detectable by NDI techniques.

Previous surface flaw growth data for 0.125-inch thick 2219-T87 aluminum weld specimens showed that a flaw will growth through the thickness and leak

6

in about 400 cycles at limit stress if the initial flaw depth is 50 percent
of the thickness. This corresponds to the number of pressurizations for
about 100 flights. Actual spacecraft tanks could not be allowed to have this
depth of flaw, however, because a scatter factor would be required for the
design fatigue life. In addition, spectrum effects of flight loads would
need to be accounted for if the tanks are integral with the structure.

Finally, a partial exploration of the influence of temperature on the
fatigue-crack growth problem is required. Since current data show that
fatigue-crack growth rate in 70°F air is slightly greater than that in either
liquid oxygen or liquid hydrogen, an analysis based on ambient air data would
be conservative, except that a 300°F temperature may occur in the tanks in
the latter part of a mission. Currently, there is little data available
on the effect of elevated temperature on fatigue-crack propagation behavior
of 2219-T87 aluminum.

As a result of these considerations, the program reported herein was initiated
to obtain information on the following parameters as they influence the
number of fatigue cycles to cause leakage:

- Thickness
- Initial flaw size and shape
- Temperature
- Stress ratio
- Maximum stress

Subsequent to determining the influence of these parameters on fatigue-crack
propagation a program to evaluate current NDI practices was developed to:

- Optimize current practices for penetrant, X-ray, eddy current
  and ultrasonic inspection procedures

- Obtain an estimate of the flaw detection limits of each of the
  NDI procedures listed above

● Evaluate the effect of a prior proof stress cycle on the NDI inspection capability limits

The program outlined above is described in the following sections of this report.

## 2.2 Fatigue Crack Propagation Analysis

Having established that natural flaws can exist in a structure, the rate at which the flaw propagates by fatigue and/or sustained load flaw growth is one of the major considerations in designing to prevent fracture. For a 2219-T87 aluminum pressure vessel, the fatigue-crack propagation behavior of an initial surface (or embedded) flaw is of major importance. Using current fracture mechanics concepts to analyze this fatigue-crack propagation behavior, two elements must be considered. The first is the stress intensity expression for the surface flaw used in the analysis, and second in the fatigue-crack propagation model or expression used to predict the fatigue-crack propagation behavior. These factors are discussed in the following sub-sections, respectively.

## 2.2.1 Stress Intensity Factor

The analysis of surface flaws in terms of stress intensity factors originated with Irwin[1] and was based on the elastic-stress solution of Green and Sneddon[2] for an embedded elliptical crack. The resulting basic equation was

$$K = \frac{S \, (\pi A)^{1/2}}{\phi_o} \left\{ \sin^2 \phi + \frac{A^2}{C} \cos^2 \phi \right\}^{1/4} \tag{1}$$

where  S = gross stress perpendicular to the crack

A = crack depth (one-half minor diameter)

C = one-half of surface crack length (one-half major diameter)

$\phi$ = angle from major axis to specific point on the circumference

$\phi_o$ = the complete elliptic integral of the second kind, or

8

$$\phi_o = \int_0^{\pi/2} \left[ 1 - \left( \frac{c^2 - A^2}{c^2} \right) \sin^2\theta \right]^{1/2} d\theta \qquad (2)$$

The mathematical model used in this development was based on a linear elastic solution for a fully embedded elliptical crack within an ideally elastic material. However, structural metallic materials used in real aircraft hardware are not purely elastic but exhibit various degrees of ductility. The adjustments to the elastic fracture mechanics equations are estimates of very complex effects of plasticity and free boundary surfaces. For the surface crack test specimens, there are four correction factors to be considered:

- Correction for the specimen free surface (front face) that is normal to the plane of the crack and intersects the crack along the major axis of its semi-elliptical shape.

- Correction for the net section effect. This correction accounts for the increase in stress at the plane containing the crack caused by the reduction in cross sectional area. The K values should be multiplied by the ratio of gross area-to-net area. With large test specimens or small flaws, this correction is normally neglected.

- Correction for the specimen free surface, back face. This correction factor is necessary to account for the influence of the back face free surface on the strain and stress state in the material adjacent to the crack tip as the surface crack depth approaches the specimen thickness.

- Correction for plastic deformation at the crack tip.

For this study, the surface flaw stress intensity was computed in accordance with the procedure currently employed by NASA/MSC for 2219-T87 aluminum and described in Reference 3. Briefly, two stress intensity factors were used to describe the surface flaw, one at the surface of the specimen (major axis),

$\Delta K_C$, and the other at the minor axis location, $\Delta K_A$, as shown in Figure 1. The correction factors F, G, M, and Q as defined below, were included in the analysis.

- F, correction factor for the effect of the front surface on crack growth through the thickness. The correction used was that assumed by Kobayashi and Moss[4] and is given by

$$F = 1.0 + 0.12 \ (1 - A/2C)^2 \qquad (3)$$

- G, correction factor for the effect of the front surface on crack growth in the width direction. Estimates of this correction for a surface flaw are based on the results for embedded flaws with the same minor and major axis length[5] where it was found that a constant value of 1.12 was an adequate approximation.

- M, correction factor for the effect of the back surface on crack growth through the thickness. Several approximate empirical[4,6,7,8] and experimental[9] solutions have been proposed for this correction. For this program, the proposed solution of Shaw and Kobayashi[10] was used.

- Q, is a form of Irwin's[1] plasticity correction modified to account for different cyclic load ratios such that

$$Q = \phi^2 - 0.212 \left[ \frac{(1.0 - R) \ \Delta S}{S_y} \right]^2 \qquad (4)$$

The resulting equation for the surface flaw stress intensities at the surface $(\Delta K_C)$ and the point of maximum penetration through the thickness $(\Delta K_A)$ were

$$\Delta K_C = G(\Delta S) \ A/C \ \sqrt{\frac{\pi \ C}{Q}} \qquad , A \leq C \qquad (5)$$

$$\Delta K_C = G(\Delta S) \ \sqrt{\frac{\pi \ C}{Q}} \qquad , A > C \qquad (6)$$

$$K_A = F(\Delta S)\, M\sqrt{\frac{\pi A}{Q}} \quad \text{FOR } A \le C$$

$$= F(\Delta S)\,\frac{C}{A}\sqrt{\frac{\pi A}{Q}} \quad \text{FOR } A > C$$

$$K_C = G(\Delta S)\,\frac{A}{C}\sqrt{\frac{\pi C}{Q}} \quad \text{FOR } A \le C$$

$$= G(\Delta S)\sqrt{\frac{\pi C}{Q}} \quad \text{FOR } A > C$$
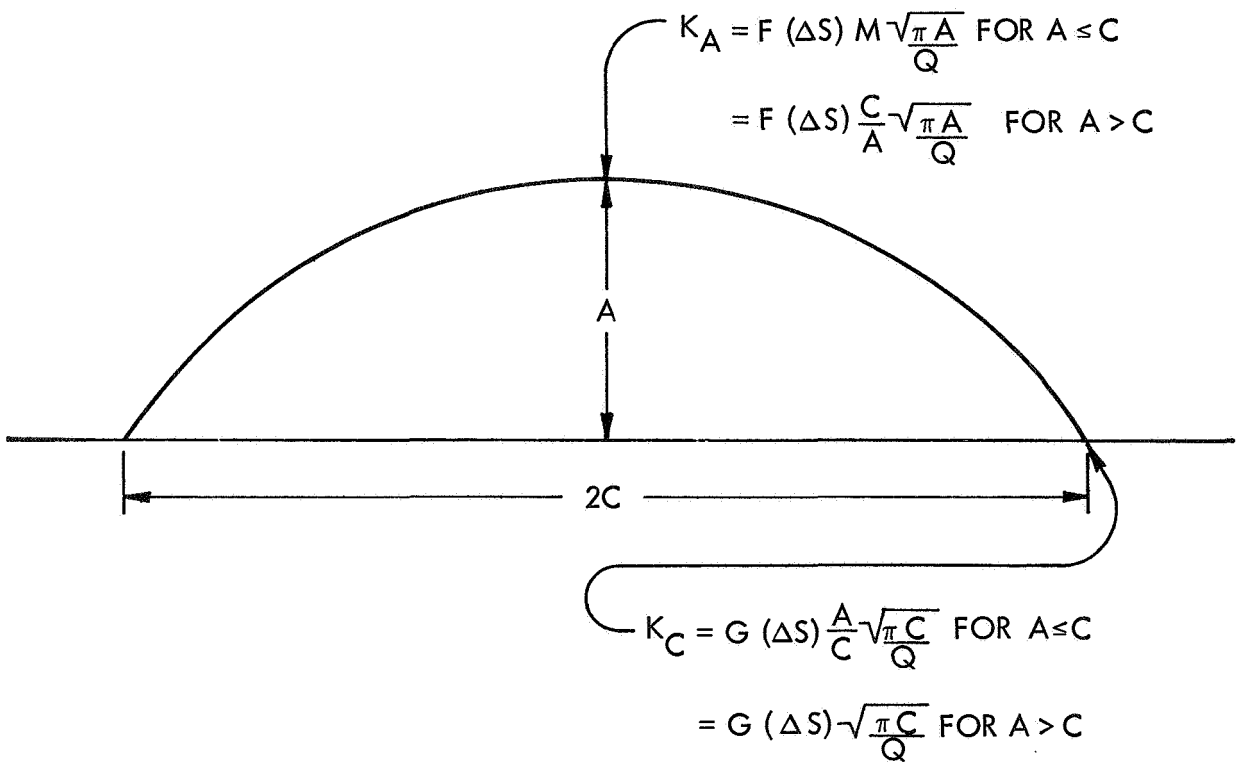
Figure 1.  Stress Intensity Expressions Used in Computation of
Fatigue Crack Propagation Behavior using Forman's
Equation and NASA "CRACK" Computer Program

$$\Delta K_A = F(\Delta S) \, M \sqrt{\frac{\pi A}{Q}} \qquad , A \le C \qquad (7)$$

$$\Delta K_A = F(\Delta S) \, \frac{C}{A} \sqrt{\frac{\pi A}{Q}} \qquad , A > C \qquad (8)$$

These equations were utilized in the data analysis as subsequently described in the results section.

## 2.2.2 Fatigue-Crack Propagation Models

Experimental studies of fatigue-crack propagation behavior are usually based on determination of fatigue crack growth rates for a given set of specimen, material, stress and environmental conditions. The crack growth rates for various combinations of conditions are related to one another by means of an analytical expression based on one of two relationships, either

$$dA/dN = C' \cdot f(A,S) \qquad (9)$$

or alternately using fracture mechanics concepts,

$$dA/dN = C' \cdot f(K) \qquad (10)$$

Where  A  =  one-half crack length or crack depth, (inch)

N  =  number of cycles

S  =  gross area stress (ksi)

K  =  stress intensity factor (ksi $\sqrt{in.}$)

At a given value of stress ratio, $R = S_{min}/S_{max}$, for a given material and environment combination, the crack growth rate can be plotted with equal success against either $K_{max}$ or $\Delta K$, with all data falling within a narrow scatterband. This band widens when the data from more than one stress ratio are included. The breadth of the band tends to be smaller when $dA/dN$ is plotted against $\Delta K$ rather than $K_{max}$, which indicates that $\Delta K$ is the primary variable. Crack growth data is often presented as a series of $dA/dN$ versus $\Delta K$ plots for various range ratios, as shown in Figure 2. For simplicity a
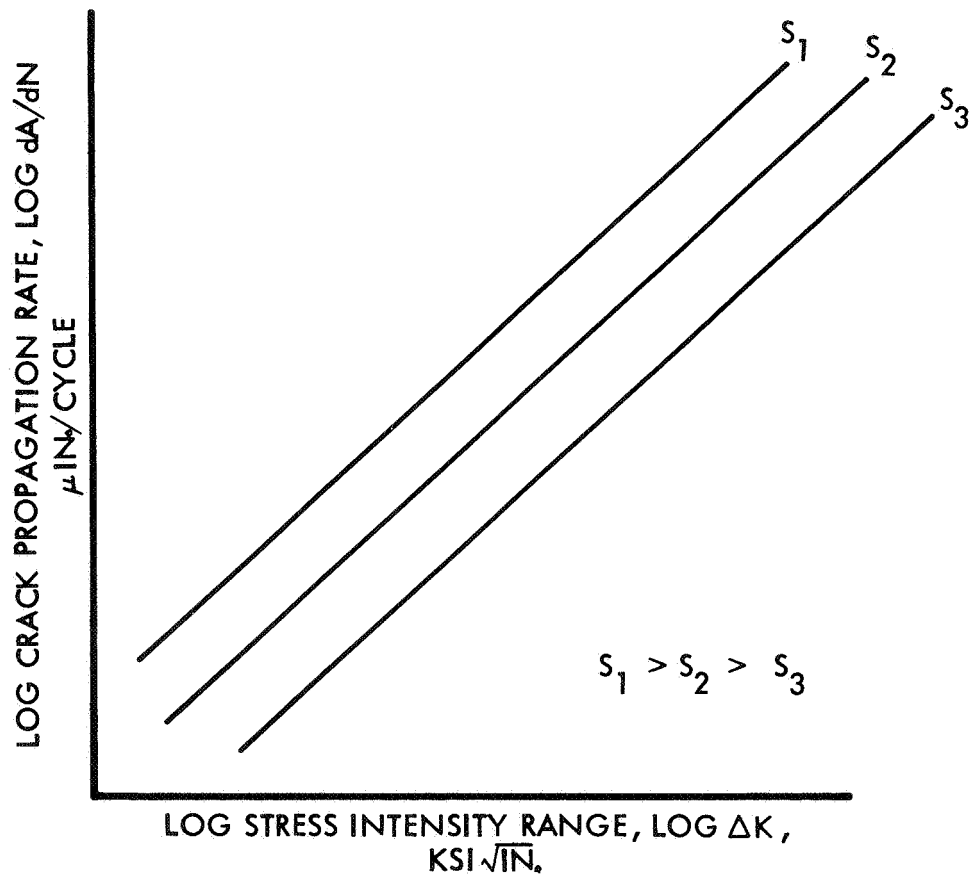
Figure 2. Typical Presentation of Fatigue-Crack Propagation
Data Based on the Stress Intensity Range, $\Delta K$, During
the Fatigue Cycle.

13

single crack-growth rate curve would be desirable. Clever choice of the stress intensity-related abscissa for the crack growth curve can lead to such a unique relationship.

Forman[11] developed an equation providing a means for comparing crack growth data obtained at different range ratios. The proposed relationship is

$$dA/dN \;=\; C' \;\; \frac{\Delta K^n}{(1 - R)\, K_c - \Delta K} \tag{11}$$

where $K_c$ is the fracture toughness of the material, while $C'$ and n are empirical constants. This model assumes a unique relationship between the fatigue crack growth rate and the alternating stress intensity for a given material and environment. This model has been quite successful in correlating fatigue crack growth data.

Another recent development of Hall[12] has proposed that surface flaw growth may be represented by

$$\frac{d(\frac{A}{Q})}{dN} \;=\; C' \;\left(\frac{S_o}{S}\right)^2 (1 + \lambda)^m \, \Delta K^n \left[ 1 - \frac{K_{max}}{K_{Ic}} \right]^{-P} \tag{12}$$

where $C'$, m, n, and P are experimental constants, $S_o$ an arbitrary stress, and $\lambda$ a function of K. The proposed equation originated from the plane-strain cycles-to-fracture criteria for surface flaws similar to that used in the Apollo program. While the $(\Delta K)^n$, $(1 - K_{max}/K_{Ic})^{-P}$, and $(1 + \lambda)^m$ terms are similar in form to those major terms used by other investigators to predict dA/dN, two major differences exist. First Hall uses the crack parameter $d(A/Q)/dN$ where A/Q is the "normalized flaw depth" and incorporates the crack shape parameter rather than using dA/dN as many investigators have and letting the shape influence of Q be reflected only in the stress intensity term. Second, the $(S/S_o)^2$ term is included to account for the the existence of an assumed unique curve when $K_{Ii}$ is plotted versus cycles-to-failure.

14

The Forman and Hall equations thus differ in their basic assumptions, the Forman equation assuming a unique $\Delta K$ versus $dA/dN$ relationship and the Hall equation assuming a unique $K_{Ii}$ versus cycles-to-failure relationship. As a result these two equations were evaluated in the present program, the Forman equation cycle by cycle integration being performed using the two-dimensional integration of the NASA "crack" program and the Hall equation being integrated on a cycle by cycle basis assuming a one-dimensional problem with a constant Q value.

## 2.3    The Fracture Mechanics/Nondestructive Inspection Interface

After the critical size flaw (here when A = B) and fatigue crack growth behavior are known for a given environment, material, and application, fracture mechanics analysis can be used to determine the maximum initial flaw size that can be allowed in the structure if a specific design life is to be obtained before leak occurs. The problem now becomes one of establishing a method of assuring that no flaws larger than the maximum permitted initial flaw are present in the structure. When proof testing is not applicable, nondestructive inspection procedures must be relied upon to detect all flaws that are larger than the maximum initial size allowed in the design.

### 2.3.1  Nondestructive Inspection Methods

Subsequent to establishing the maximum initial flaw size that can be permitted in the structure, it becomes necessary to establish a method by which flaws larger than this crack size can be screened. However, it is becoming imperative that not only the detection limits of current NDI methods be defined, but also that the statistical reliability of flaw detection be known.

The size, shape, and location of probable flaws are influenced by metallur-gical factors, product form, fabrication methods, and the load history of the structure that may produce fatigue cracks and/or corrosion damage. Flaws in structural components can be present in the raw sheet, plate or forged

15

material or can be imparted during processing or service. Common non-destructive techniques employed to reveal these flaws include surface penetrant, X-ray, ultrasonics, and eddy current. All of these methods were examined in this investigation, and are discussed in this section.

Surface penetrants are commonly used in surface flaw detection. When the limit of surface flaw detection from penetrant inspection in a fracture mechanics application is considered, it is immediately obvious that an important parameter is missing. This inspection method only detects the length of flaw open to the surface, and gives no indication of the shape or amount of flaw beneath the surface. Therefore, to use fracture mechanics we must assume the hidden flaw dimensions. If the flaw has been generated by fatigue in three point bending, for example, the unknown dimension can be estimated reasonably well. However, if the flaw is a heat treating crack or a welding defect, the estimate of sub-surface size may be very poor. It becomes obvious that penetrant inspections can detect surface flaws but are of limited value for characterizing flaw shapes.

Another standard NDI method is radiographic or X-ray inspection. It is possible to locate and define a flaw by taking exposures from several angles. This method is very sensitive to experimental technique since an X-ray exposure taken from an incorrect angle will completely miss a crack type flaw. Also, the accuracy depends on the visual interpretation of the film. Packman et al[13] showed X-ray to be the least reliable method for detecting 0.05-0.50-in. long flaws. The minimum reliably detectable flaw size using X-ray techniques was larger than the proposed thickness for 2219-T87 tanks. Therefore, X-ray is anticipated to be of limited value in detection small surface defects and cracks in this material.

Various researchers have reported the detection of extremely small flaws by ultrasonic techniques. These research efforts are not in question; however, in most cases the flaw was built-in or known in some manner and the researcher adjusted his equipment to detect the known flaws. For example,

ultrasonic flaw indication is particularly sensitive to the gain setting. Sattler[14] reports that examination with ultrasonic Delta C-scan of a test block containing several flat bottom holes at different depths required two gain settings. At the lower gain setting the closer holes were distinctly visible while the more distant holes were undectable. At the higher gain setting the more distant holes were detectable but the indications of the closer holes were quite distorted, large, and difficult to interpret. Packman et al[13] also reported using different gain settings to detect cracks of different sizes. Cellitti and Carter[15] established good correlation between ultrasonic inspection recording and inclusion content in steels. They proved that ultrasonics can be used to select material with the best fatigue strength based on the inclusion content.

Based on Sattler's and Packman's research using various gain settings, it appears that an ultrasonic instrument tuned to record inclusion content could not be used to characterize a large flaw or crack. Further, it appears that for particular instrument settings there is a range of flaws and a range of depths that will be characterized while extraneous indications may be present. The true flaw characterization may be indistinguishable from extraneous indications unless several scans at different instrument settings are made.

Ultrasonic testing has been standardized sufficiently to insure reproducible results for a given set of conditions by the use of fabricated standards such as those fabricated for the C-5 aircraft program and those reported by Pless, Weil, and Lewis for NASA use[16]. As yet, however, the state-of-the-art has not progressed to a universal set of standards for ultrasonics, therefore many laboratory-to-laboratory differences in techniques exist. Although Krautkramer[17] discusses a method for characterizing a flaw using ultrasonics, most NDI efforts are concerned with finding, not characterizing a flaw. This is partially due to the previous lack of necessity for quantitative flaw characterization and partially due to the high cost (in time) to obtain adequate data.

The use of eddy current techniques may prove to be one of the most useful for inspection of cryogenic tankage but has not been extensively evaluated at the present time.

## 2.3.2 Factors that Influence Flaw Detection

In addition to equipment and operating/operator variables, many external factors influence the detectability of defects by NDI methods. Three main variables are flaw characteristics, history, i.e., the separation of the crack surface due to prior or current loading, and surface conditions. The influence of each of these variables is discussed below.

Corbley et al[18], showed that ultrasonic NDI response was proportional to the stress in a part containing a flaw. Sattler[14] also pointed out that NDI was enhanced when flaws were opened by the application of a stress. Packman[19] showed actual measurements of air gap required to obtain an NDI indication of a crack. Therefore, if a crack is formed in fatigue and closes upon release of load, it will be harder to detect than an open crack or void. At the present state-of-the-art, it is difficult to be specific as to the amount of crack opening; but the general concept of an open versus a tightly closed crack can be visualized. For this reason, surface fatigue cracks are assumed to be representative of the worst flaw condition likely to occur in non-welded structure. On the other hand, the effect of a prior proof load and a high fatigue stress would produce a plastic zone at the crack tip. Upon release of the load, the residual plastic zone would tend to resist the complete closure of the crack. This in turn would result in an increase in the crack surface separation distance and the crack could be more easily detected. A measure of the expected crack tightness and consequently the NDI response would be the applied stress intensity to yield stress ratio, although this measure can only be qualitative with present knowledge.

Processing of parts is a distinct variable that can only be accounted for in a qualitative manner. For example, surface finish is very critical in surface crack detection. A smooth finish is an asset to all NDI methods as

long as the material is not soft enough to flow over the crack during the surface finishing process. The sensitivity of ultrasonics for detecting an internal flaw is especially enhanced by a smooth finish. Plating can also be a significant factor. The plating material can cover an existing crack or a fatigue crack could exist under a soft plating material without cracking through the plating. The effect of surface finish is one variable not examined in this current program but is being examined on other NASA funded research programs.

A previous AFML contract[13] investigated the accuracy of detection of surface flaws in aluminum and steel cylinders. Typical results for aluminum are presented in Figure 3. Similar work by Sattler[14] is presented in Table 3.

Using delta configuration ultrasonics, Automation Industries, Inc.[20] inspected several types of flaws in weldments and compared the delta configuration to 60 degree angle beam ultrasonics and X-ray inspection. These data are summarized in Table 4. The material was 2014 and 2219 aluminum sheet 0.063 to 1 inch thick; lack of fusion was from 0.010 to 0.130 inch long, lack of penetration was 0.070 inch wide and cracks were up to 0.250 inch long (intergranular). These data show that large porosity, cracks, and micro fissuring all were detected by the delta configuration; however, the four tests identified do not represent a complete statistical sampling. In addition, there is a discrepancy between the number of flaws detected and the correlation with destructive tests, probably due to differences in flaws thought to be present and those verified by destructive test.

The influence of these variables (excluding surface finish) are examined in the program reported herein. The standard reference blocks selected for use were fatigue cracks of known dimension in 2219-T87 aluminum. Details of the study are presented in subsequent sections.
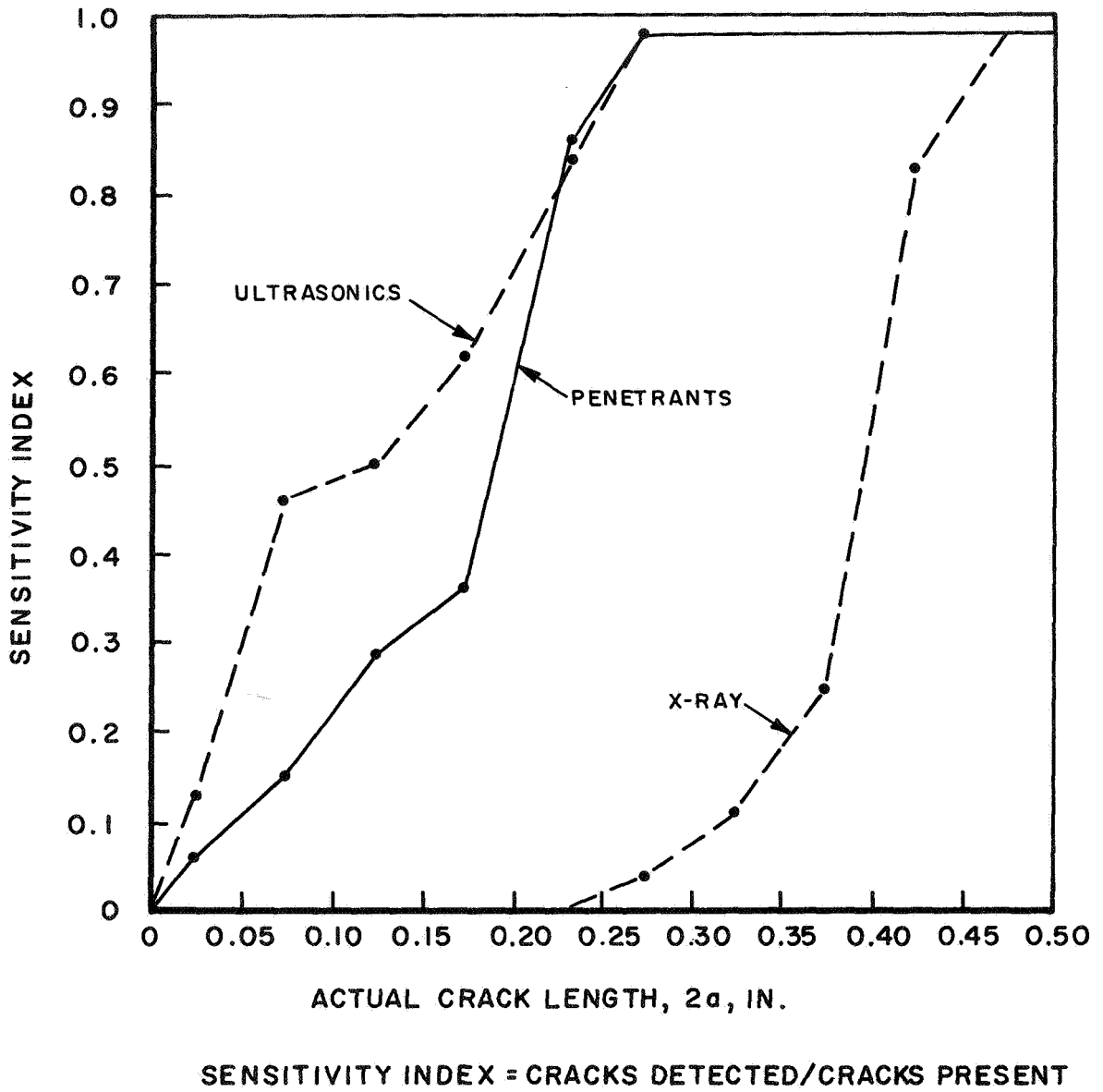
Figure 3. Comparison of NDI Inspection Methods for Aluminum Cylinders[13]

TABLE 3

FLAW DETECTABILITY LIMITS[1] IN 0.020-1.0-INCH THICK
ALUMINUM AND TITANIUM PLATE, REFERENCE 14

| NDI Technique | 0.020-Inch Aluminum | 0.020-Inch 6Al-4V Ti | 0.020-Inch 5Al-2.5Sn Ti | 0.125-Inch Aluminum | 0.125-Inch 6Al-4V Ti |
|---|---|---|---|---|---|
| Ultrasonic | 0.05 | 0.10 | 0.03 | NC | 0.09 |
| Penetrant | 0.04 | 0.032 | | 0.03 | 0.05 |
| X-ray | NC[2] | 0.07 | | ND[3] | 0.13 |
| Delta Ultrasonics | | | | | 0.034 |

| NDI Technique | 0.5-Inch Aluminum | 0.5-Inch 6Al-4V Ti | 0.5-Inch 5Al-2.5Sn Ti | 1.0-Inch Aluminum |
|---|---|---|---|---|
| Ultrasonic | 0.29 | 0.15 | 0.07 | |
| Penetrant | ND | 0.025 | | ND |
| X-ray | 0.46 | ND | | 0.21 |
| Delta Ultrasonics | (4) | 0.09 | 0.10 | |

Notes: (1) Determined by statistical method based on extrapolated flaw length measured versus actual length. Flaw location was known and all specimens contained flaws.

(2) NC designates no correlation of data; therefore, no statistical evaluation was possible.

(3) ND designates no flaws detected by this method.

(4) This number was negative, an illogical result.

TABLE   4

QUANTITATIVE NDI PERFORMED BY AUTOMATION INDUSTRIES

| Detection of Flaws in Selective Area of Weld | | | | | | | |
|---|---|---|---|---|---|---|---|
| Types of Flaws Found | Flaw Occurrence in 5 ft of Weld | Delta Wheel | | 60° Angle Beam | | X-Ray | |
| | | No. | % | No. | % | No. | % |
| Lack of Penetration | 14 | 12 | 86 | 7 | 50 | 5 | 36 |
| Lack of Fusion | 36 | 34 | 94 | 16 | 45 | 31 | 91 |
| Porosity >0.010 in. | 4 | 4 | 100 | 4 | 100 | 4 | 100 |
| Porosity <0.010 in. | 6 | 4 | 67 | 1 | 17 | 4 | 67 |
| Cracks | 4 | 4 | 100 | 3 | 75 | 2 | 50 |
| Microfissuring | 4 | 4 | 100 | 0 | 0 | 0 | 0 |

| Comparison of NDI with Destructive Evaluation | | | |
|---|---|---|---|
| Flaw Types | Delta Inspection Correlation with Destructive Tests | 60° Angle Beam Correlation with Destructive Tests | Radiography Correlation with Destructive Tests |
| Lack of Penetration | 73% | 50% | 37% |
| Lack of Fusion | 98% | 45% | 84% |
| Porosity >0.010 in. | 92% | 100% | 83% |
| Porosity <0.010 in. | 49% | 17% | 37% |
| Cracks | 90% | 75% | 60% |
| Miscrofissuring | 100% | 0% | 14% |

Section 3

MATERIALS


## 3.1  Parent 2219-T87 Aluminum Alloy

Parent material for this study was supplied to Lockheed by NASA/MSC in the
form of 0.125, 0.250, and 0.500 inch thick plates of 2219-T87 aluminum.  The
material then was chemically milled by Anadite, Inc. to the desired testing
thickness (viz., 0.040, 0.080, 0.160, 0.30 inch).  Following the chem milling
operation, metallographic sections were made and the material examined to
detect any unusual chem milling effects.  Typical results, shown in Figure 4,
show no unusual effects.  Thickness variations were determined for six
pieces of 0.250-inch thick material chem milled to 0.157-inch nominal
thickness.  For all six specimens the thickness was found to be 0.157 $\pm$0.002
inch.  Typical room temperature tensile properties of the chem milled
material, presented in Table 5, were representative of normal parent material.
All NDI panels were made 0.020-inch thicker than the test thickness.


## 3.2  Welded 2219-T87 Aluminum Alloy

Subsequent to chem milling the supplied sheets to the desired specimen
thickness, the sheets were sheared to the desired specimen blank size, the
joint chemically cleaned and scraped and mechanized gas tunsten arc welding
(GTAW) employed with 2319 aluminum filler wire to make the welds necessary
for the fabrication of the cross weld and longitudinal weld specimens.
The welding parameters agreed to by NASA and Lockheed personnel for the
0.080, 0.160, 0.300 inch thick (cycles-to-leak specimens) and 0.100, 0.180,
and 0.320 inch thick (NDI panels) welds are given in Table 6.  A typical
weld cross section is shown in Figure 5.

Tensile tests were conducted according to ASTM Standard E-8 on representative
welded specimens with the weld bead machined off flush to the specimen surface.
The tensile test results at room temperature and at 300°F were found to be
representative of welded 2219 aluminum and are presented in Table 7.

23
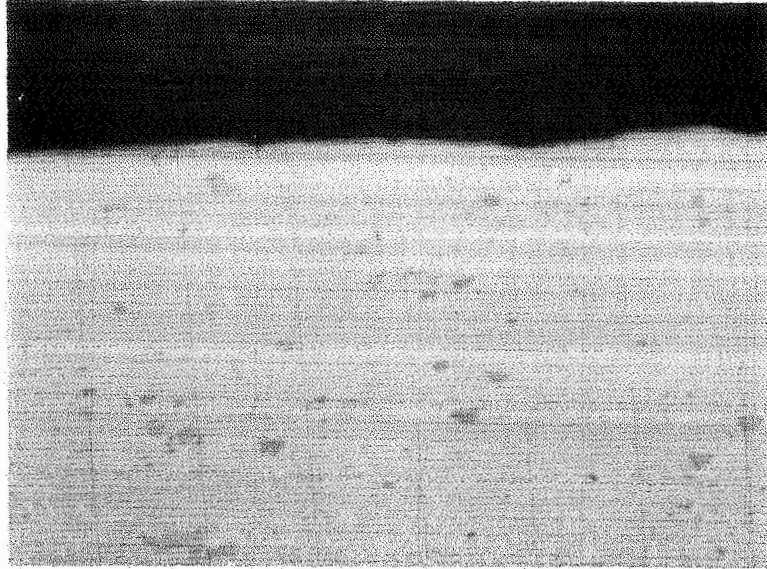
a. Longitudinal Section, As Polished. 500X
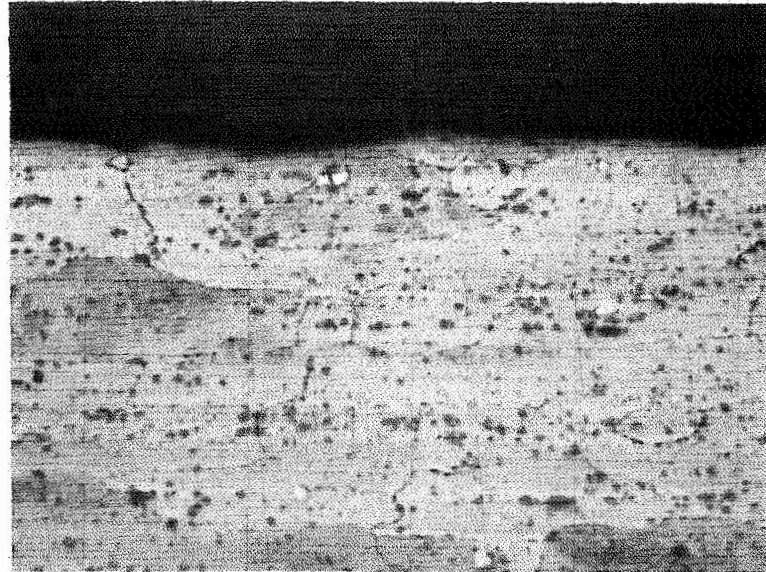


b. Longitudinal Section, Modified Keller
Etch, 500X.

Figure 4 . Metallographic Results for Chem Milled Parent
2219-T87 Aluminum.

TABLE  5 .   ROOM TEMPERATURE TENSILE RESULTS FOR
PARENT 2219-T87 ALUMINUM ALLOY
MATERIAL FOLLOWING CHEM MILLING TO
THICKNESS FROM 0.125-INCH THICK SHEET

| Specimen Number | Thickness B, inch | Ultimate Strength $S_{tu}$, ksi | 0.2% Yield Strength $S_y$, ksi | % Elongation in 2 inches |
|---|---|---|---|---|
| B-1-1 | 0.043 | 67.1 | 54.2 | 9.5 |
| B-1-2 | 0.043 | 66.5 | 53.5 | 9 |

TABLE 6 . WELDING PARAMETERS FOR 2219-T87 ALUMINUM ALLOY

| Thickness, inch | 0.080 | 0.100 | 0.160 | 0.180 | 0.300 | | 0.320 | |
|---|---|---|---|---|---|---|---|---|
| Weld Parameter | | | | | | | | |
| Pass | 1 | 1 | 1 | 1 | 1 | 2 | 1 | 2 |
| Equipment | Sciaky | Sciaky | Sciaky | Sciaky | Miller | Miller | Miller | Miller |
| Amperage | 106 | 106 | 165 | 183 | 300 | 295 | 330 | 295 |
| Volts | 12.8 | 12.8 | 13.5 | 13.5 | 18 | 17 | 18 | 17 |
| Weld Speed, ipm | 12.5 | 12.5 | 12.5 | 12.5 | 5-1/4 | 6-1/2 | 5-1/4 | 6-1/2 |
| Wire Speed, ipm | 65 | 65 | 70 | 70 | 19-1/2 | 20 | 19-1/2 | 20 |

Constant Parameters, All Thicknesses

| | | |
|---|---|---|
| Type | – | GTAW Mechanized |
| Weld Wire | – | 1/16 in. 2319 Aluminum |
| Shielding Gas | – | Helium |
| Electrode | – | 2% Thoriated Tungsten |
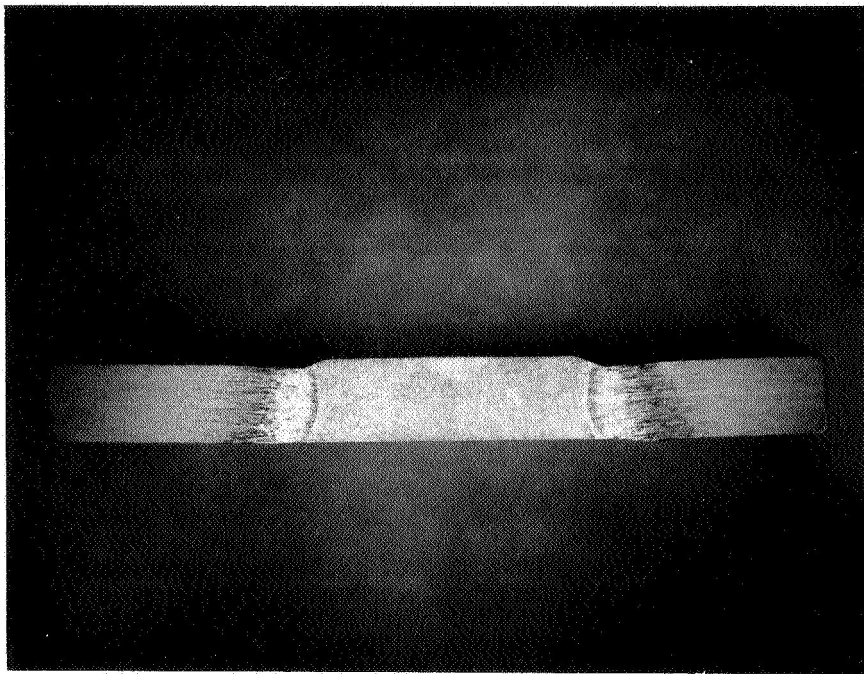
M176                                                    5X

Figure 5.   Typical Macrograph of 0.080-inch Thick
            Welded 2219-T87 Aluminum.   Etched.

TABLE 7. TENSILE TEST RESULTS FOR CROSS-WELDED
2219-T87 ALUMINUM ALLOY MATERIAL, WELD
BEAD MACHINED FLUSH TO SURFACE

| Specimen Number | Temperature, T, °F | Thickness B, inch | Ultimate Strength $S_{tu}$, ksi | 0.2% Yield Strength $S_y$, ksi | % Elongation in 2 inches |
|---|---|---|---|---|---|
| 1 | RT | 0.080 | 36.0 | 25.7 | * |
| 3 | | 0.080 | 36.0 | 24.7 | * |
| 4 | | 0.080 | 36.0 | 25.0 | * |
| | | Average | 36.0 | 25.1 | |
| 1 | 300 | 0.080 | 34.2 | 21.9 | 8 |
| 2 | | 0.080 | 33.5 | 21.8 | 8 |
| 3 | | 0.080 | 34.1 | 23.0 | 8 |
| | | Average | 33.7 | 22.2 | 8 |

*Not recorded

28

Section 4

PHASE I TEST PROCEDURES

In this section of the report, the detailed test procedures used in the
Phase I tests are presented. Included are specimen preparation, cycles-to-
leak test procedures and fatigue-crack growth rate (dA/dN) test procedures.

4.1    Specimen Preparation

Due to a limitation of the amount of material available, it was necessary to
use minimum possible size specimens. Using the criteria that the specimen
width should be greater than three times the maximum surface crack length at
breakthrough and the specimen length should be three times the specimen
width, the specimen configurations shown in Figure 6 were adapted for the
various thicknesses. The specimens for this study were oriented with the
crack transverse to the rolling direction.

Three types of specimens were used in this program; parent material, welded
specimens with the weld perpendicular to the applied load (hereafter
referred to as cross weld), and welded specimens with the weld parallel to
the load (hereafter referred to as a longitudinal weld). For the parent
material tests, the flaw was located at the specimen center. For the
longitudinal welds two flaw locations were examined; one at the weld center-
line and one at the weld fusion line. For the cross weld specimens, a
series of preliminary tests were conducted to determine the most critical
flaw location in the weld. The results, shown in Figure 7, indicated that
the weld center was more critical from a fatigue-crack propagation standpoint
than the fusion line. As a result, the flaws were located at the weld
centerline in  the cross weld specimens for cycles-to-leak tests.

| THICKNESS* (INCH) | W (INCH) | L (INCH) |
|---|---|---|
| .040, A | 2 | 12 |
| .080, A | 2 | 12 |
| .160, B | 3,4 | 16 |
| .300, B | 5 | 18 |
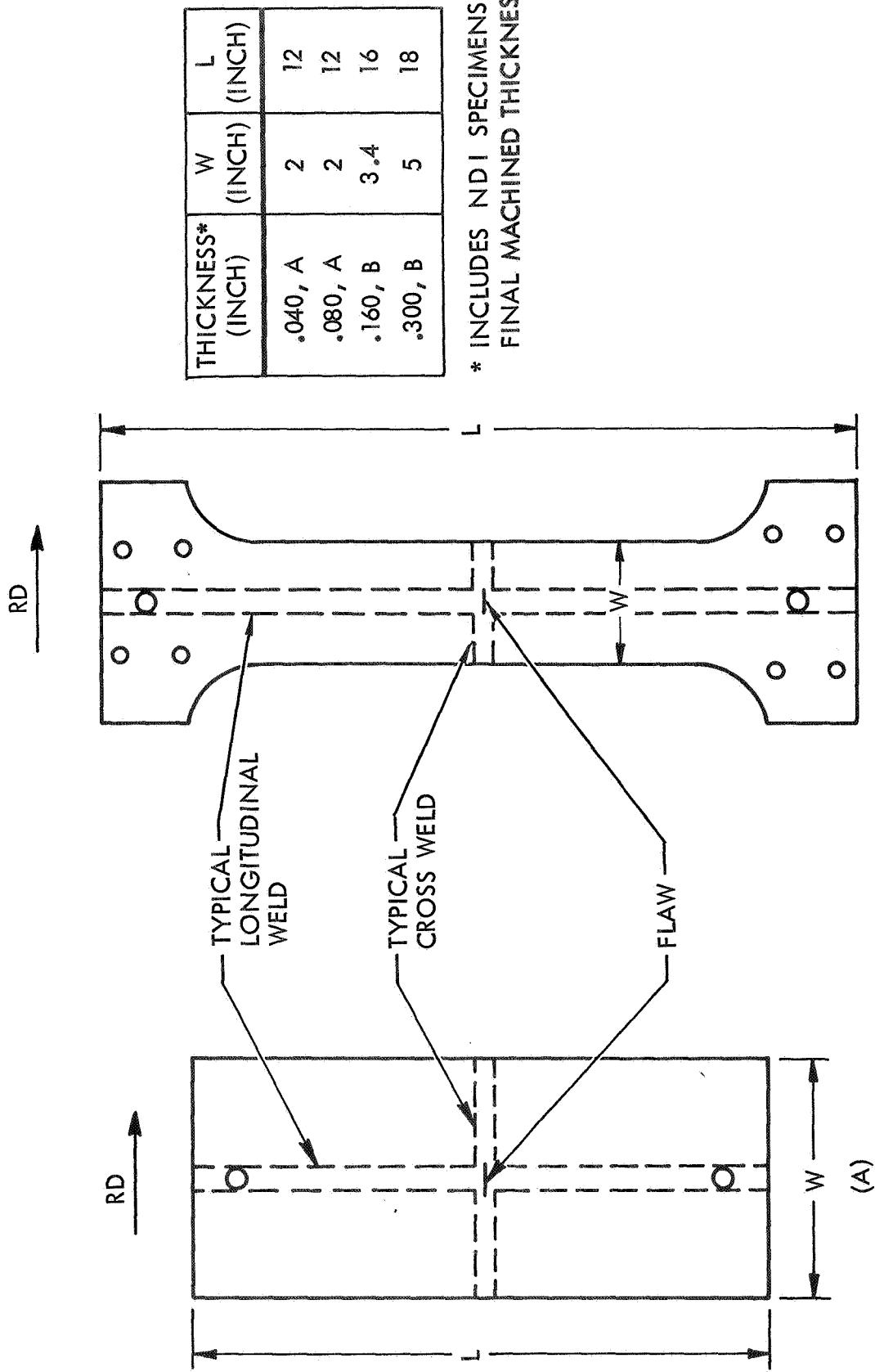
\* INCLUDES NDI SPECIMENS,
FINAL MACHINED THICKNESS

TYPICAL LONGITUDINAL WELD

TYPICAL CROSS WELD

FLAW

RD

L

W

(B)

RD

W

L

(A)

Figure 6.  Specimen Configurations

30
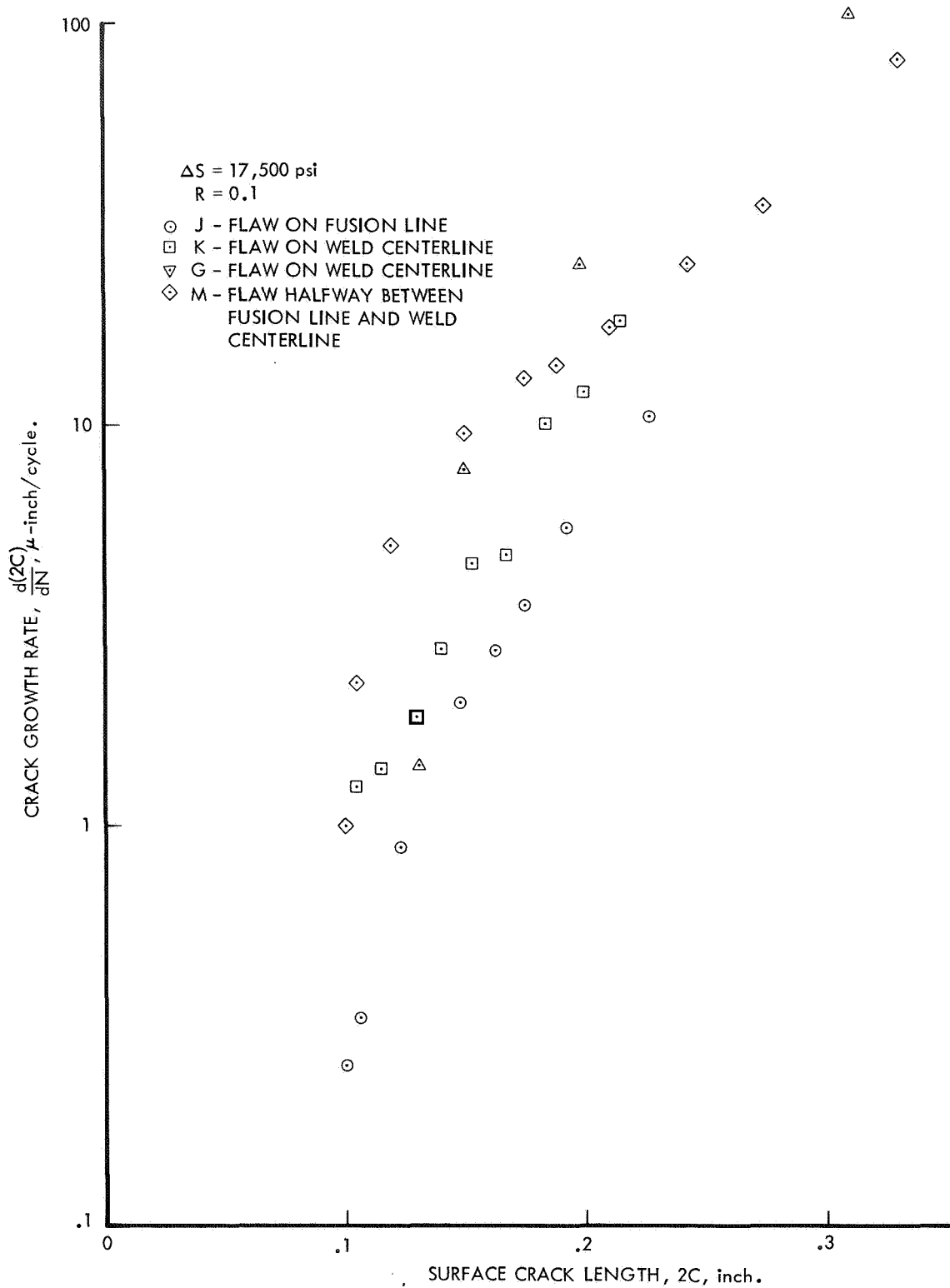
Figure 7. Fatigue Crack Growth Rates for Various Flaw Locations in Welded 0.080-inch Thick 2219-T87

31

The initial flaws were produced in each specimen by low stress fatigue cycling from an appropriately located EDM slot. Three flaw configurations were examined in this program; A/2C = 0.5, 0.3, and 0.15. The fatigue precracking sequence for each flaw configuration is given below.

$\underline{A/2C = 0.5.}$ Tension-tension fatigue, R = 0.1, $K_{max}$ < subsequent initial $K_{max}$ of the fatigue-crack propagation test; crack propagated from an EDM slot with $(A/2C)_{EDM}$ = 0.5.

$\underline{A/2C = 0.3.}$ Tension-tension fatigue, R = 0.1, $K_{max}$ < subsequent initial $K_{max}$ of the fatigue-crack propagation test; crack propagated from a rectangular EDM, $(A/2C)_{EDM}$ = 0.25.

$\underline{A/2C = 0.15.}$ Cantilever bending fatigue (except for 0.040 inch thick parent material where four point bending was used), R = 0.1 with the maximum bending stress on the surface equal to 0.5 yield for the parent material and 0.6 yield for the welded material. Cracks were propagated from EDM slots with $(A/2C)_{EDM} \approx 0.2$.

The crack lengths were measured during precracking with a 30X microscope attached to a 0.001 inch division dial gage mounted on an optics bench as shown in Figure 8. The target crack depths were estimated based on preliminary specimens precracked by the same procedures from the same initial flaw and then fractured to determine the relationship between the crack depth and surface crack length.

4.2    Cycles-to-Leak Test Procedures

All cycles-to-leak tests were conducted in a 100 kip capacity MTS electro-hydraulic testing machine. In the initial program the test frequency was one-half Hz until leak or 5000 cycles had occurred. However, early in the program it was found that many of the flaw/load conditions initially specified did not result in a leak condition in 5000 cycles. Subsequently, tests were conducted to determine the effect of test frequency on fatigue-crack propagation. The results that are shown in Figure 9 showed no effect of increasing the test frequency from 1/2 Hz (30 cpm) to 4 Hz (240 cpm).

32
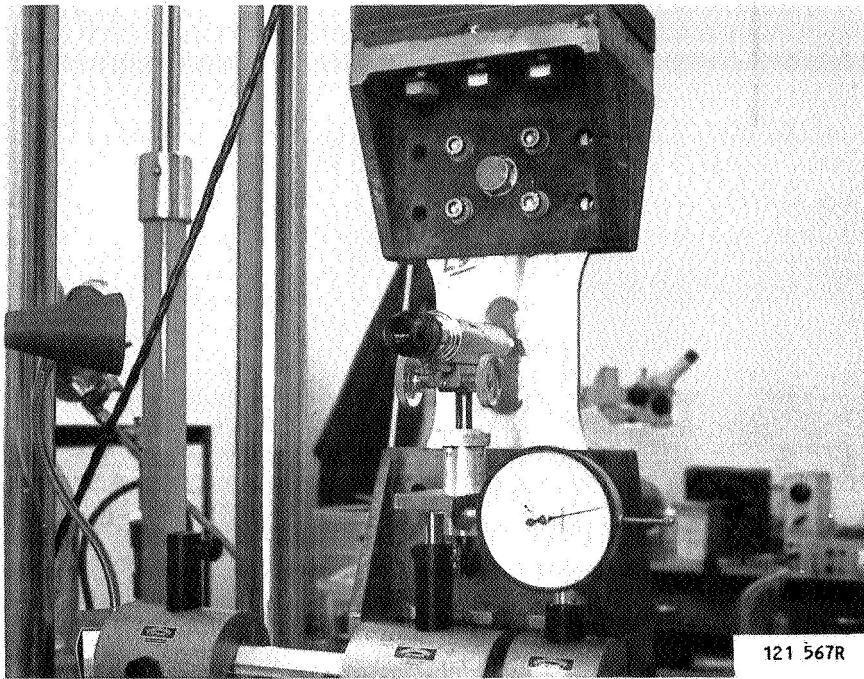
Figure 8. Typical Precracking Crack Measuring Equipment
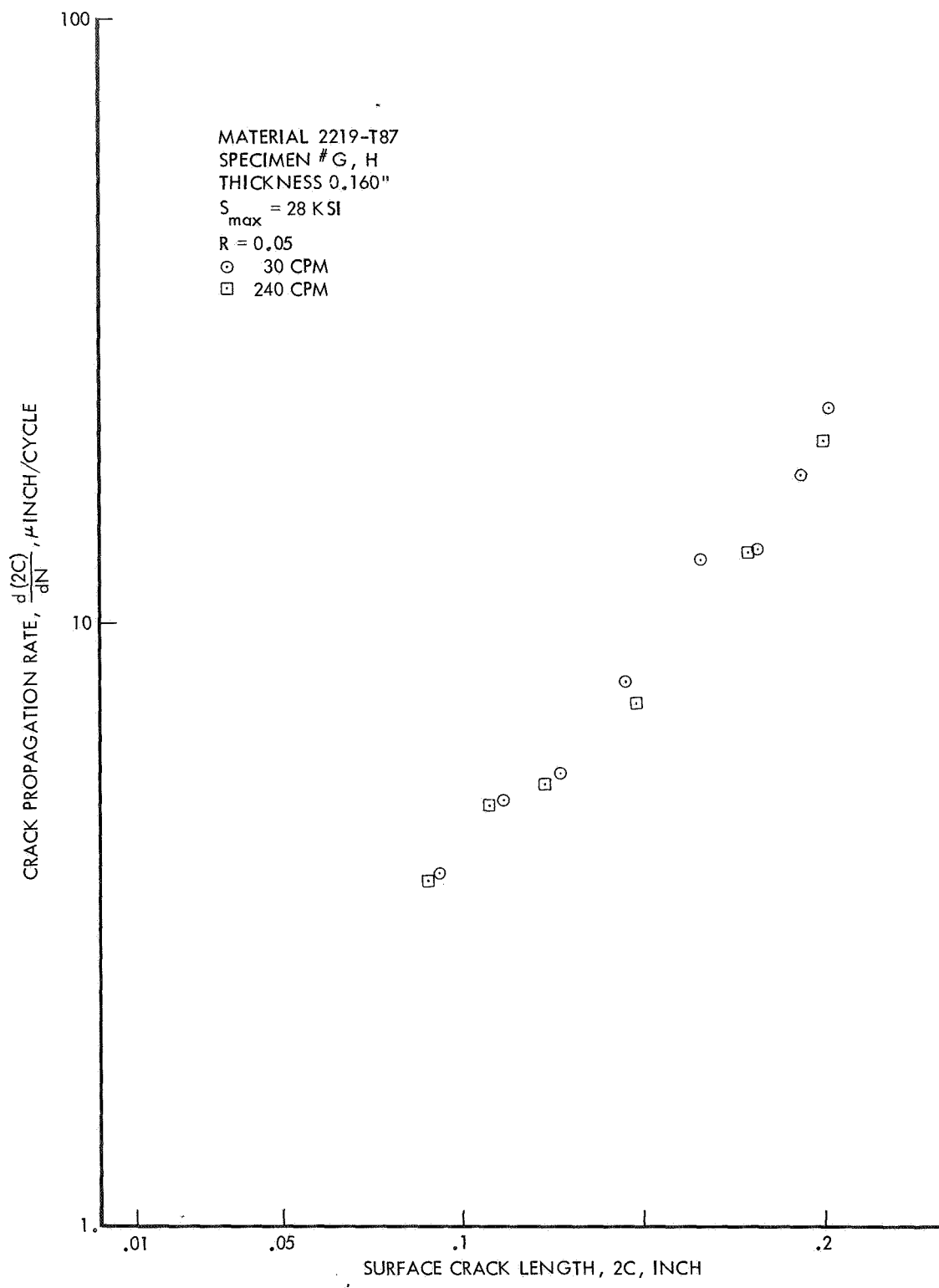
Figure 9.  Effect of Frequency on the Fatigue Crack Propagation
Behavior on 2219-T87 Aluminum Tested in Laboratory Air

34

These results were confirmed by NASA/MSC[21]. All subsequent tests were conducted at 3 Hz until leak or 20,000 cycles occurred.

## 4.2.1  Crack Marking Procedure

Preliminary tests revealed that the initial fatigue crack front could not be reliably defined on a post test fractographic examination, even using polarized light methods. As a result the use of a 10 percent NaOH solution such as used by NASA/MSC personnel to stain the initial crack location was considered. Figure 10 shows the results when fatigue-crack propagation testing was interrupted, a 10 percent NaOH solution applied to the crack tip for 30 seconds with the specimen under the mean precracking load, the specimen removed and vacuum baked at 200°F for 30 minutes, and the fatigue crack propagation test resumed. As shown in Figure 10, no effect of the NaOH marking procedure was noted on the subsequent fatigue-crack propagation rate. This confirmed the NASA/MSC results[21]; this marking procedure subsequently was used for the cycles-to-leak and dA/dN testing in this program.

## 4.2.2  Room Temperature Test Procedure

After the initial crack front had been marked and the specimen vacuum baked, it was placed in a 100 kip MTS electro-hydraulic test machine for testing. The occurrence of crack breakthrough was determined by use of the system shown schematically in Figure 11. A chamber containing distilled water was attached to the back surface of the specimen and pressurized to 20 psi gauge with $N_2$ gas. An electrical grid covered by an absorbent (gauze) cloth was placed over the center of the crack on the opposite surface. When crack breakthrough occurred and water was forced through the crack by the 20 psig pressure, the gauze absorbed the water and shorted the low potential voltage between the two sides of the grid. When the grid was shorted, a circuit switch stopped the test. The typical test set-up is shown in Figure 12. Use of this system showed it to be very reliable and accurate. An attempt also was made to detect crack breakthrough on the back
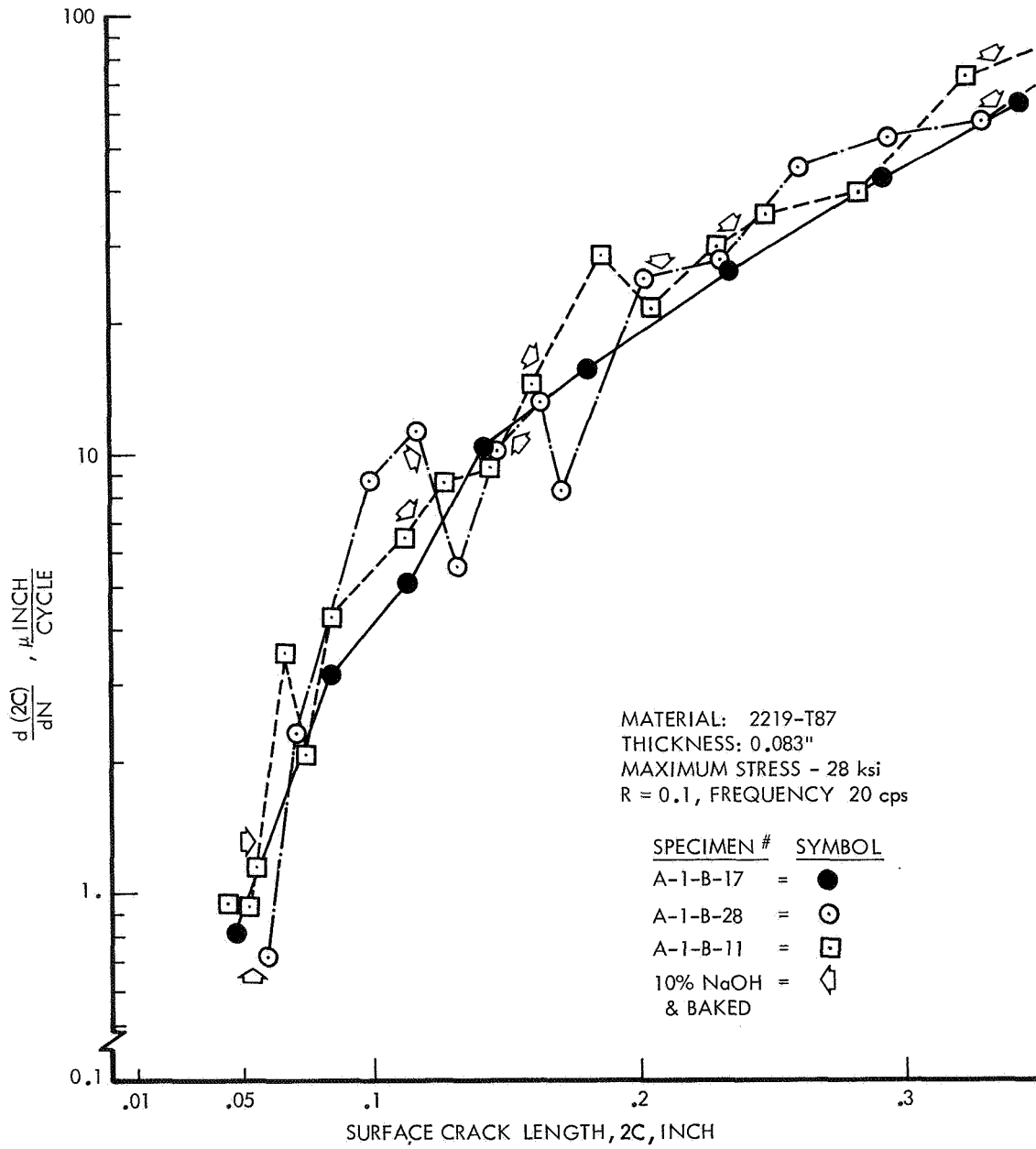
Figure 10. Effect of NaOH Crack Marking Procedure on Crack Growth Rate
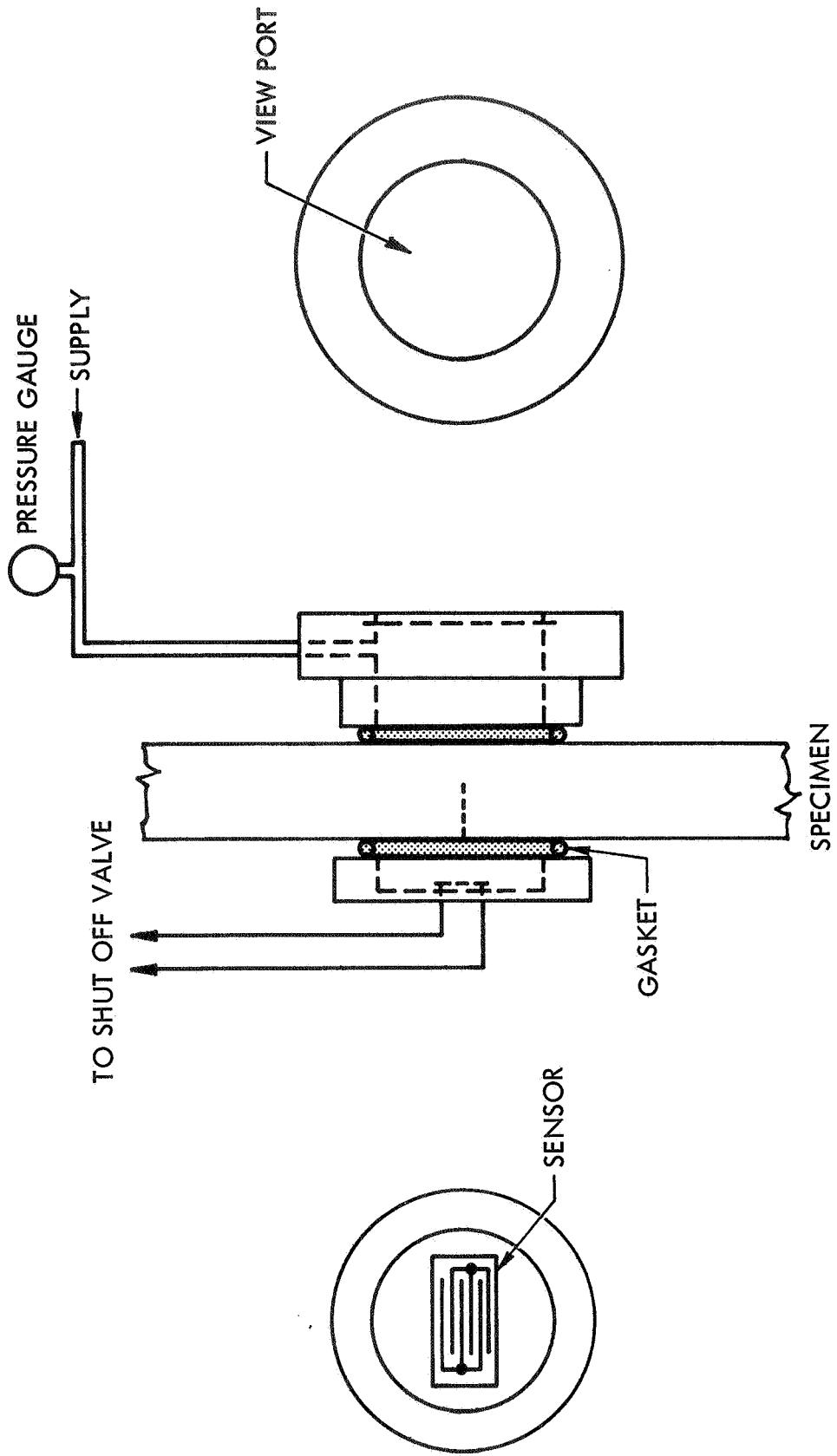
Figure 11. Room Temperature Leak Detection System

37
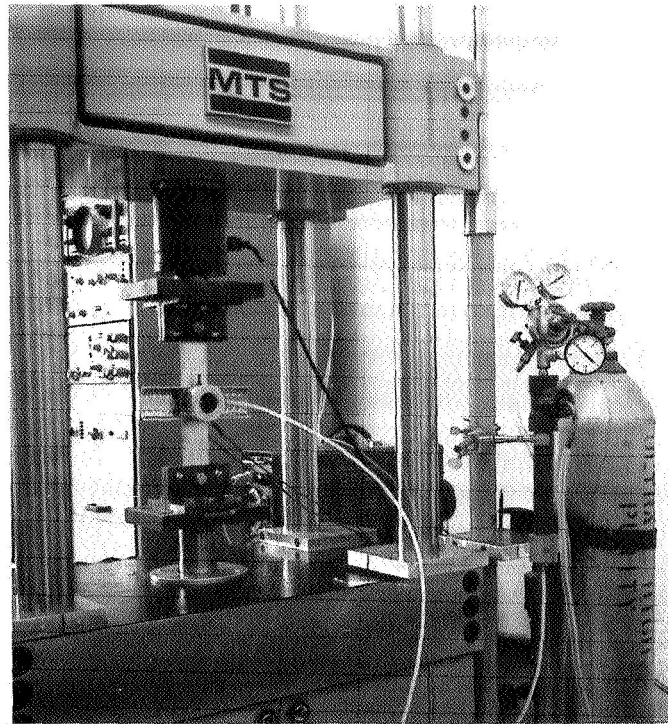
a. Pressure Chamber (20 psig) on Back of Specimen
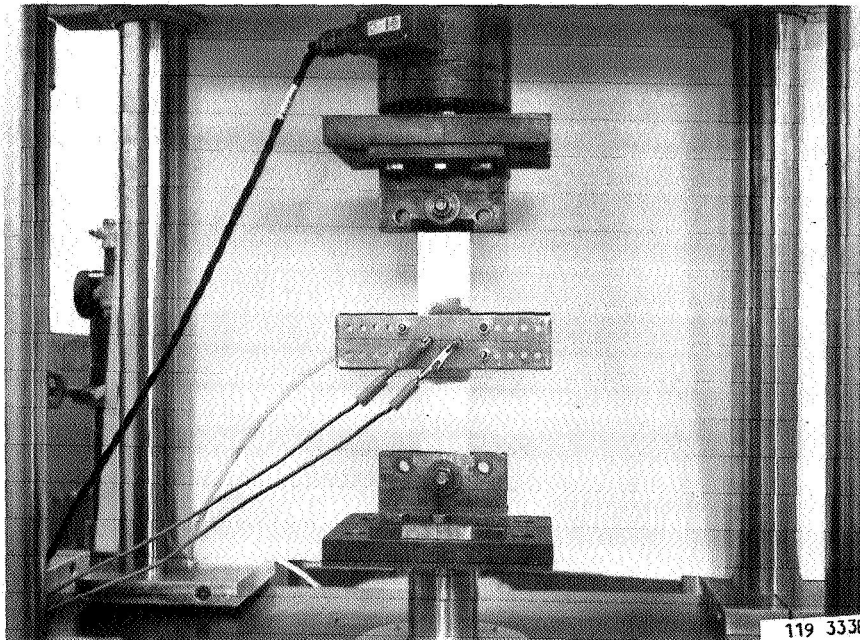


b. Electrical Grid on Front of Specimen

Figure 12. Leak Detection System in Use on Specimen

38

surface optically.  However, the observance of the crack at breakthrough was generally not possible even at 30X under maximum fatigue loads.

Following the occurrence of leak or 20,000 cycles, the specimens were fractured and the initial and final crack lengths measured with a tool-maker's microscope.

### 4.2.3   300°F Test Procedure

All test procedures for the 300°F tests were the same as for the room temperature tests with the exception of the method of leak detection.  For the 300°F tests, the 20 psig chamber was used containing only $N_2$ gas.  The electrical grid was replaced with a low volume pressure sensor attached over the crack.  The equipment was set to shut down if the pressure increased 0.5 psig on the surface flaw side of the specimen.  Test results showed this system to accurately detect leak.

The specimen and leak detector  were enclosed in an insulated box with a hot air blower attached.  Temperature was controlled to $\pm5°$F by use of a thermocouple attached to the specimen and a Foxboro controller.  Each specimen was brought to 300°F and held for five minutes to stabilize the temperature before testing.

### 4.3    Fatigue-Crack Propagation Rate Tests

All fatigue-crack propagation rate tests were conducted in laboratory air in a 100 kip MTS electro-hydraulic test machine at a stress ratio of 0.05.  Each specimen was fatigue cycled at the test temperature a sufficient number of cycles to produce approximately 0.050 inch of crack growth.  The specimens were then statically fractured and the initial and final crack dimensions measured on a toolmaker's microscope.  The average crack propagation rate then was determined.

39

Section 5


PHASE II NDI TEST PROCEDURE


The NDI test program was conducted according to the flow chart shown in
Figure 13. The detailed procedure for each element of the program is
presented in the following sections.


## 5.1    Specimen Preparation

Two types of specimens were used in this phase of the program.  The first
specimens were reference specimens containing cracks of a known size.
These specimens were used to optimize and calibrate the NDI test
procedures.  However due to the large number of variables represented in
the three thicknesses and four specimen configurations (parent, riser, cross
weld, and longitudinal weld) with only one or two unknown specimens per
condition, the number of reference specimens restricted the variety of
known flaw conditions.  The reference specimens selected with NASA/MSC
personnel approval are shown in Table 8.


The cracks in both the reference and unknown specimens were produced by
fatigue cycling to propagate a fatigue crack from various sized EDM slots
(always less than 0.020 inch deep) in specimens that were 0.020 inch
thicker than the required specimen.  The surface of the specimen containing
the EDM/crack then was machined off to remove the EDM flaw, leaving only the
fatigue crack.  The specimens then were cleaned and given a light alkaline
etch to remove any smeared metal due to the machining operation.  The final
specimen configurations for the reference and unknown specimens are shown
in Figures 14 and 15, respectively.


41
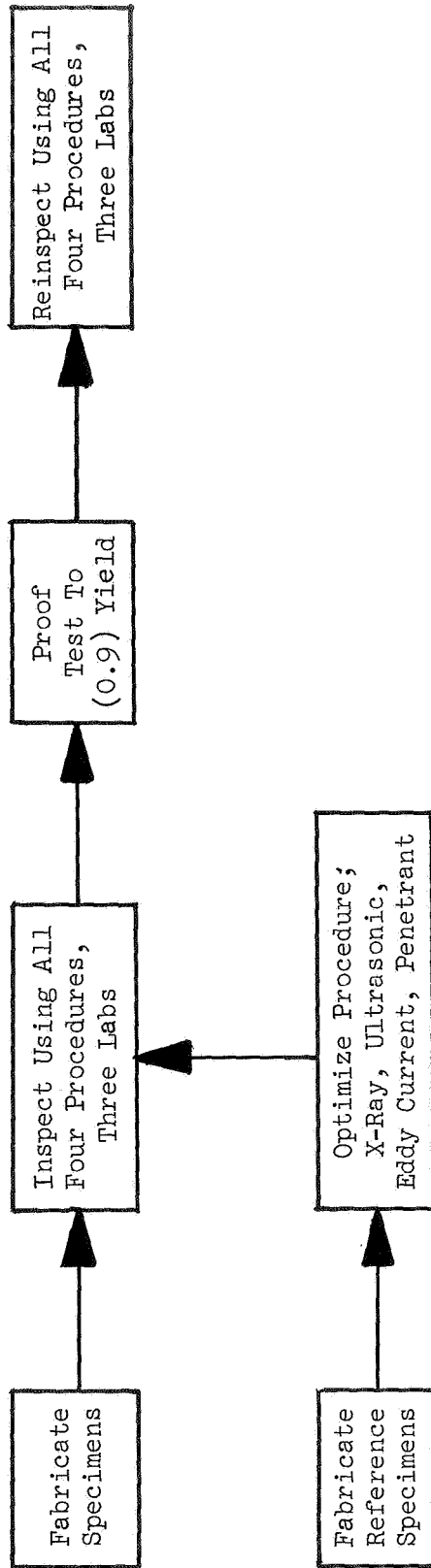
Figure 13. NDI Test Program

TABLE 8.   NDI REFERENCE SPECIMENS

| Specimen | Thickness, B, inch | Condition | Surface RMS | Crack Depth A, inch | Surface Crack Length 2C, inch |
|---|---|---|---|---|---|
| SP 3 | 0.036 | Parent | 50 | a - 0.021<br>b - 0.024 | 0.123<br>0.074 |
| C-1-1 | 0.142 | Parent | 60 | a - 0.047<br>b - 0.052 | 0.124<br>0.249 |
| SW-1 | 0.077 | Cross Weld | 50 | 0.030 | 0.154 |
| SW-1 | 0.076 | Cross Weld | 55 | 0.028 | 0.129 |
| SW-10 | 0.300 | Cross Weld | 60 | 0.030 | 0.157 |
| SW-11 | 0.300 | Cross Weld | - | Failed during precracking | |
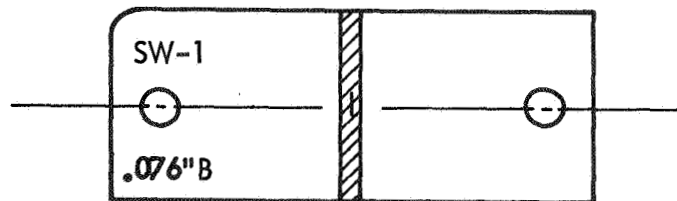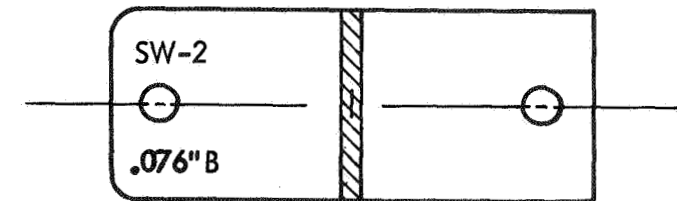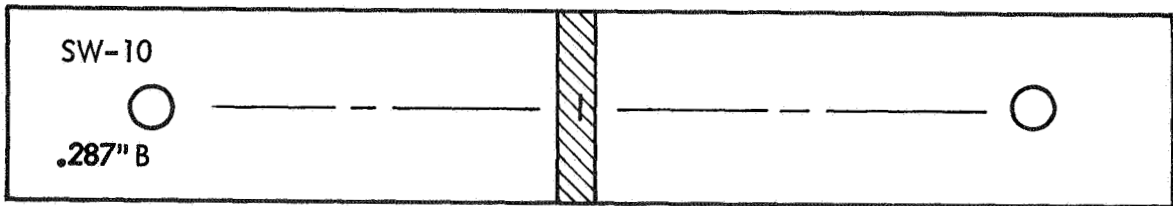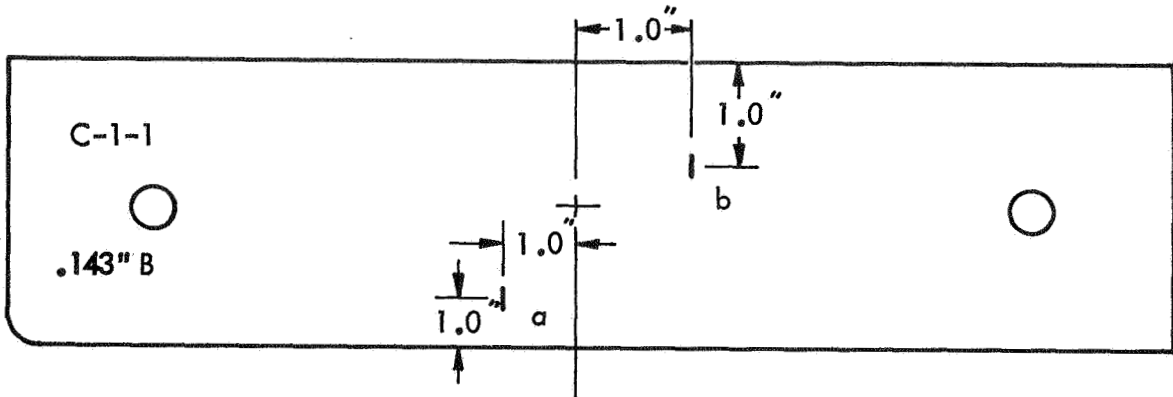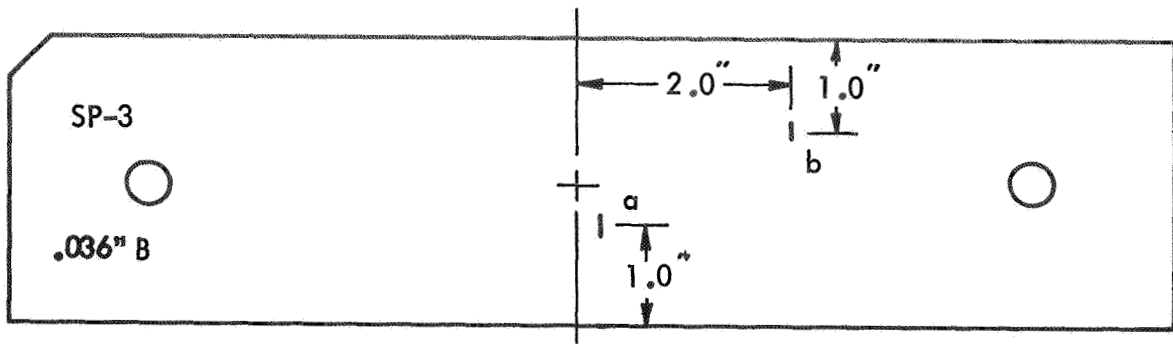
Figure 14.  Fatigue Cracked NDI Reference Specimen Configurations

FATIGUE CRACKS
RANDOMLY
LOCATED WITH
DIFFERENT
LENGTHS AND
DEPTHS (TYP)

BASE METAL
SPECIMEN
(A)

CROSS WELD
SPECIMEN
(B)

6"
(TYP)

18" (TYP)

LONGITUDINAL
WELD SPECIMEN
(C)
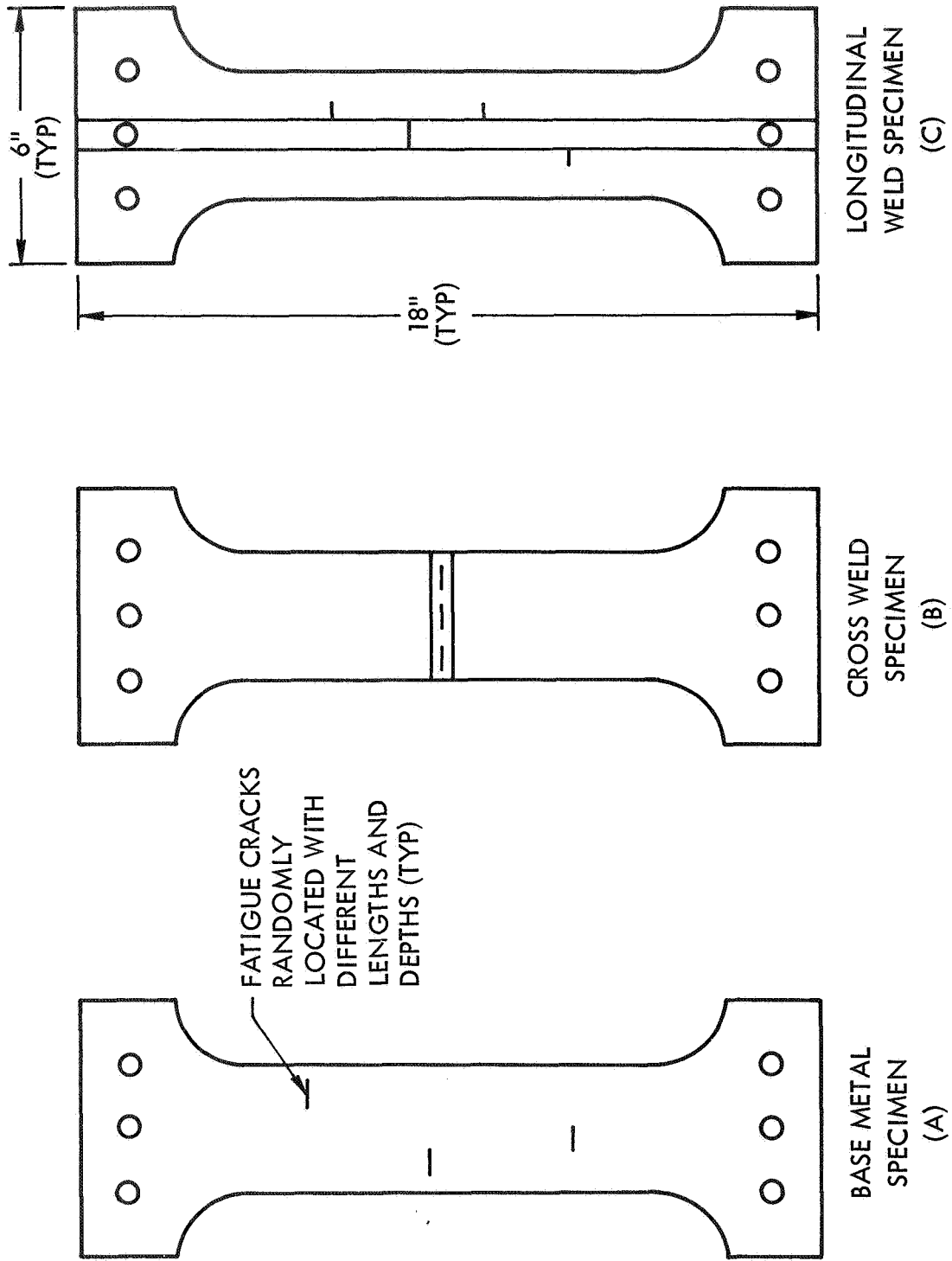
Figure 15. Flaw Detection Specimen Configurations for Base
Metal, Cross Weld, and Longitudinal Weld Panels

.080" OR .150"

.500"

.100"

FATIGUE CRACKS
RANDOMLY SPACED
WITH DIFFERENT
LENGTHS AND DEPTHS

6"

18"

(D)
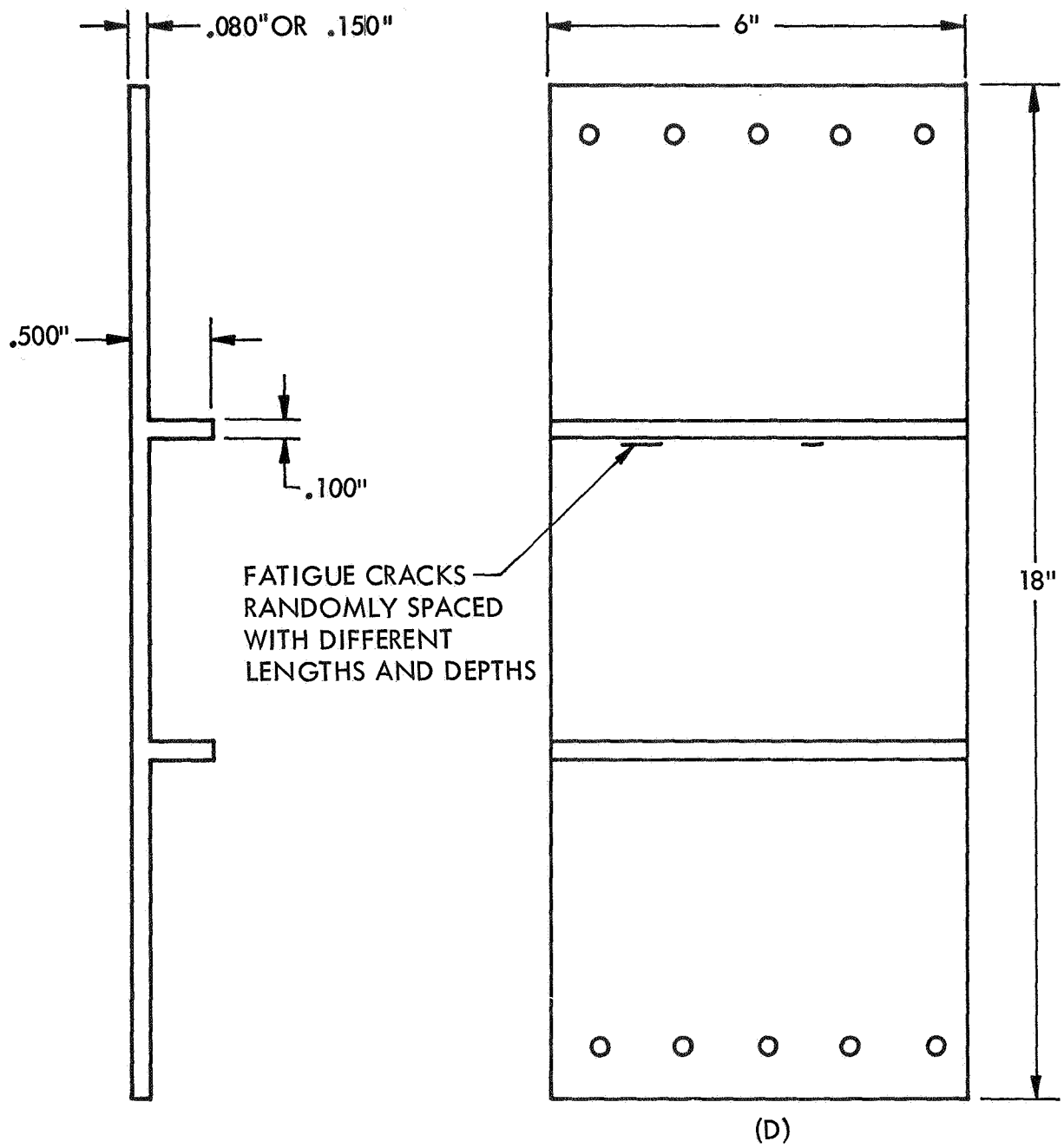
Figure 15 (Cont'd). Flaw Detection Specimen Configuration
for Stiffened Panels

46

## 5.2    Optimization of NDI Inspection Procedures

The four current state-of-the-art NDI procedures included in this program were radiography, penetrant, ultrasonic, and eddy current.  The reference specimens were supplied to each of three inspecting laboratories, Lockheed, Magnaflux, and NASA/MSC, for use in optimizing the calibration and set-up of each of the NDI procedures to be used.  The final procedure selected by each of the three laboratories is listed by method in the following sections.  Only the results of the optimization are presented for Magnaflux and NASA/MSC since detailed written reports were not required.

### 5.2.1  Radiographic Inspection Procedures

#### Lockheed

X-ray techniques were explored wherein a variety of X-ray tubes, film type and processing methods were utilized.  X-ray tubes utilized in this effort were:  50 KV Picker, 100 KV Picker Ranger, 100 KV Picker Hot Shot and a 200 KV Andrex with film focal distances of from 30 to 60 inches at various MA's.  Kodak M, AA, Single Coat R film, as well as Gevaert film types D-4 and D-7, were used.  Hand processing and automatic processing by Kodak X-O-Mat film processor were also evaluated.

This preliminary exploration disclosed that the most favorable radiographic results would be obtained by utilizing the 100 KV Hot Shot tube using Kodak Single Coat R film with automatic film processing.  The following procedure was used:

1.  Specimens were placed with the crack-containing surface adjacent to the film.

2.  The film focal distance (FFD) chosen for optimum resolution was 60 inches.

3.  Film cassettes were utilized with the anticipation of production applications.

47

TABLE 9.  MAGNAFLUX RADIOGRAPHIC SETTINGS

| Plate* | Double Load DuPont NDT 45 Film | | | Kodak M Film | | |
|--------|-----------|-----------|-------------|-----------|-----------|-------------|
| | Kilovolts | Milliamps | Time, Sec. | Kilovolts | Milliamps | Time, Sec. |
| 1 | 60 | 5 | 120 | 55 | 5 | 70 |
| 3 | 95 | 5 | 110 | 70 | 5 | 120 |
| 4 | 95 | 5 | 110 | 70 | 5 | 120 |
| 10 | 85 | 5 | 210 | 70 | 5 | 120 |
| 11 | 85 | 5 | 180 | 70 | 5 | 120 |
| 14 | 80 | 5 | 120 | 55 | 5 | 100 |
| 15 | 80 | 5 | 120 | 55 | 5 | 100 |
| 16 | 85 | 5 | 180 | 70 | 5 | 120 |
| 17 | 85 | 5 | 180 | 70 | 5 | 120 |
| 18 | 85 | 5 | 270 | 65 | 5 | 270 |
| 19 | 85 | 5 | 270 | 65 | 5 | 270 |
| 20 | 85 | 5 | 270 | 65 | 5 | 270 |
| 23 | 80 | 5 | 120 | 55 | 5 | 100 |
| 68 | 85 | 5 | 270 | 65 | 5 | 270 |
| A | 80 | 5 | 90 | 55 | 5 | 90 |
| B | 60 | 5 | 120 | 55 | 5 | 70 |
| C | 80 | 5 | 90 | 55 | 5 | 90 |
| D | 85 | 5 | 270 | 65 | 5 | 270 |
| E | 85 | 5 | 90 | 55 | 5 | 70 |
| F | 85 | 5 | 180 | 70 | 5 | 120 |

*See Appendix I

48

4. Radiographic inspection proved very poor in the detection of the cracks in the submitted reference specimens. The larger crack in the 0.076-inch thick specimen was the only defect detected by the use of X-ray.

## Magnaflux

A Willich Eng. 150 KV tube with a 1.5 M.M. focal spot was used with a 42 inch specimen focal distance (SFD). Two shots were taken per specimen using Double Load Dupont NDT 45 and Kodak Ready Pac M film. The details of the exposures for each specimen is listed in Table 9.

## NASA/MSC

A Norelco PG 140 KUP X-ray machine was used at a tube current of 4 ma and a source to film distance of 34 inches. Hand processed Kodak Ready Pac M film with a density of 2.5-2.7 was used. The voltages and exposure times are given in Table 10.

TABLE 10

NASA/MSC RADIOGRAPHIC PROCEDURE

| Specimen Thickness, Inch | Kilovoltage | Exposure Time, Sec. |
|---|---|---|
| 0.040 | 65 | 180 |
| 0.080 | 70 | 180 |
| 0.150 | 70 | 240 |
| 0.300 | 80 | 300 |

One exposure was taken on cross weld specimens with beam alignment on transverse centerline, while two exposures were taken of all other specimens with beam alignment two inches from the specimen's transverse centerline.

## 5.2.2 Penetrant Inspection Procedure

### Lockheed

A high sensitivity water wash fluorescent penetrant (Uresco P-133) with dry powder which meets MIL-I-25135 Group VI sensitivity level was used with the following procedure:

1. Specimens were preheated to 150°F by being placed in the dryer for twenty minutes, then dipped in the penetrant tank assuring complete immersion. The penetrant dwell time was ten minutes.

2. At the end of the dwell time, the specimens were water washed to remove surface penetrant using a Tricon Nozzle on the water line. The specimens were dried in the dryer at 150°F, then developed for five minutes.

3. Inspection was accomplished in a conventional black light illuminated booth.

4. All of the reference crack defects were detected and their respective lengths noted.

5. Since crack location and size correlated favorably with the data supplied, no further penetrant work was done.

### Magnaflux

Pre-Penetrant Cleaning - Standard vapor degrease with trichlorethylene

Penetrant Application - Dipped in ZL2A penetrant, 30 minutes dwell time

Emulsification - Dipped in ZE4A for 1 minute

Development - Dryed, applied ZP4A dry powder developer for 15 minutes

### NASA/MSC

Pre-Penetrant Cleaning - 15 minutes hot vapor degrease with trichlorethylene; 5 minutes immersion in acetone

Penetrant Application - Uresco P-301 high sensitivity visible red dye brush applied; penetration time 30 minutes

Emulsification - Two minutes immersion in E-142 spray scrubber diluted two parts water to one part spray scrubber

Wash and Dry Cycle - Water spray rinse approximately 10-15 seconds; warm air dry minimum 15 minutes

Development - Apply Unesco D-499C spray developer; minimum of 30 minutes development before interpretation

Post Penetrant Cleaning - Water rinse; dry; 30 minutes immersion in acetone

## 5.2.3 Ultrasonic Inspection Procedure

Lockheed

Optimization of techniques for the detection of the defects in the specimens included an evaluation of the following operational variables:

1. Choice of test mode, i.e., contact: surface/shear wave; immersed: shear and various delta array

2. Transducer frequency and size (range utilized 2.25 MHZ through 15 MHZ, both flat and focused)

3. Use of collimator and collimator size (immersed)

4. Optimum incident angle (applicable to some but not all of the above-listed test modes)

5. Specimen configuration (i.e., surface condition, thickness, homogeneity), while not a manipulatable test variable, has a very decided effect on the ability to detect a flaw of specific size and orientation

While the evaluation included a limited amount of contact ultrasonics, this method was discarded in favor of the immersed method due to the inability to automatically record the ultrasonic results obtained by the contact method. An automated system was used to give a permanent two-dimensional C-scan record.

51

Due to inherent differences between the parent material specimens and the welded specimens, efforts were made to optimize techniques for each of these two specimen types. The results are reported on the basis of this categorization.

## Parent Material Specimens

1.  The use of a 15 MHZ, 0.375 inch diameter lithium sulfate transducer with a 1/8-inch collimator in the shear wave mode at a 27 degree incident angle provided the optimum crack detection capability for the 0.036 inch thick specimen.

2.  The same transducer using a 1/4-inch collimator at a 25 degree incident angle proved optimum for use on the 0.143 inch thick specimen.

3.  While both above-listed inspections could be accomplished without the use of collimators, their use enhanced the resolution of the defects due to elimination of signals received from the entry surface. Although there was some difficulty due to surface finish variation from specimen to specimen and between the top and bottom surfaces (chem milled and machined) of each specimen, the optimized technique provided crack detection from either surface.

4.  The basic delta technique, using various transducer combinations, was able to detect the larger crack in the 0.036 inch thick specimen and both cracks in the 0.143 inch thick specimen. Since the smaller crack in the 0.036 inch thick specimen could not be detected by the delta technique, it was abandoned in favor of the shear wave technique described above.

## Weld Specimens

1.  As in the inspection of the parent material, the shear wave and the basic delta transducer array were explored. In addition, a "shuttle delta" method wherein the receiver is held fixed was tried.

2. The basic delta technique provided limited results on the thick
   specimens but adequate defect detection in the thin welded specimens.

3. The shear wave technique proved adequate in the detection of the cracks
   using 15.0 MHZ transducers.

4. The shuttle delta technique appeared best for the detection of defects
   over the complete range of thicknesses.  Consequently, this technique
   with a 5 MHZ/5 MHZ transducer pair was chosen as the optimum technique
   for this inspection.  All of the reference defects were detected
   utilizing this technique.

Magnaflux

A contact hand scan procedure was employed using a Magnaflux PS 901
ultrasonic unit.  A 1/4-inch Magnaflux 45 degree transducer was used
at 5.0 MHZ with glycerine as the contact media.

NASA/MSC

Note two ultrasonic procedures (surface and shear wave) were used since
no eddy current inspection was conducted.

Equipment
        Branson Model 50C Sonoray Flaw Detector
        Branson, straight, immersed, 10 MHZ, Pb metaniobate, 1/4-inch transducer

Technique
        Water immersion
        Surface wave angle 32 degrees
        Shear wave angle 20 degrees

Procedure

Gain settings optimized on calibration specimens; for surface wave a single
gain setting was sufficient for all specimens; for shear wave gain settings
varied depending on specimen type and thickness.

Scanning was semi-automatic in that the transducer scanning bridge was
mounted on wheeled tracks which provided movement in the x and y directions.

Bridge manipulation was done by hand. The scan was indexed every 1/4-inch in the x direction. Flaw locations were determined by recording specimen end and edge locations on the x and y axes, optimizing flaw signal and recording x and y axis readings.

## 5.2.4 Eddy Current Procedures

### Lockheed

Exploratory tests indicated that it would be desirable to automate the performance of the eddy current testing both to enhance precision and in order to generate an objective record of inspection results. Two eddy current instruments were utilized in these tests, the Magnaflux ED 520 and the Nortec NDT-3. The laboratory ultrasonic tank C-scan bridge was used to provide the mechanics for automatic scanning capability. Two types of recordings were generated. A plot plan two-dimensional view of the specimen surface depicting the location of the cracks was obtained through the use of the standard ultrasonic C-scan recording system after a specially developed electronic circuit was added to the system. A dual channel Sanborn strip chart recorder was used to record the amplified eddy current signal generated by the presence of the flaw. Special electrical leads were provided to both the ED 520 and NDT-3 to permit the transmission of the output from the respective instrument to both recording systems.

The following results were noted:

1. The NDT-3 instrument, using a variety of modules and probes to provide different operating frequencies, was used only in exploration. The 100 KHZ module (F-100) and probe (Sp-100) provided the best results. At this frequency, variations due to surface roughness, slight probe tilt caused by probe drag, and conductivity changes due to the weld zone, were minimized.

2. The ED 520 instrument and supplied probes proved adequate in the detection of the defects in all of the specimens. The lack of spring loading capability made setting up very critical with regard to leveling the specimens to the bridge.

54

3. All of the cracks in the welded and the parent material specimens were
   defined using the strip chart recorder. Scan rates varying between 35
   and 50 feet/minute were used with no adverse effect on flaw resolution.
   Index steps of 0.020 inch to 0.050 inch were used in conjunction with
   the different scan rates. The optimum condition for scanning/recording
   was found to be 43 feet/minute with an index step of 0.020 inch. The
   limiting factor in scan rate is the inability of the electro/mechanical
   recorder to keep up with the eddy current instrument when using high
   probe scan speeds.

Magnaflux

A Magnaflux ED 510 instrument was used with a hand scan procedure employing
a B-nut probe with a 1/4-inch diameter spring loaded Boeing probe operated
at 80 KHZ.

5.3    Inspection Procedure

The sequence of NDI testing that would result in minimal interference with
defect detection by the successive NDI tests was selected. Thus, eddy
current testing with a potential effect of masking of the defect by possible
smearing of the metallic surface from repetitive probe contact was placed
last in the sequence. Penetrant testing, which requires a dry, clean surface
for proper defect detection, was accomplished first. Radiography was
accomplished after penetrant inspection, and the ultrasonic inspection
was accomplished after the radiography.

Each laboratory was instructed to conduct each inspection method independent
of the preceding methods, using different personnel for each procedure when
possible. Following fabrication, all unknown specimens and reference
specimens were inspected at Lockheed, then sent to Magnaflux for inspection,
and then sent to NASA/MSC for inspection. The specimens then were returned
to Lockheed, and the unknown specimens loaded statically to 90 percent of the
respective material yield strength in a 50,000 lb Baldwin universal test
machine. The proof tested unknown specimens and the reference specimens

then were reinspected at Lockheed, Magnaflux, and NASA/MSC. The unknown specimens then were fractured by NASA/MSC and the actual crack sizes and locations recorded. For each inspection a listing of estimated crack size and crack location was supplied to Lockheed for each method and inspection. These data formed the basis for the NDI analysis, reported in Section 7.

PHASE I RESULTS

## 6.1 Analytical Expressions

Two basic analytical expressions were evaluated to determine the accuracy with which fatigue-crack propagation expressions could be used to predict the cycles required to produce crack breakthrough. One expression examined was that of Forman[11]

$$dA/dN = \frac{C_1 (\Delta K)^n}{(1 - R) K_c - \Delta K} \tag{12}$$

and the other that proposed by Hall[12]

$$\frac{d(A'Q)}{dN} = C_2 \left(\frac{S_o}{S}\right)^2 (\Delta K)^{n_2} \left(1 - \frac{K_{max}}{K_{Ic}}\right)^P (1 + \lambda)^m \tag{13}$$

where $C_1$, $C_2$, $n_1$, $n_2$, m, P = experimental constants

$\Delta K$ = alternating stress intensity, $(K_{max} - K_{min})$

$K_c$ = critical fracture toughness

$K_{Ic}$ = critical plane strain fracture toughness

R = stress ratio, $S_{min}/S_{max}$

A = crack depth

Q = Irwin's plasticity corrected shape parameter

$S_o$ = arbitrary stress for determination of $C_2$

$\lambda$ = $K_{min}/\Delta K$

When viewed in mathematical terms, Forman's equation is basically a two parameter experimental fit of the crack propagation data with a stress ratio correction added to satisfy the condition that

$$\lim_{\Delta K \to (1 - R) K_c} \left[\frac{dA}{dN}\right] = \infty \tag{14}$$

57

Hall's expression is more complicated in that the degree of anticipated fit is improved by using four experimentally determined constants (plus one arbitrary stress) rather than the two parameter fit used by Forman. While this may increase the accuracy somewhat (assuming the general form is valid), it does require more experimental data to allow a reasonably accurate determination of the various experimental constants. In addition, the equation in its original form yields the crack propagation rate of the normalized crack depth, $A/Q$, rather than the physical crack depth, thus accounting for the change in shape as well as crack depth. For the purpose of this study, the assumption used at NASA/MSC was made that, for the range of crack size studied, the parameter Q could be treated as a constant based on the initial crack shape. The equation then was rewritten as

$$dA/dN = QC_2 \left(\frac{S_o}{S}\right)^2 (\Delta K)^{n_2} (1 - K_{max}/K_{Ic})^{-P} (1 + \lambda)^m \quad (15)$$

where $Q = Q_{initial} = $ constant.

A review of existing $dA/dN$ data showed sufficient data existed for the parent 2219-T87 material at room temperature and some limited data existed at elevated temperature near 300°F[21,22]. Some cross weld data at room temperature also was found, but no weld data was found at 300°F. As a result, a few of the cycles-to-leak tests were converted to·dA/dN tests, the results of which are shown in Table 11 along with recent 70°F weld results obtained at NASA/MSC[23].

Using the weld data presented in Table 11 and the parent data presented in Reference 21, the experimental constants shown in Table 12 were obtained. Several important points concerning the relation of these experimental constants warrant further comment.

First, the range of data and number of data points available are not sufficient to develop a high degree of precision on the experimental constants. This is especially true for the weld data where the range

TABLE 11

FATIGUE CRACK PROPAGATION DATA FOR 2219-T87 CROSS WELD SPECIMENS

| Specimen Number | Thickness inch | Maximum Stress, S, ksi | Initial Surface Crack Length, $2C_i$, inch | Initial Crack Depth, $A_i$, inch | Final Surface Crack Length, $2C_f$, inch | Final Crack Depth, $A_f$, inch | Cycles N | $\Delta A/\Delta N$ inch/cycle | Data Source |
|---|---|---|---|---|---|---|---|---|---|
| 300°F Results | | | | | | | | | |
| 1 | .3 | 20.0 | .232 | .114 | .324 | .159 | 7,400 | $1.28 \cdot 10^{-5}$ | Lockheed R = 0.05 |
| 2 | .3 | 17.5 | .263 | .140 | .515 | .211 | 10,000 | $2.5 \cdot 10^{-5}$ | |
| 3 | .3 | 17.5 | .407 | .159 | .503 | .206 | 3,000 | $3.3 \cdot 10^{-5}$ | |
| 4 | .135 | 17.5 | .166 | .067 | .199 | .137 | 4,000 | $0.18 \cdot 10^{-5}$ | |
| 5 | .150 | 15.0 | .195 | .081 | .232 | .093 | 10,000 | $0.37 \cdot 10^{-5}$ | |
| 6 | .150 | 17.5 | .253 | .092 | .291 | .103 | 2,000 | $1.90 \cdot 10^{-5}$ | |
| Room Temperature Results | | | | | | | | | |
| 31W | .241 | 13.78 | .593 | .131 | .711 | .200 | 5,000 | $13.8 \cdot 10^{-6}$ | NASA/MSC R = 0.01 |
| 33W | .240 | 13.79 | .580 | .120 | .630 | .157 | 2,500 | $14.8 \cdot 10^{-6}$ | |
| 34W | .252 | 19.73 | .597 | .129 | .712 | .190 | 500 | $122 \cdot 10^{-6}$ | |
| 35W | .244 | 20.37 | .603 | .129 | .636 | .156 | 200 | $135 \cdot 10^{-6}$ | |
| 36W | .244 | 6.82 | .595 | .137 | .657 | .196 | 40,000 | $1.47 \cdot 10^{-6}$ | |
| 37W | .240 | 6.94 | .600 | .152 | .662 | .187 | 20,000 | $1.75 \cdot 10^{-6}$ | |
| 40W | .243 | 16.33 | .640 | .140 | .724 | .202 | 2,000 | $31 \cdot 10^{-6}$ | |

TABLE 12. EXPERIMENTAL CONSTANTS DETERMINED FOR 2219-T87
FORMAN'S AND HALL'S EQUATIONS

| PARAMETER | PARENT MATERIAL | | WELD MATERIAL | |
| --- | --- | --- | --- | --- |
| | 75°F | 300°F | 75°F | 300°F |
| Forman Equation | | | | |
| $C'$ | $1.4 \cdot 10^{-11}$ | $1.4 \cdot 10^{-11}$ | $3.1 \cdot 10^{-15}$ | $5.44 \cdot 10^{-22}$ |
| $n$ | 2.5 | 2.5 | 3.5 | 5.23 |
| $K_c$, psi $\sqrt{in.}$ | 40,000 | 40,000 | 30,000 | 30,000 |
| $S_y$, psi | 55,000 | 45,000 | 25,000 | 21,000 |
| Hall Equation | | | | |
| $C'$ | $3.6 \cdot 10^{-16}$ | $3.60 \cdot 10^{-16}$ | $9.7 \cdot 10^{-21}$ | $1.77 \cdot 10^{-27}$ |
| $n$ | 2.5 | 2.5 | 3.74 | 5.42 |
| $P$ | 1 | 1 | 1 | 1 |
| $\Delta S_o$, psi | 19,700 | 19,700 | 13,785 | 17,500 |
| $K_{Ic}$, psi $\sqrt{in.}$ | 40,000 | 40,000 | 30,000 | 30,000 |

of $\Delta K$ was limited, particularly for the 300°F tests where $6.6 \leq \Delta K \leq 10.9$ ksi $\sqrt{\text{in.}}$ due to the low maximum stress defined by 0.8 yield strength. As a result the experimental constants used are considered tentative pending the development of additional dA/dN data.

Second, available data on $K_{Ic}$ and $K_c$ is very limited[22]. The values shown in Table 12 are best estimates based on the data available to NASA/MSC at the time of this report. However, some variation in $K_{Ic}$ can be tolerated since it enters into the equations only as a difference with a parameter $(\Delta K)$ which is typically of the same order of magnitude. As a result, a variation in $K_{Ic}$ would produce only a small scalar shift on predicted dA/dN values.

Finally, for the case of R = 0 (for nearly all available data), there is little difference in the functional form between Forman's and Hall's equation as shown below:

$$dA/dN = C_1 Q \left( \frac{\Delta S_o}{\Delta S} \right)^2 (\Delta K)^n (1 - K_{max}/K_{Ic})^{-1} \qquad (16)$$

Similarly Forman's equation can be rewritten by using the relationship that, for R = 0,

$$(1 - R)K_{Ic} - \Delta K = K_{Ic} \left( 1 - \frac{K_{max}}{K_{Ic}} \right) \qquad (17)$$

but $K_{Ic}$ = constant so

$$dA/dN = \frac{C'\Delta K^n}{\left( 1 - \frac{K_{max}}{K_{Ic}} \right)} \qquad (18)$$

where $C' = C_2/K_{Ic}$.

A comparison of these two equations shows both to be of the form

$$dA/dN = \frac{C'(\Delta K)^n}{(1 - K_{max}/K_{Ic})} \qquad (19)$$

The only functional difference is in the scalar multiplier which is a constant for Forman's equation but is a variable in Hall's. As a result Hall's equation predicts an increase in dA/dN for increasing Q (i.e., increasing A/2C) for a constant $\Delta K$ and a decrease in dA/dN with an increase in $\Delta S$. Neither trend is predicted by Forman's equation. Unfortunately, no consistent body of data is available for 2219-T87 to statistically prove or disprove these trends. If, however, the available data is carefully examined, indications of such trends should become apparent.

The maximum practical variation in the predicted dA/dN values due to the shape parameter, Q, is expected to be approximately 2, the variation in Q as the A/2C ratio is varied from 0.2 to 0.5. The influence on the predicted dA/dN for this variation in Q is shown in Figure 16a for the 300°F results for welded material. As can be seen, the variation due to Q is small enough that normal scatter in the data masks the accuracy of the predicted trend.

The influence of the stress level, $\Delta S$, however, is more apparent since the term $\Delta S_o/\Delta S$ is squared. Figure 16 shows the predicted variation in dA/dN with $\Delta S$. While it would appear that the data may show a slight shift to higher dA/dN values as $\Delta S$ decreases for a constant $\Delta K$, the true shift in the data is very minor if it statistically can be shown to exist at all. Figure 16c shows the relatively large shift in dA/dN with $(1/\Delta S)^2$ that is predicted by Hall's equation to be unwarranted for these thicknesses of parent 2219-T87.

The fit of Forman's equation to the existing data is shown in Figure 17. The results show Forman's equation to fit all of the data quite well, the room temperature and 300°F parent material data falling on an approximately common curve. The functional similarity between Hall's and Forman's equation is again shown in Figure 18, the Forman equation providing a good
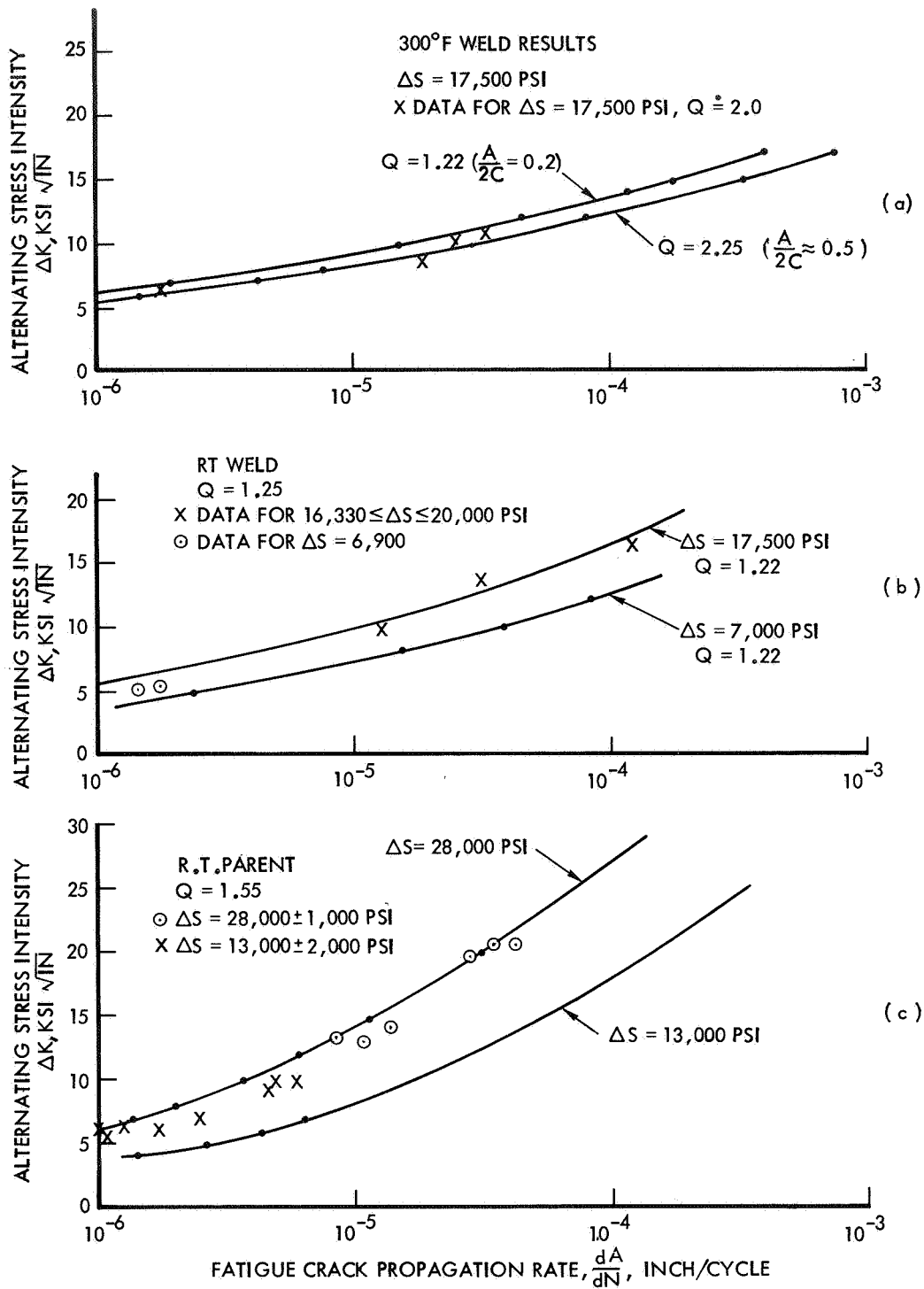
Figure 16. Comparison of the Predicted Fatigue Crack Propagation Rates Using Hall's Equation with Room Temperature and 300°F 2219-T87 Data (R = 0.05)
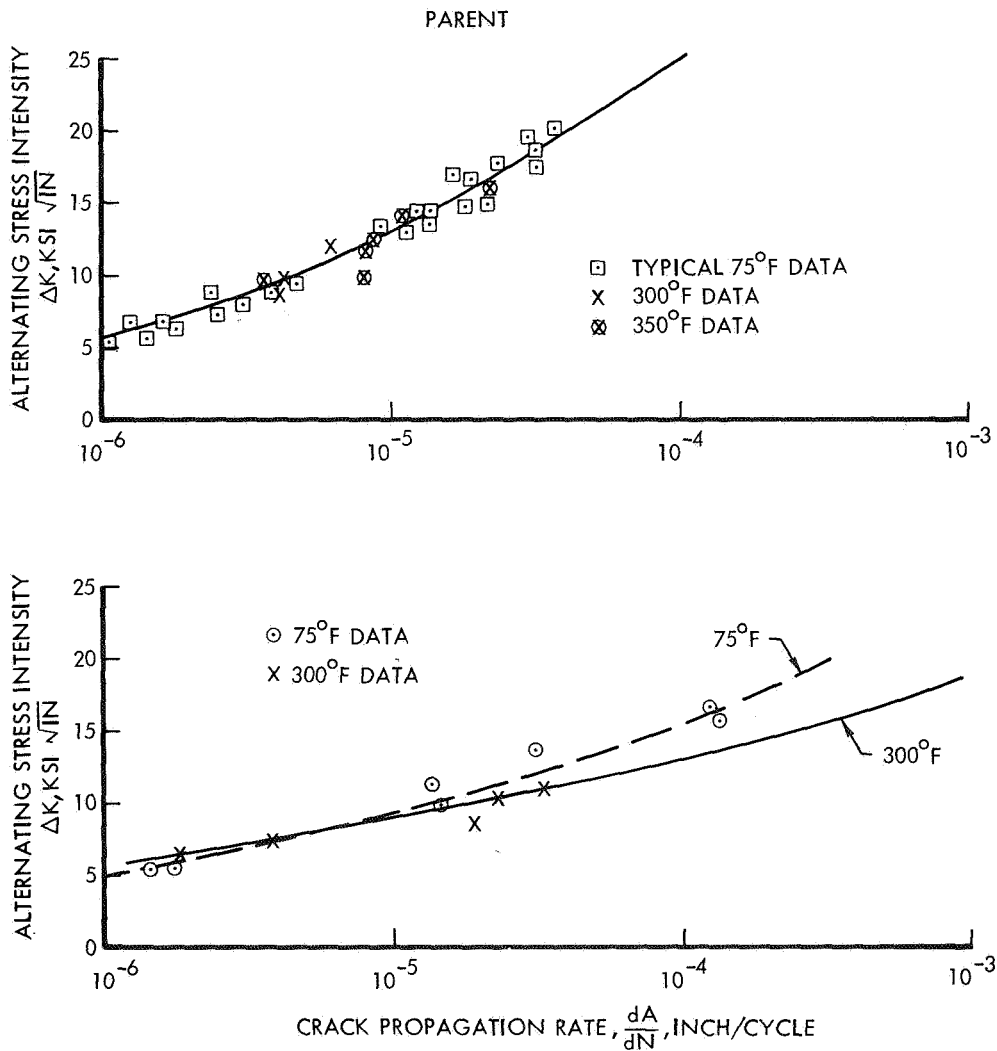
Figure 17. Comparison of the Predicted Fatigue Crack Propagation Rates Using Forman's Equation with Room Temperature and 300°F 2219-T87 Data (R = 0.05)
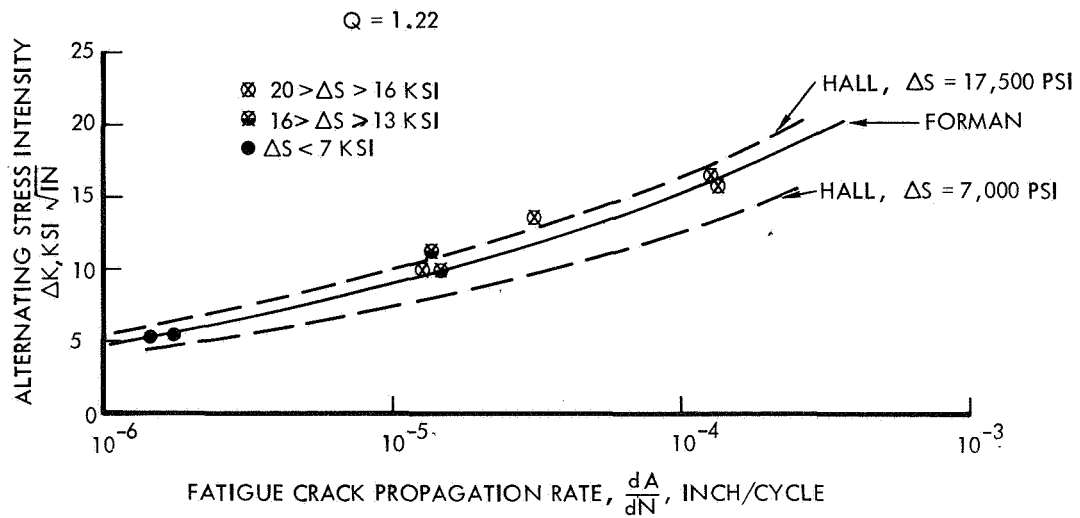
Figure 18. Comparison of the Predicted Fatigue Crack Propagation Rates
Using Hall's and Forman's Equation for Room Temperature
2219-T87 Weld Material (R = 0.05)

65

correlation with the data developed at different stress levels. This similarity in form between the two equations is again shown by the nearly equal values of the exponent in the $\Delta K$ term which were obtained for the two equations. The values are in quite good agreement considering the limited data available for their determination.

In view of the apparent invalidity for 2219-T87 of the $(1/\Delta S)^2$ term is Hall's equation and the excellent agreement of Forman's equation with the data, the main emphasis was shifted to the use of Forman's equation. Since no data was available at stress ratios other than $0.1 > R$, the room temperature cycle-to-leak data for parent material at $R = 0.5$ was screened and specimens that did not leak during the test were identified. These results, nearly all of them being in the 0.041 inch thickness, then were used to compute average $dA/dN$ data at $R = 0.5$. The results, along with the results predicted by Forman's equation, are shown in Figure 19. The predicted values are in relatively good agreement with the data, the predicted rates tending to be slightly higher than the measured rates.

## 6.2    Room Temperature Cycles-to-Leak Results

In view of the lack of correlation of the data in the previous section with the $1/(\Delta S)^2$ term in Hall's equation, the parent material cycles-to-leak data ($R = 0.05$) were first compared with Hall's equation to determine if it fit the trends in the data. The typical results, shown for the 0.08 parent material in Figure 20, show that the Hall equation does not follow the trend in the data. As noted for the $dA/dN$ data, the $1/\Delta S^2$ term results in an over estimate of fatigue life at high stress, $\Delta S = 45,000$ psi, and an under estimate of the life at low stress, $\Delta S = 28,000$ psi. In addition, the presence of the $Q$ term does not predict the consistent layering of the data with $Q$, lower $A/2C$ values (lower $Q$) having shorter lives than the same depth flaw with a high $A/2C$ (higher $Q$). It should be pointed out, however, that the form of the Hall equation being considered by NASA (i.e., $Q$ = constant and the equation integrated as a one-dimensional expression) is not strictly consistent with its original form where $d(A/Q)/dN$ is the calculated parameter.
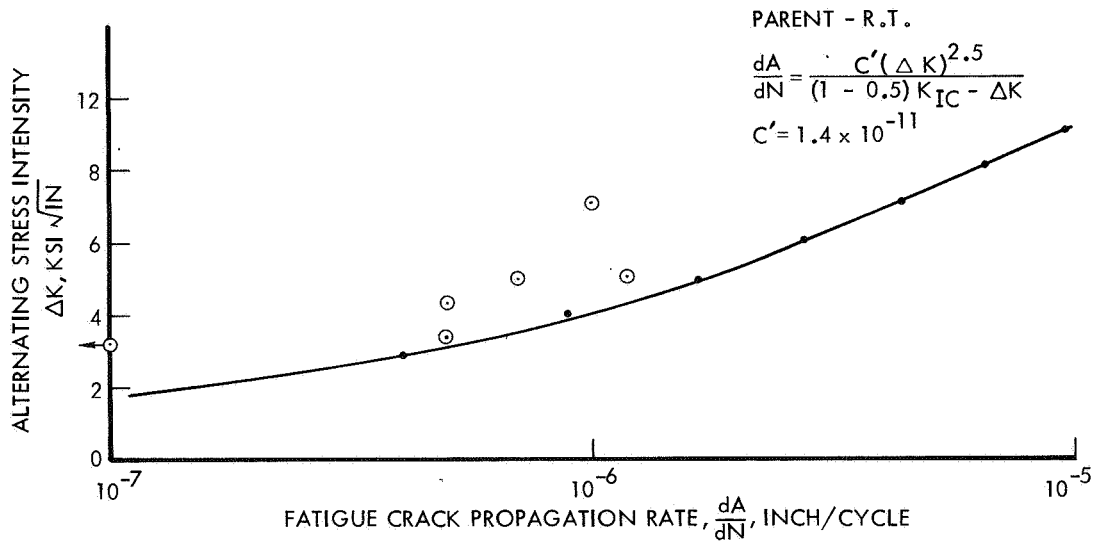
Figure 19. Comparison of the Predicted Fatigue Crack Propagation Rates
Using Forman's Equation with Room Temperature Parent Material
Results, R = 0.5
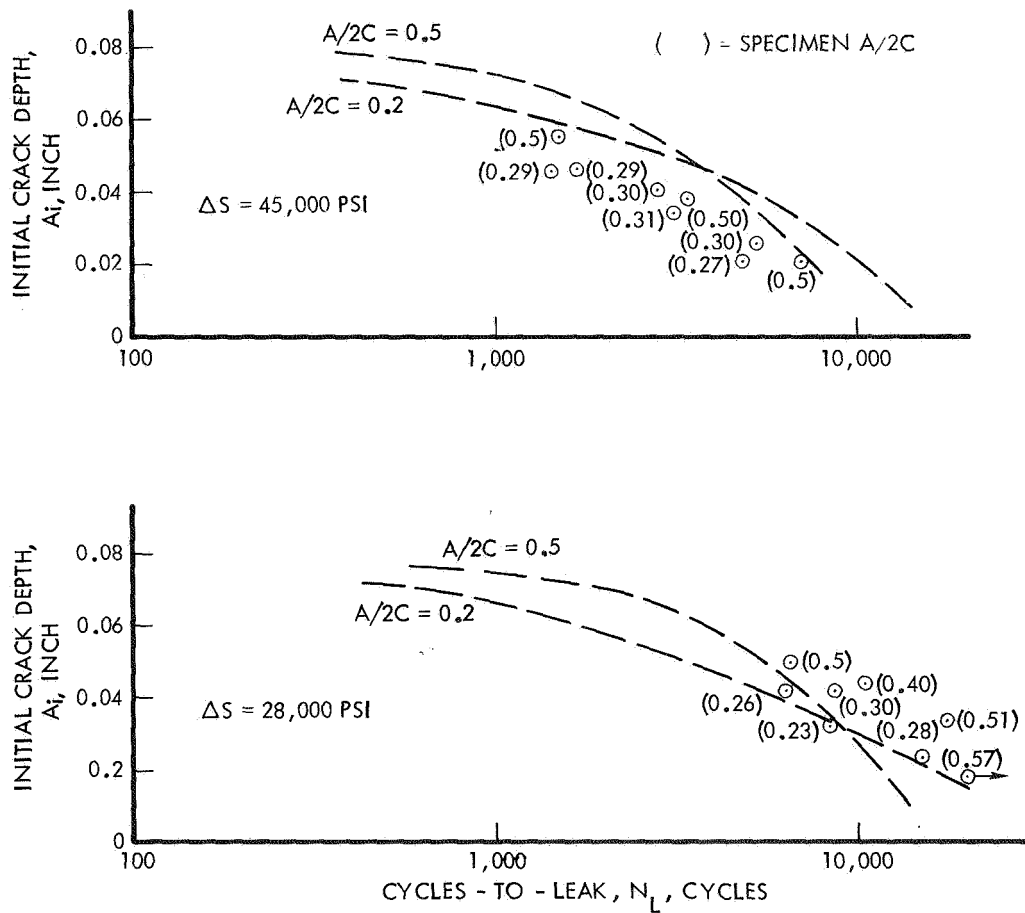
Figure 20. Comparison of Cycles-to-Leak Results for 0.080 inch Parent Material with the Life Predicted by Hall's Equation

However, for the form of the Hall equation used in this program, it does not satisfactorily predict the cycles-to-leak behavior of 2219-T87.

Figures 21 to 23 present the parent material data (R = 0.05) along with the predicted results using the Forman equation. As shown, the predicted values using the Forman equation do follow the trends in the data for various thicknesses, initial A/2C value, and alternating stress level. While the predicted values do follow observed trends in the data, the predicted results were usually conservative, i.e., the predicted life being equal to or somewhat shorter than that observed from the data. The confidence in obtaining experimentally a life equal to or greater than that predicted by the Forman equation would appear to be good.

The cycles-to-leak data for the cross weld specimens tested at room temperature and R = 0.05 is presented in Figures 24 to 26 along with the results predicted by Forman's equation. As for the parent material, the predicted results fit the data trends reasonably well, generally being conservative and forming a lower bound life for the data at a given A/2C value.

Cycles-to-leak results for the longitudinal weld specimens are presented in Figures 27 to 29 along with the results predicted by the Forman equation using the cross weld constants. Data from specimens with the flaw at the center line of the weld are shown as open symbols while data from specimens with the flaw at the edge of the weld are shown as filled symbols. A comparison of the two flaw locations in the weld show the results to be comparable. When compared with the cross weld results, the longitudinal welds exhibit consistently longer lives for the same conditions. This is reflected in the poorer fit of the results predicted by the Forman equation, the predicted values being quite conservative (approximately a factor of 2 to 4). The increased life is believed to be due to the reinforcing effect of the adjacent parent material. If the parent material predicted curves are compared with the data, as shown by the dotted lines in Figures 27 to 29, the results agree fairly well as shown. However, the
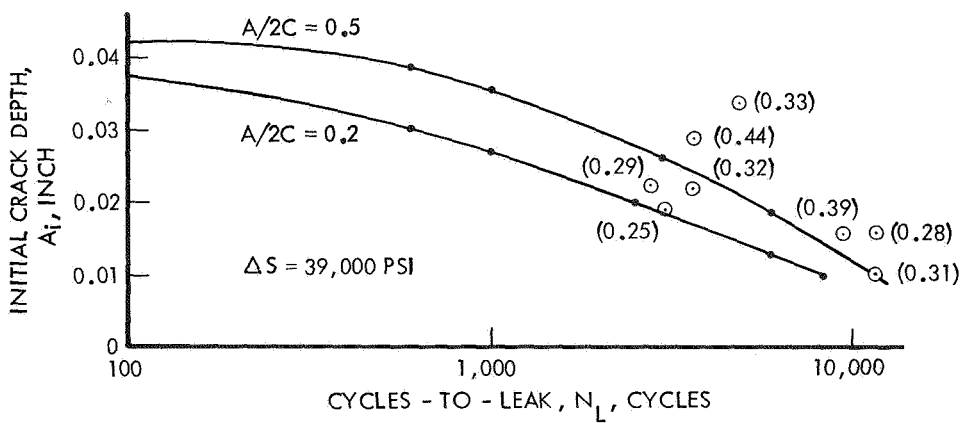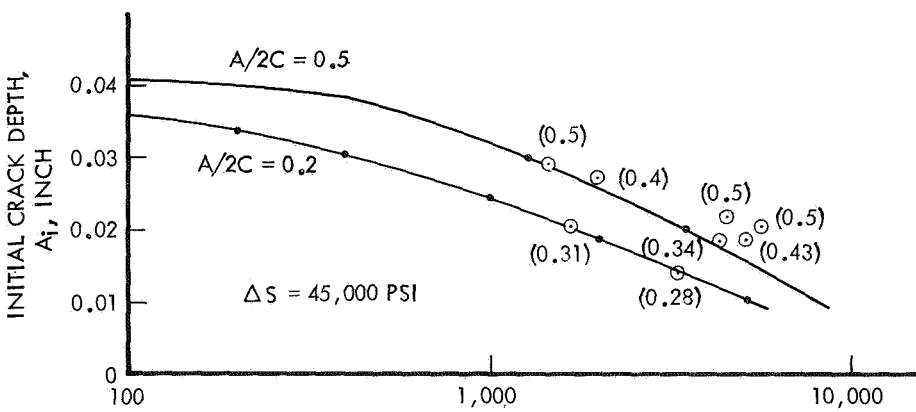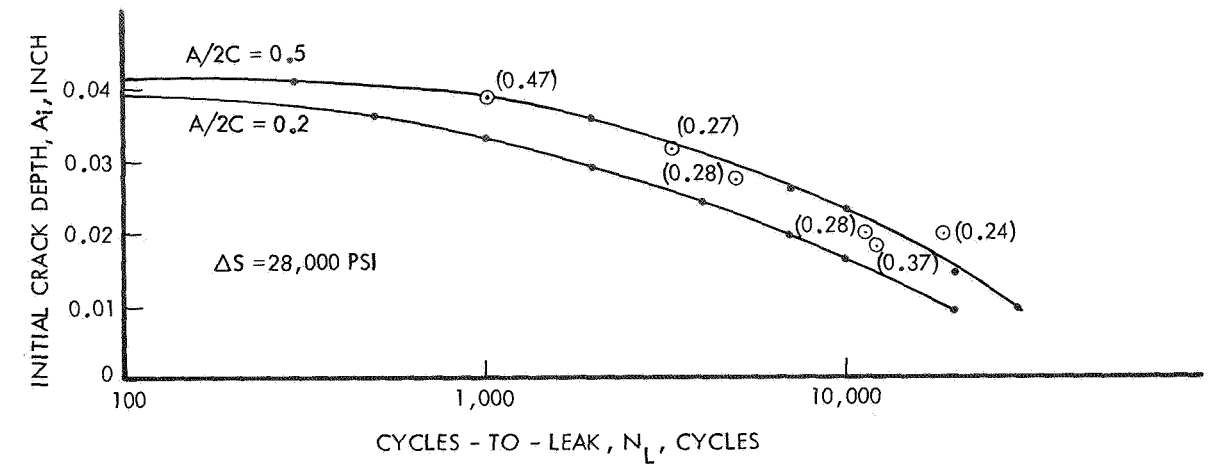
Figure 21. Cycles-to-Leak Results for 0.040 inch Parent Material at Room Temperature, R = 0.05
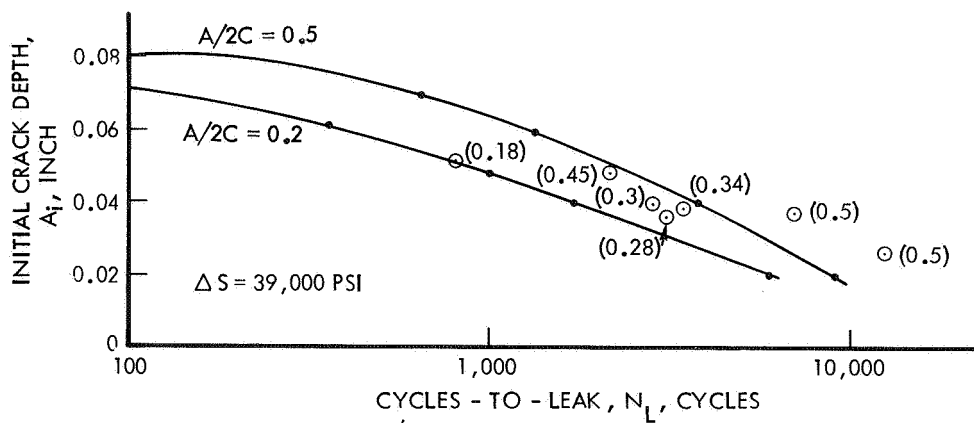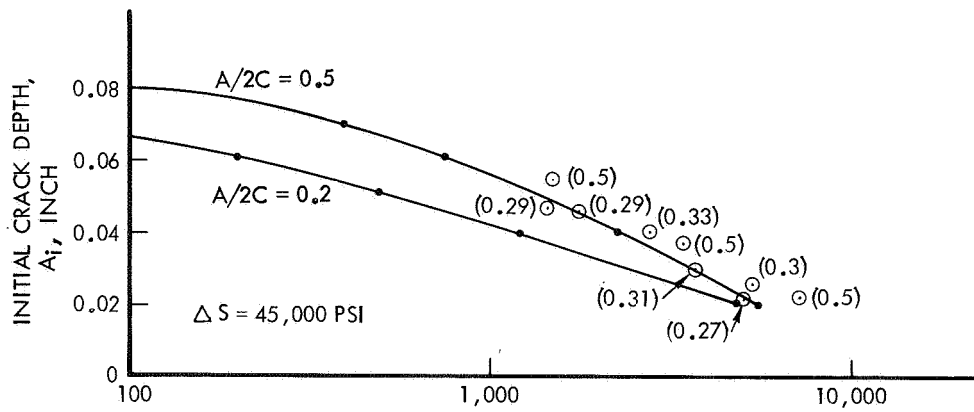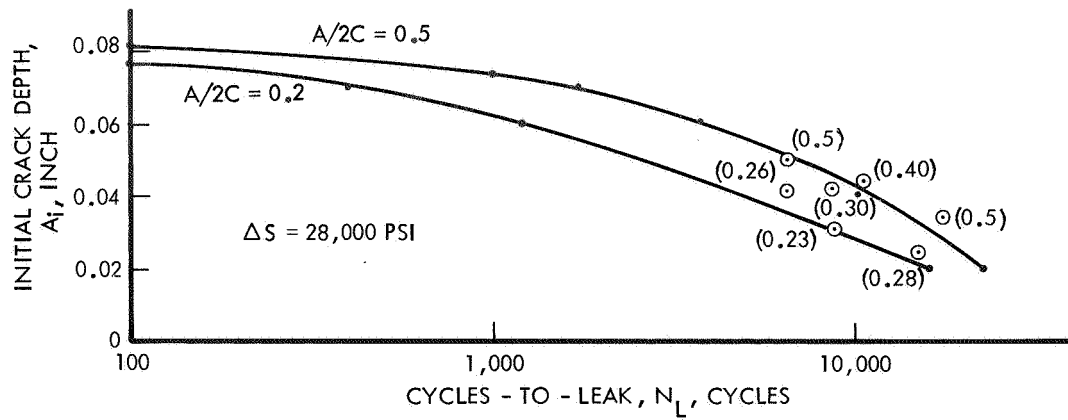
Figure 22. Cycles-to-Leak Results for 0.081 inch Parent Material at Room Temperature, R = 0.05

71
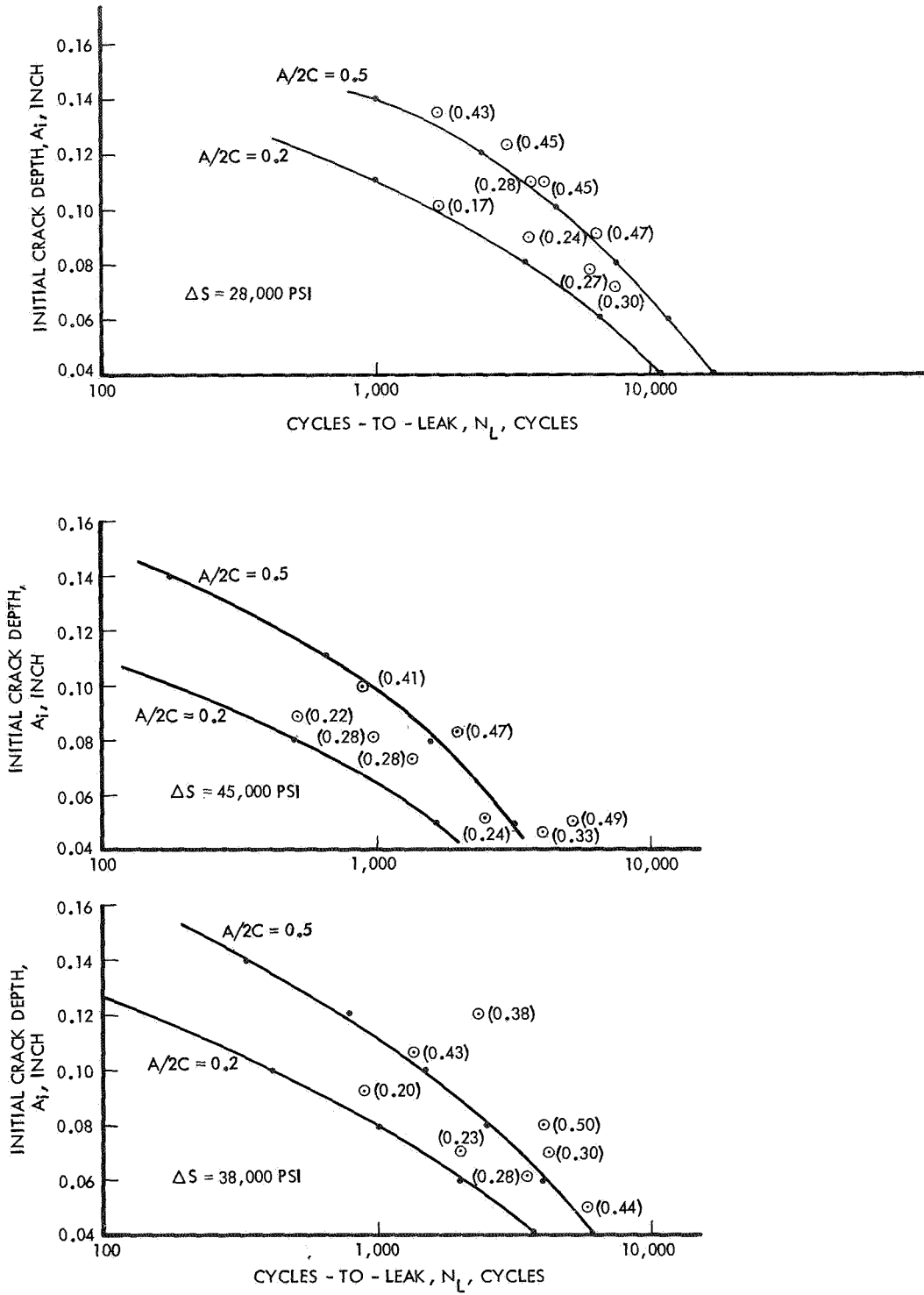
Figure 23. Cycles-to-Leak Results for 0.158 inch Parent Material at Room Temperature, R = 0.05
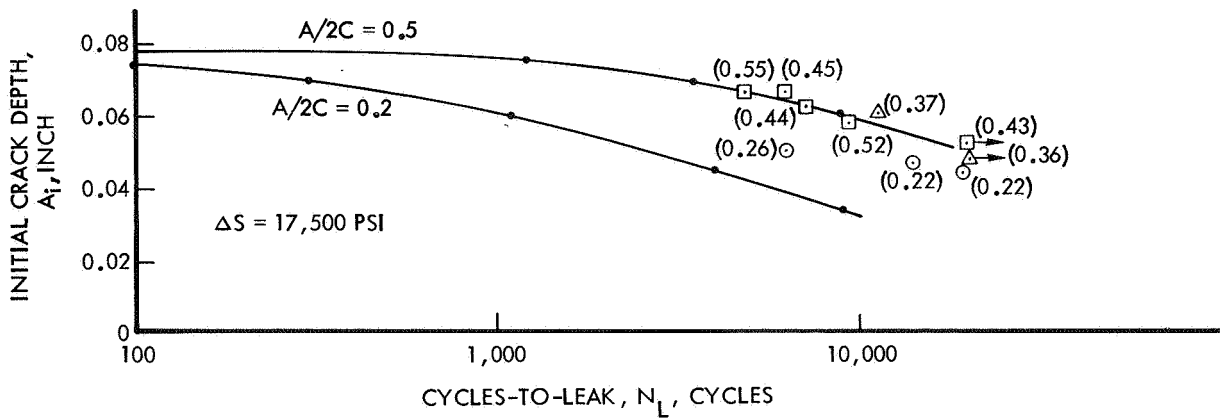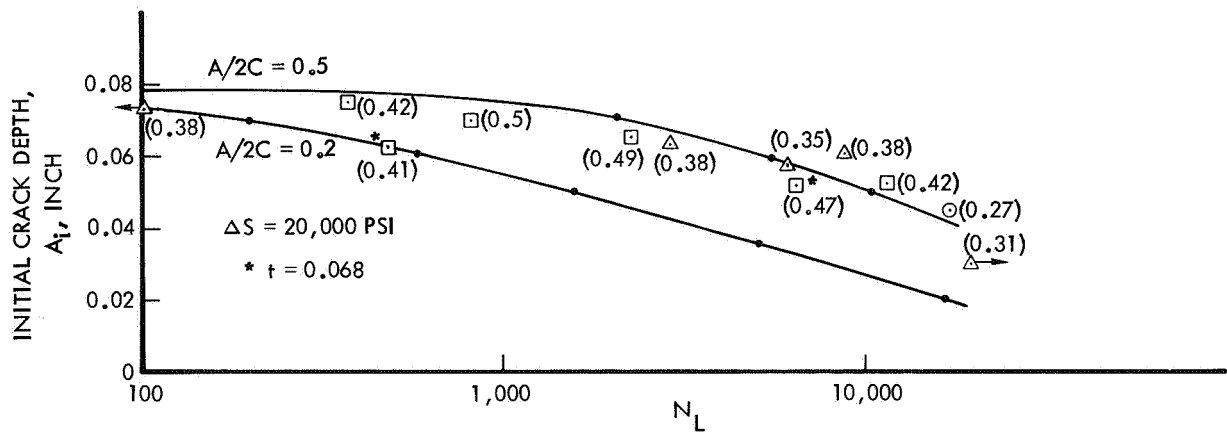
Figure 24. Cycles-to-Leak Results for 0.078 inch Cross Weld Material at Room Temperature, R = 0.05

73
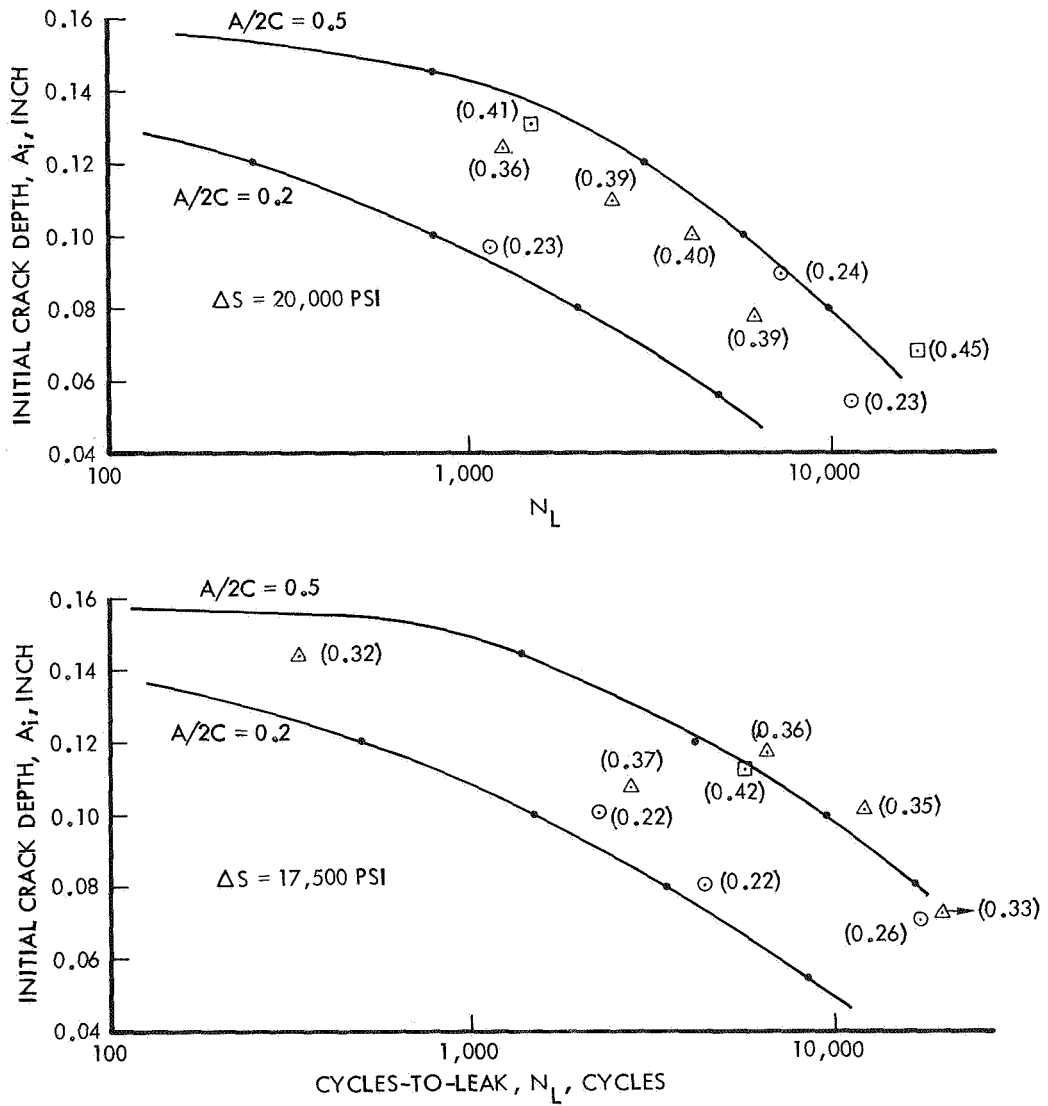
Figure 25. Cycles-to-Leak Results for 0.158 inch Cross Weld Material at Room Temperature, R = 0.05

74
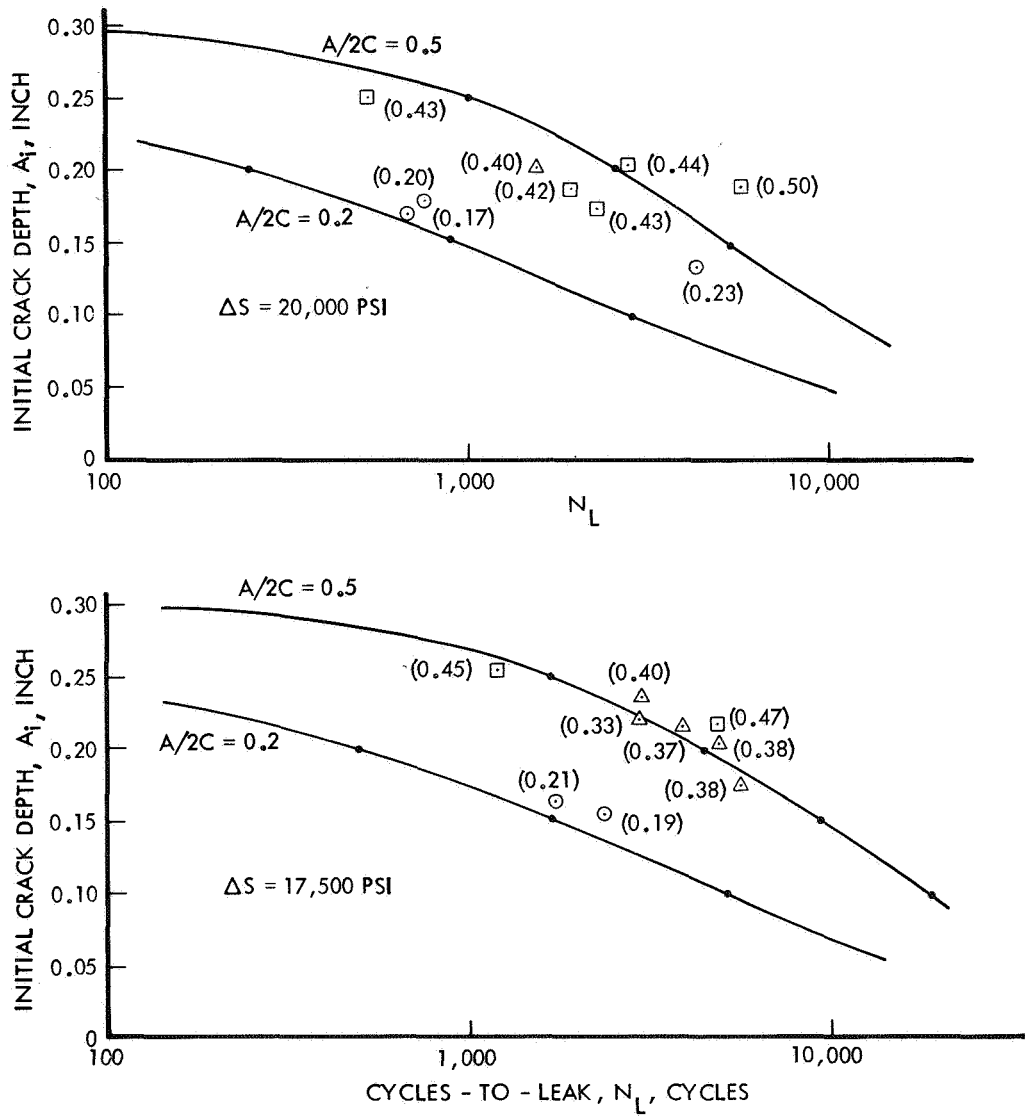
Figure 26. Cycles-to-Leak Results for 0.300 inch Cross Weld Material at Room Temperature, R = 0.05

75
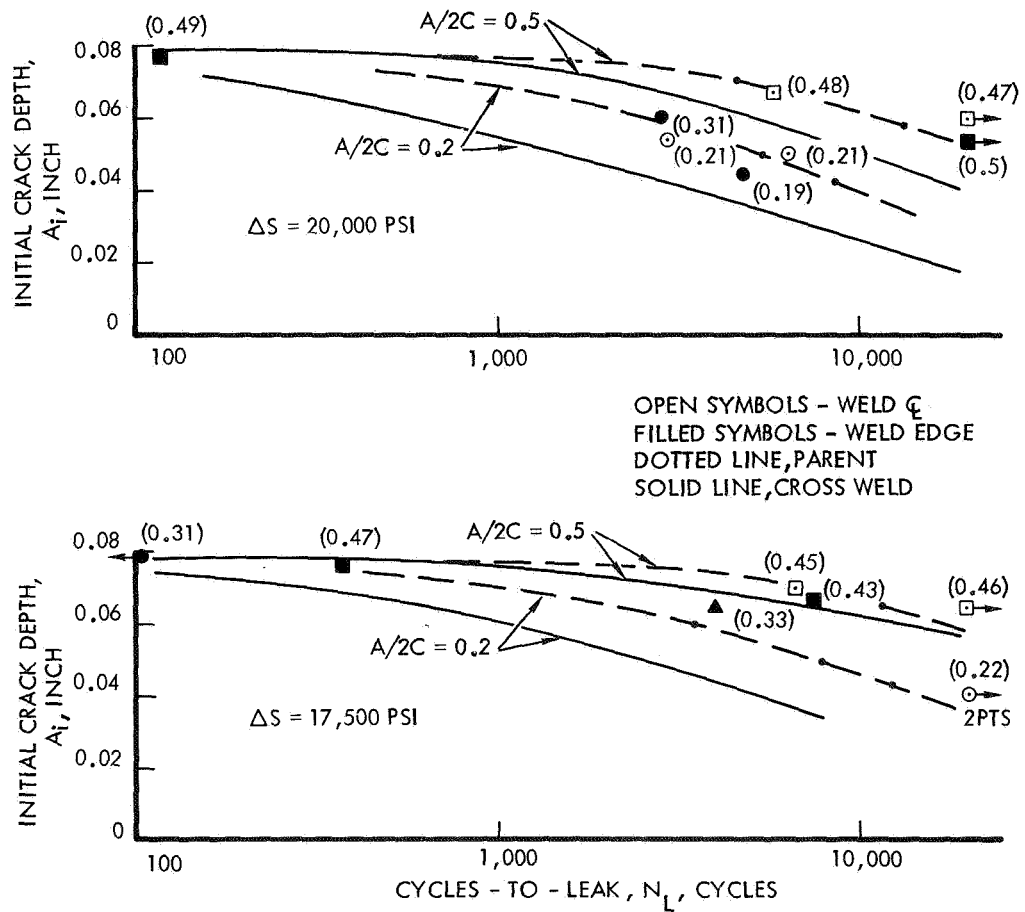
Figure 27. Cycles-to-Leak Results for 0.078 inch Longitudinal Weld Material at Room Temperature, R = 0.05

76
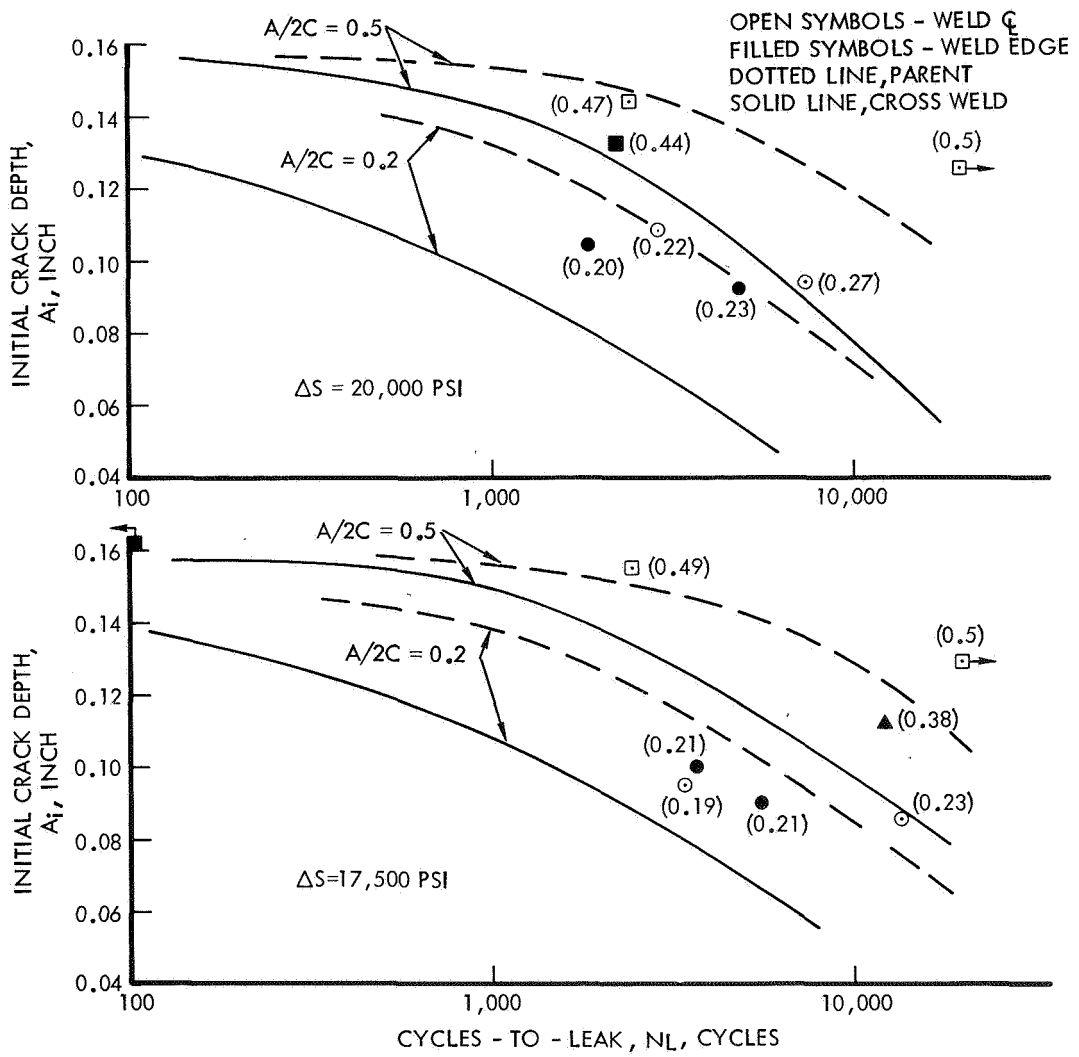
Figure 28. Cycles-to-Leak Results for 0.158 inch Longitudinal Weld
Material at Room Temperature, R = 0.05

77
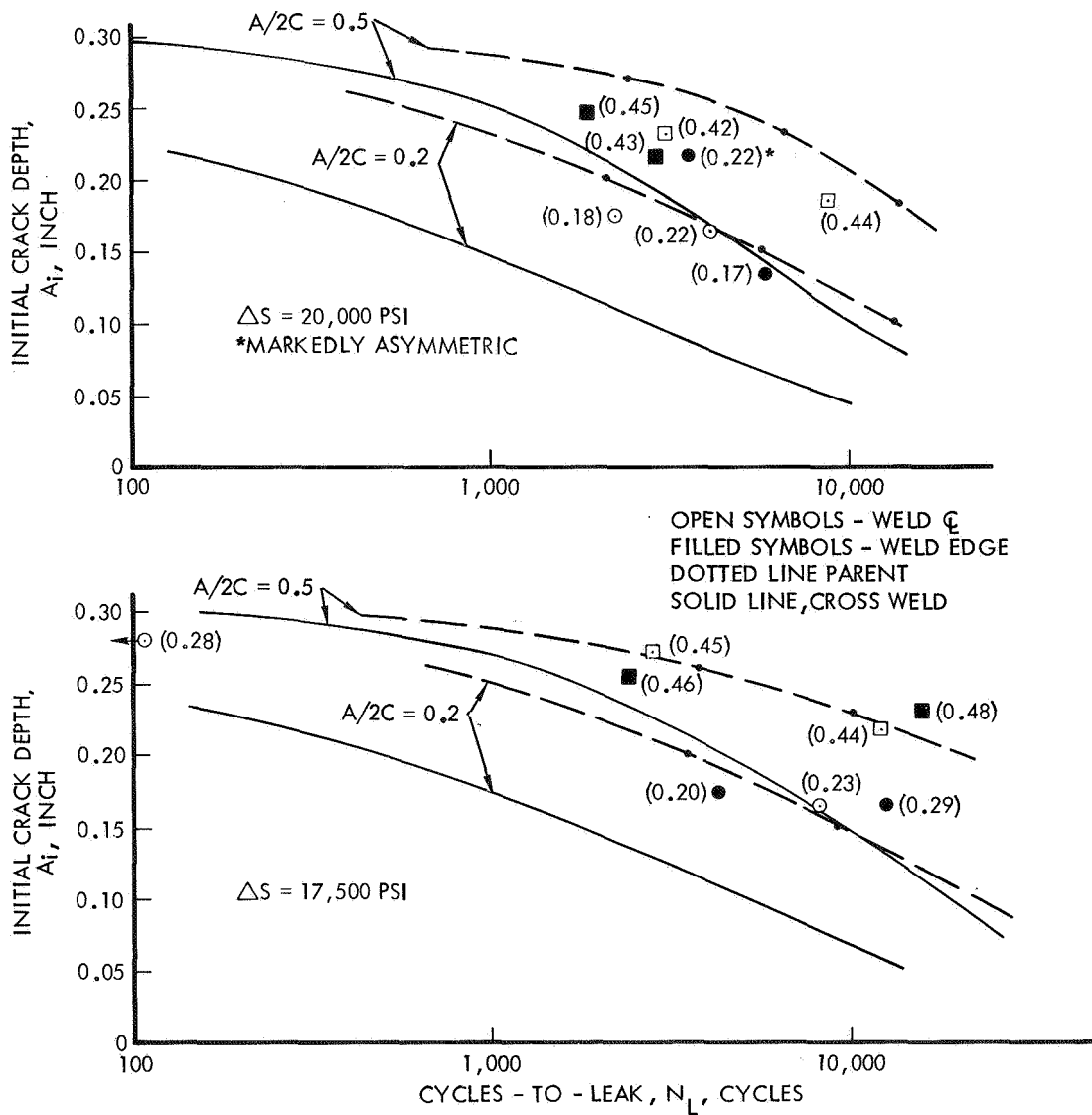
Figure 29. Cycles-to-Leak Results for 0.300 inch Longitudinal Weld
Material at Room Temperature, R = 0.05

78

results obtained based on the parent data do tend to be non-conservative. Examination of the specimens with the flaw at the edge of the weld shows that the cracks tended to propagate more rapidly in the parent material, leak usually occurring in parent material near the fusion line.

The cycles-to-leak test results at R = 0.5 are shown in Figures 30 to 33 for parent and cross weld specimens along with the results predicted by Forman's equation. As for the R = 0.05 data, the predicted values follow the data trends satisfactorily, the predicted values tending to yield conservative results (i.e., shorter lives). Comparison of the data shows that the difference between the predicted and actual values are approximately the same for the R = 0.5 data as for the R = 0.05 data. This indicates that for 2219-T87 parent and weld material at room temperature, the $(1 - R)K_{Ic}$ term in Forman's equation provides an adequate correction for stress ratio effects under constant amplitude conditions.

## 6.3 Cycles-to-Leak Results at 300°F

Results of the cycles-to-leak tests conducted at 300°F, R = 0.05, are presented in Figures 34 to 37 along with the values predicted by the Forman equation. The predicted values correlate quite well with the data, again the predicted values being generally conservative, the accuracy of the predicted values being slightly better than for the room temperature results. The raw data for both the room temperature and 300°F data is presented in Appendix I.
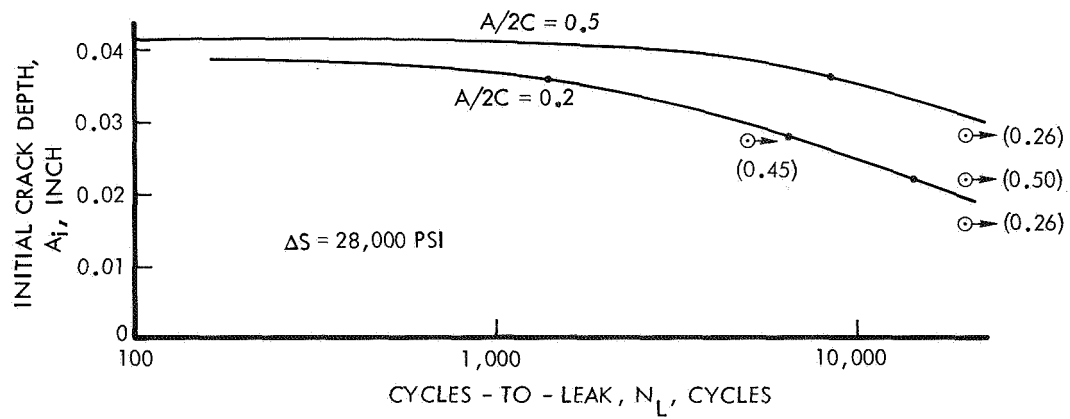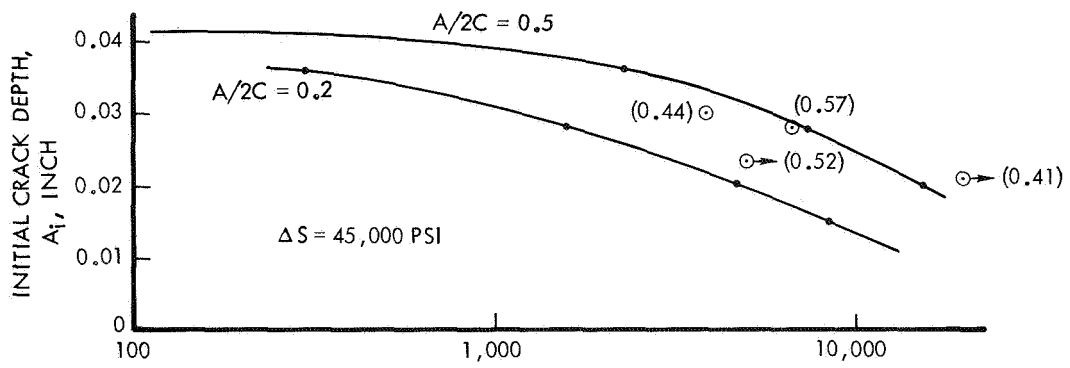
Figure 30. Cycles-to-Leak Results for 0.041 inch Parent Material Tested at Room Temperature, R = 0.5
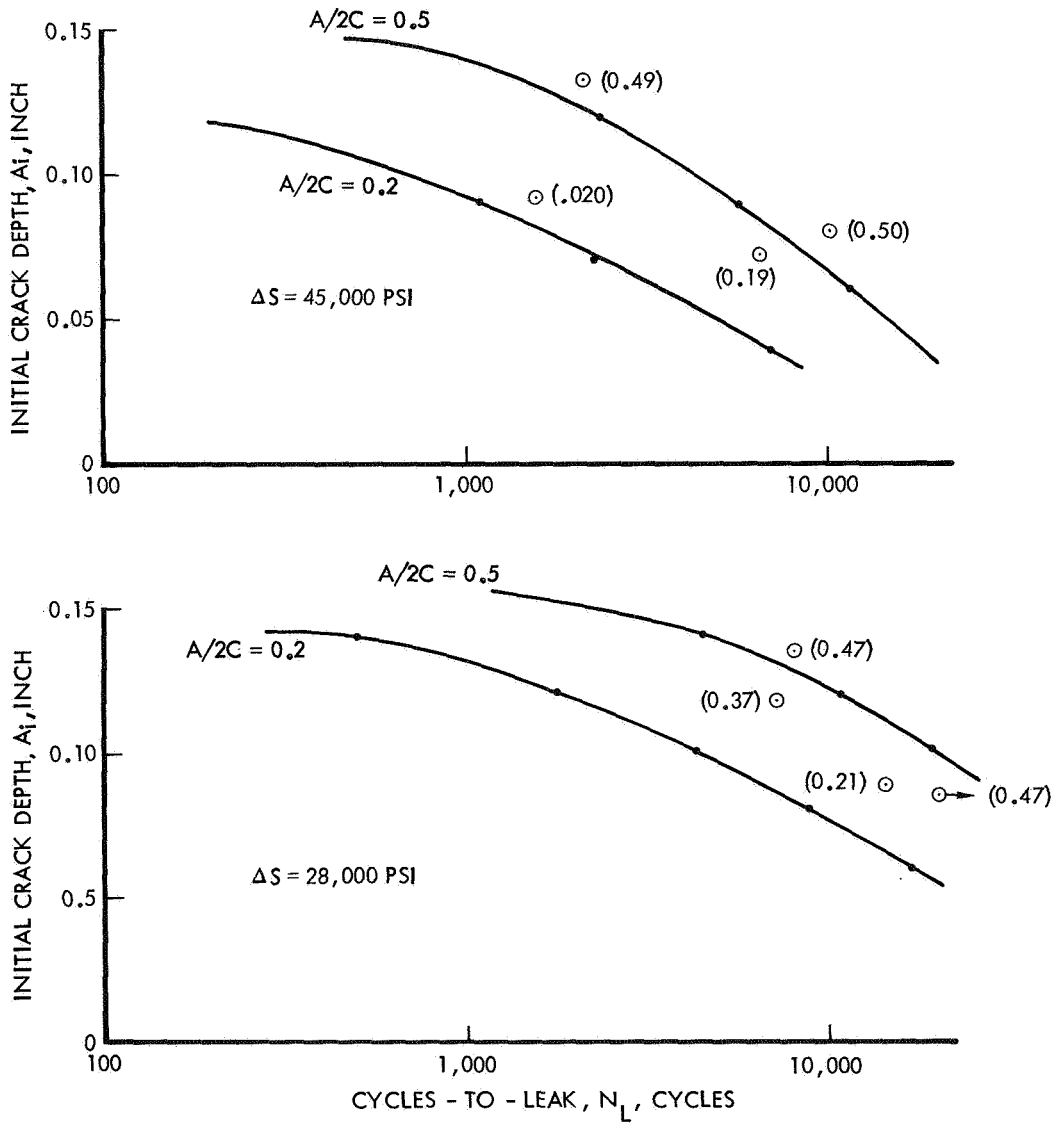
Figure 31. Cycles-to-Leak Test Results for 0.158 inch Parent Material Tested at Room Temperature, R = 0.5
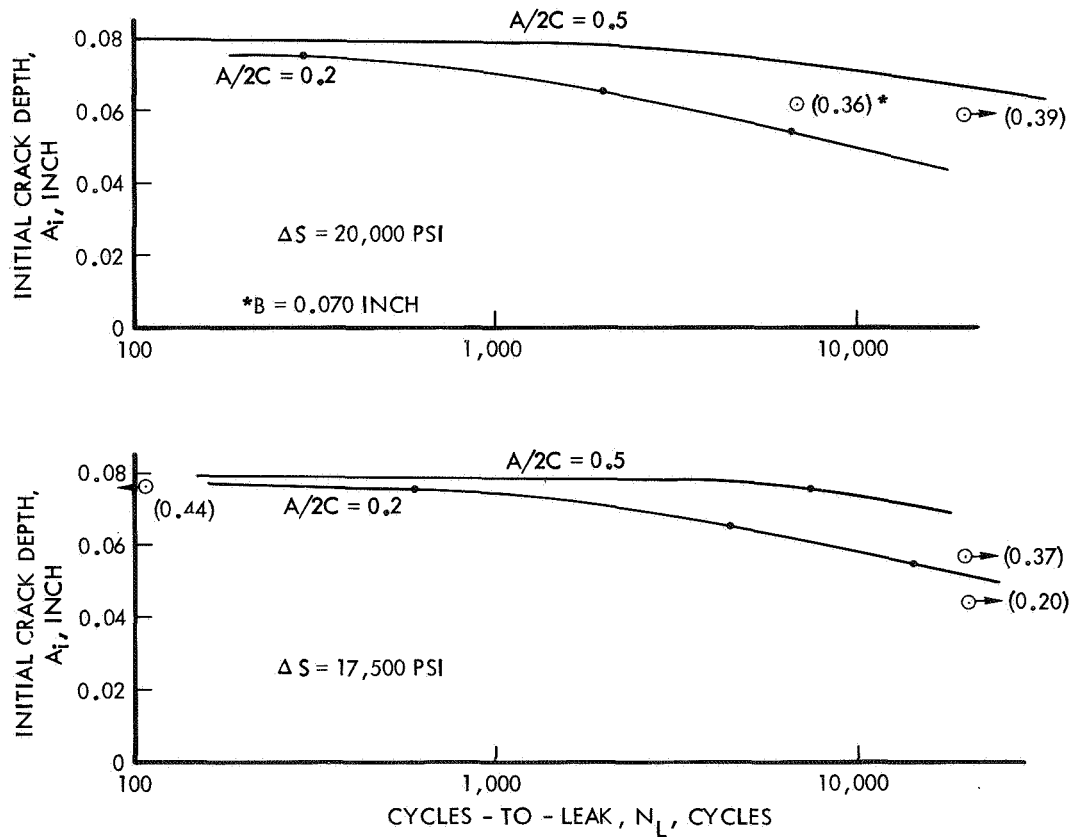
Figure 32. Cycles-to-Leak Results for 0.078 inch Cross Weld Material
Tested at Room Temperature, R = 0.5
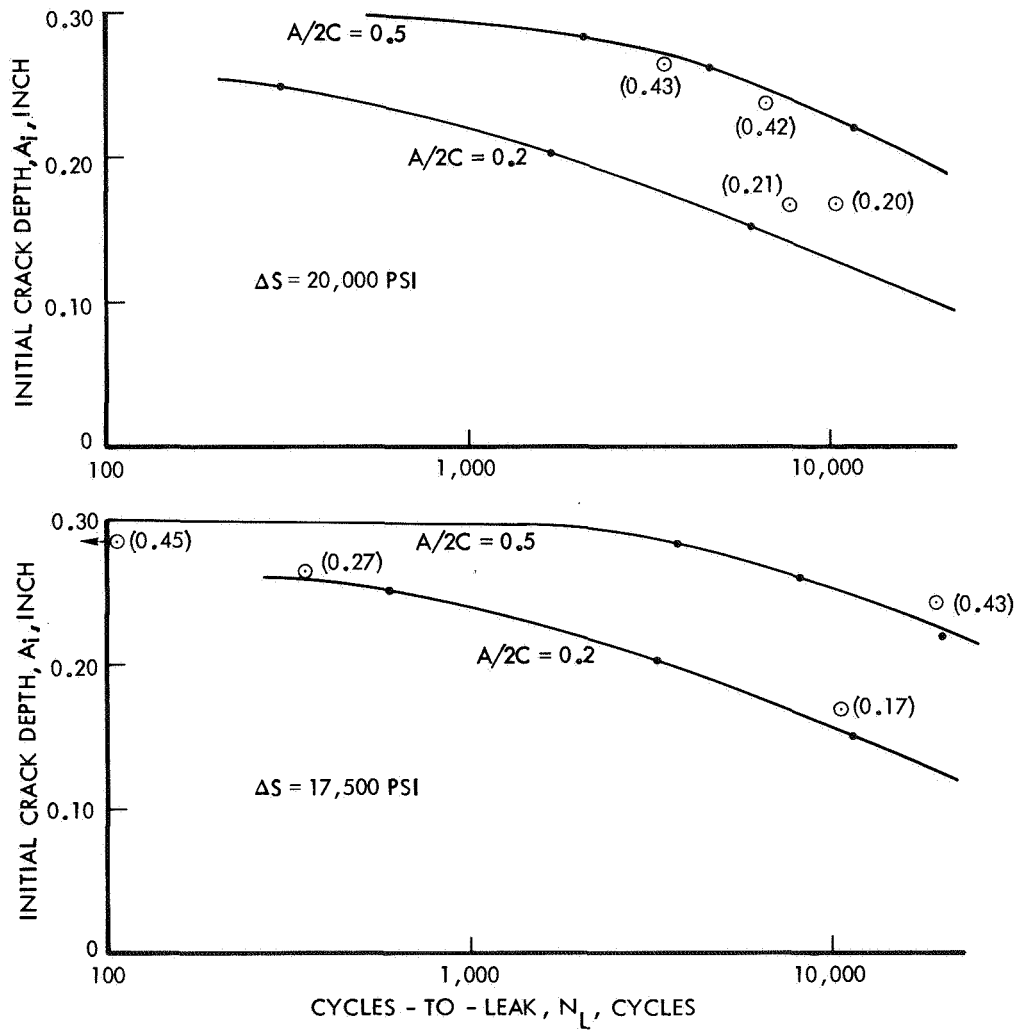
Figure 33. Cycles-to-Leak Results for 0.300 inch Cross Weld Material Tested at Room Temperature, R = 0.5
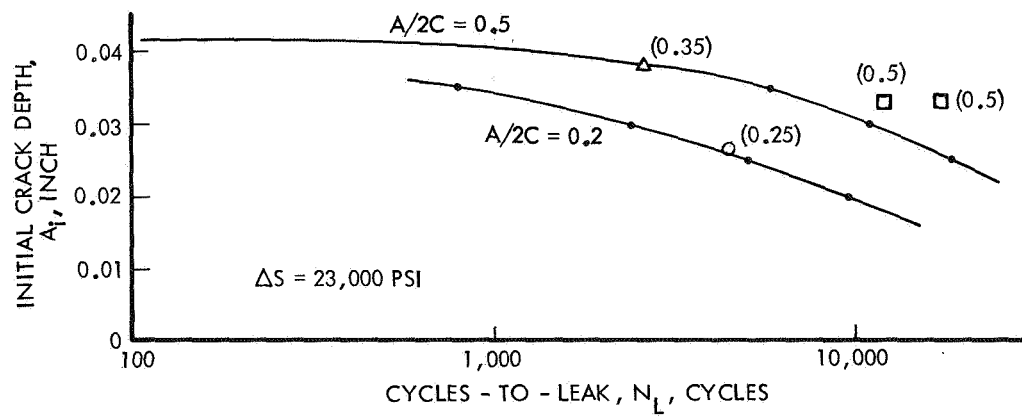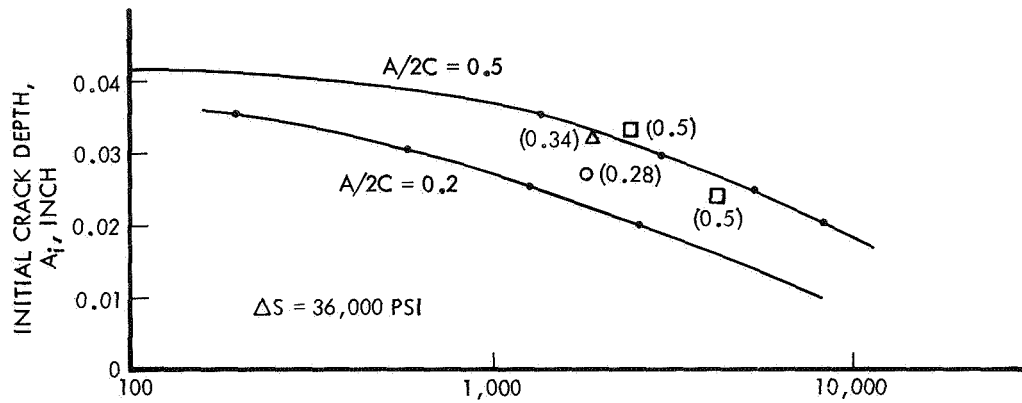
Figure 34. Cycles-to-Leak Results for 0.041 inch Parent Material
Tested at 300°F, R = 0.05

84
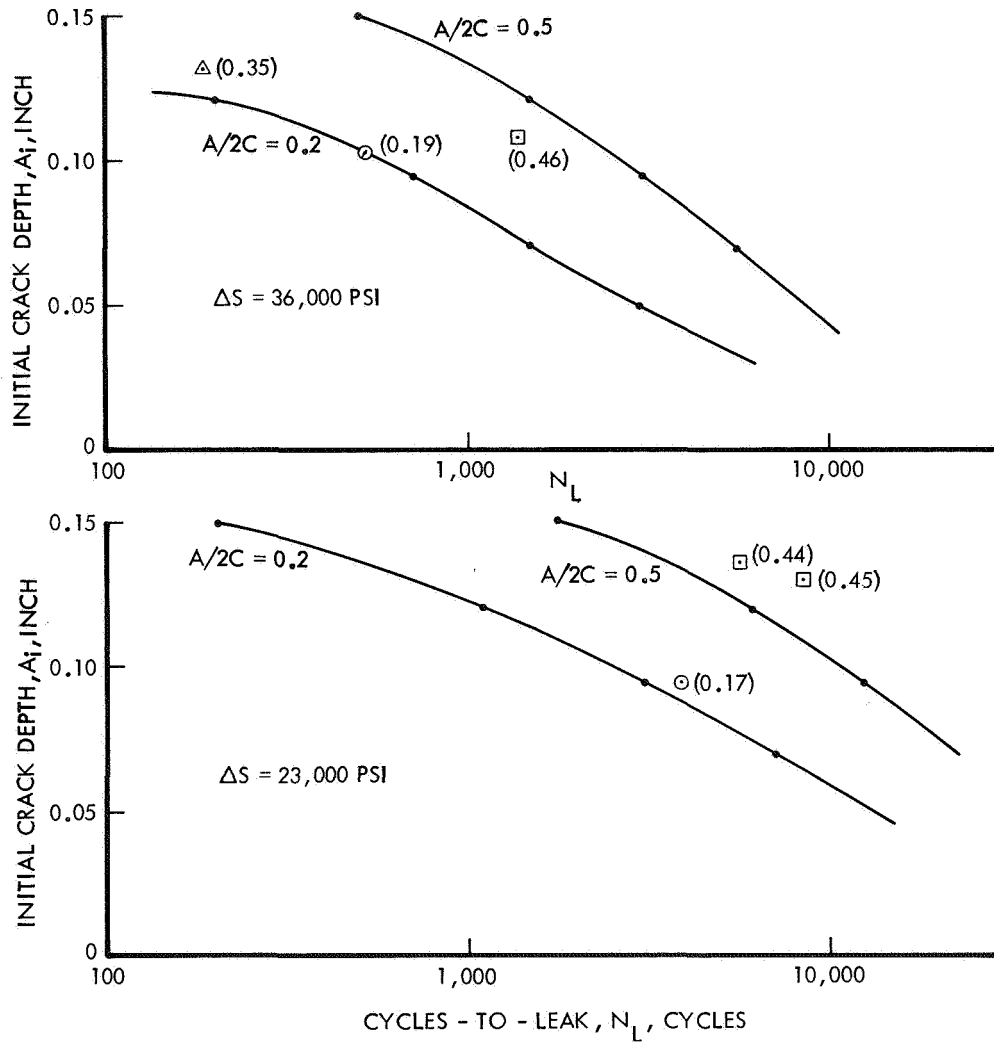
Figure 35. Cycles-to-Leak Results for 0.158 inch Parent Material
Tested at 300°F, R = 0.05
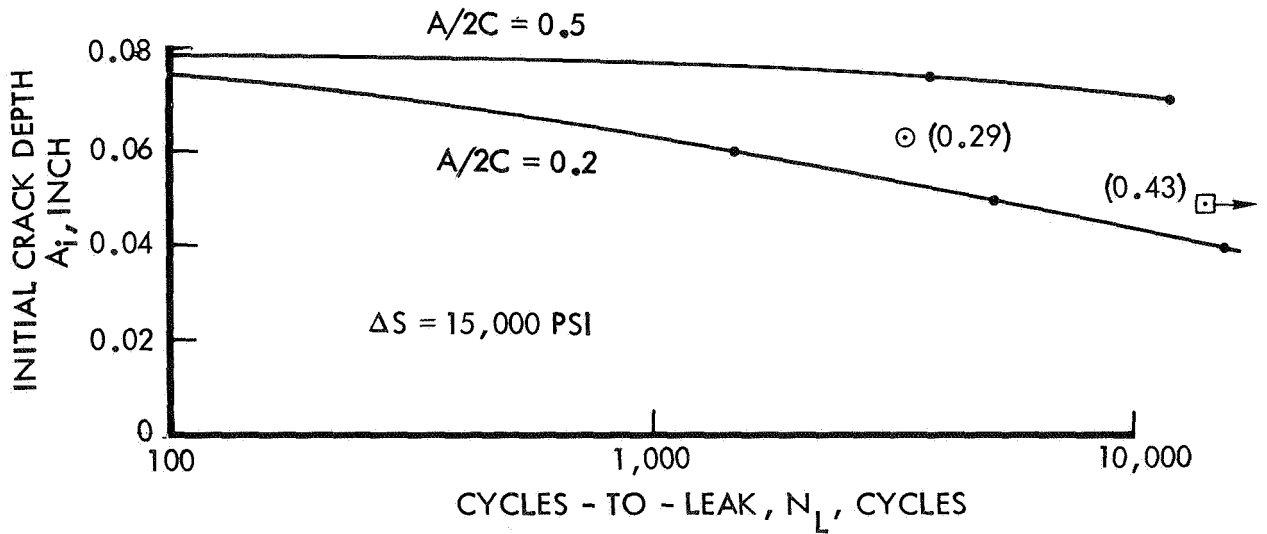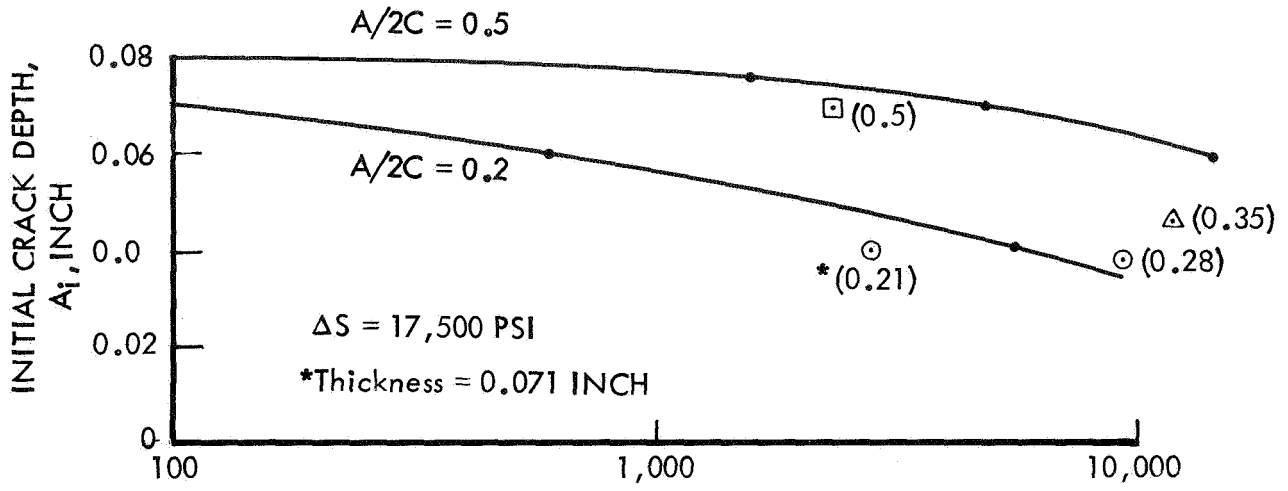
Figure 36. Cycles-to-Leak Results for 0.078 inch Cross Weld Material
Tested at 300°F, R = 0.05
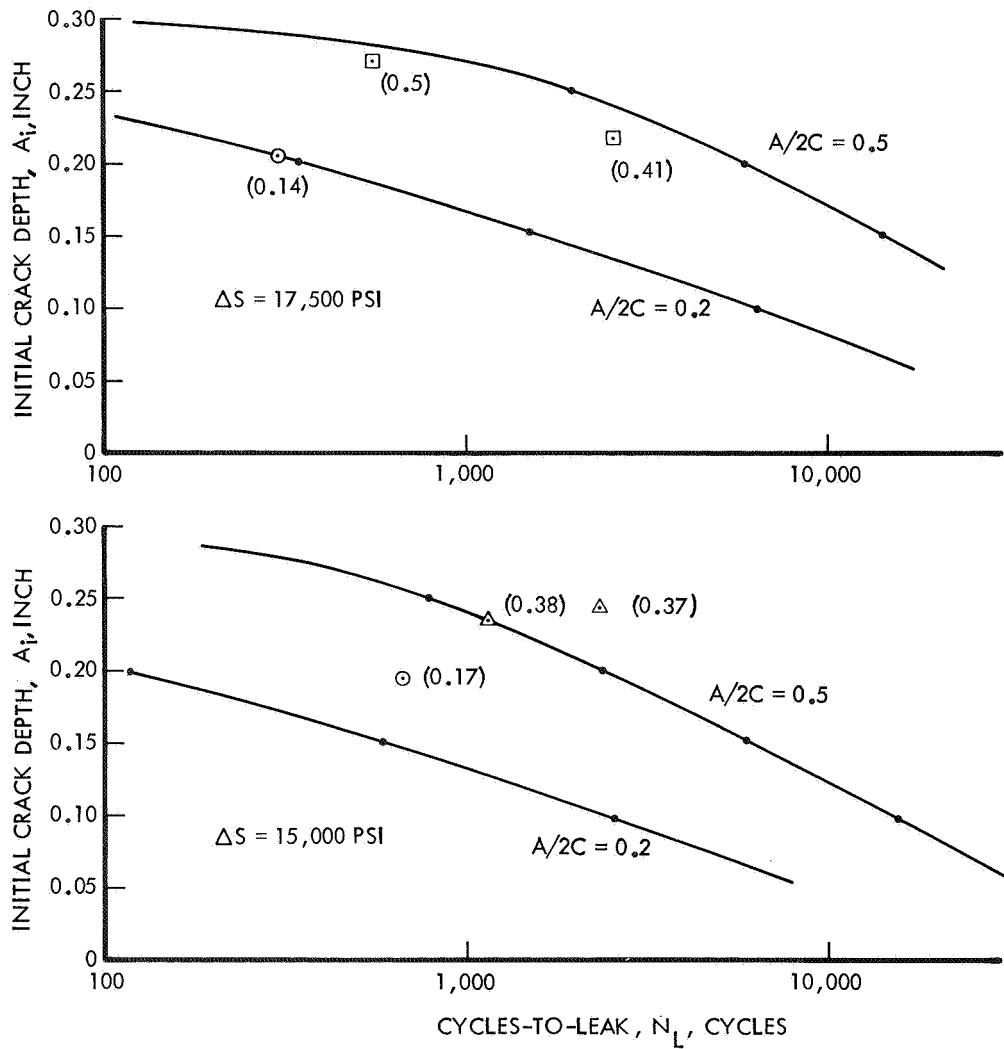
Figure 37. Cycles-to-Leak Results for 0.300 inch Cross Weld Material
Tested at 300°F, R = 0.05

Section 7

PHASE II NDI RESULTS AND ANALYSIS

A variety of flaw size parameters exist that can be used to evaluate the detection limits of various NDI methods. Typical parameters include surface crack length, crack depth, normalized crack depth, crack area, and crack area/thickness. The difficulty in comparing the four methods examined in this study then centers on which crack parameter to base the comparison on since each of the methods is most sensitive to different parameters. For example, penetrant results are sensitive to surface crack length but relatively insensitive to crack area or thickness. X-ray, on the other hand, is very dependent on crack area rather than surface crack length. As a result it is possible to bias the results somewhat in favor of a given method by the selection of the flaw parameter used in the comparison. For the data in this study, nearly all of the cracks were in the range $0.2 \leq A/2c \leq 0.45$ so that the flaws generally would fall in the same relative crack size parameter grouping for most crack parameters. This was particularly true since the very limited sample size necessitated that relatively large flaw size intervals be used to obtain a meaningfully large flaw population in each interval.

Based on these considerations and limitations in the size of the data base, the data in the study are presented as a function of the surface crack length. This crack parameter was selected as a typical parameter, but is not the only parameter that could be used to evaluate the data. The use of this parameter also allows a comparison of actual versus measured crack size to be made, the surface crack length being the only flaw parameter consistently estimated during inspection.

The small sample size also required that rather extensive data combining be done to develop a large enough flaw population to provide a meaningful evaluation. This required data combination procedure is undesirable since

89

it may mask significant variations in the individual elements of the data. This might be expected to be particularly true for the effect of thickness when a specific technique was somewhat different for various thicknesses. If sufficient data existed (it does not on this program) to warrant a separation of the results by thickness, the trends of these data appear to indicate that smaller flaws can be reliably detected in the thinner thicknesses. The use of the combined data, however, does allow a statistically based flaw detection limit to be determined that is valid for use in the entire thickness range of the data, i.e. $0.040 \leq B \leq 0.16$ inch for parent and $0.080 \leq B \leq 0.30$ inch for welded material.

## 7.1   NDI Results

The results of the NDI study of the unknown flawed panels are listed in Appendix II and are plotted in terms of percent flaws detected in Figures 38 through 42 for the four NDI procedures examined. The results shown are for the following arbitrary grouping of surface flaw lengths:  0-0.049, 0.050-0.074, 0.075-0.099, 0.100-0.149, 0.150-0.199, 0.200-0.249, and 0.250-0.299 inch surface crack length.  Within a given size range, the percent of flaws detected is plotted as the average value of the range.

It should be noted that the results shown in Figures 38 to 42 are representative of trends only since the number of flaws, i.e., sample size, for each crack size increment per condition is very limited.  As a result a 50 percent detection limit may be representative of finding one of two cracks as well as ten of twenty cracks.  The figures do show, however, relative trends in the data and do show relative variations between laboratories, i.e., procedures and personnel.

It was found during the study that natural secondary flaws (weld porosity, etc.) sometimes occurred in the "unknown" specimens.  However since the true population of these flaws, i.e., the total number and size present, was not known, these secondary flaws were not included in the analysis.  As a result, the data discussed in this section include only those cracks intentionally
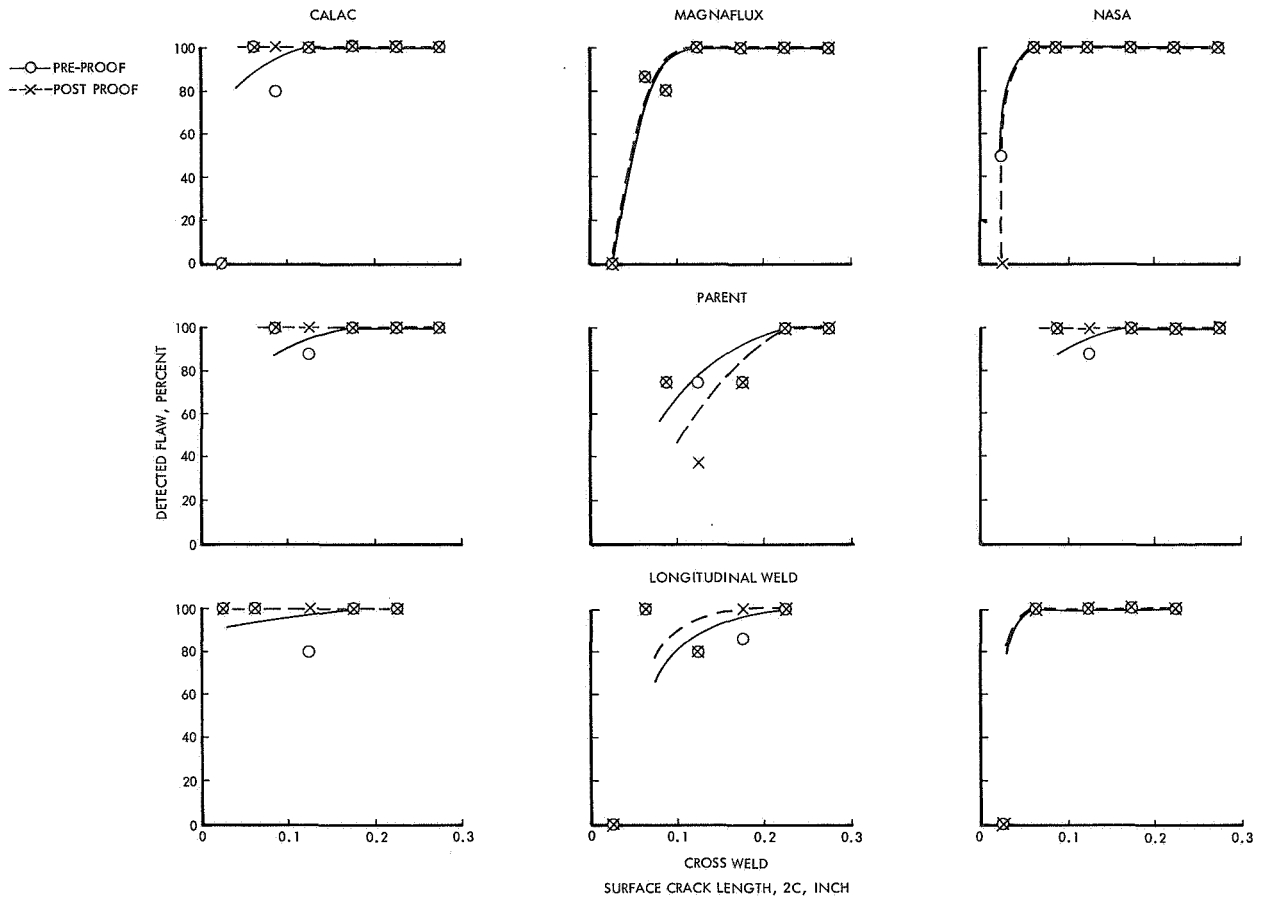
Figure 38.   Penetrant Inspection Results by Investigating Laboratory
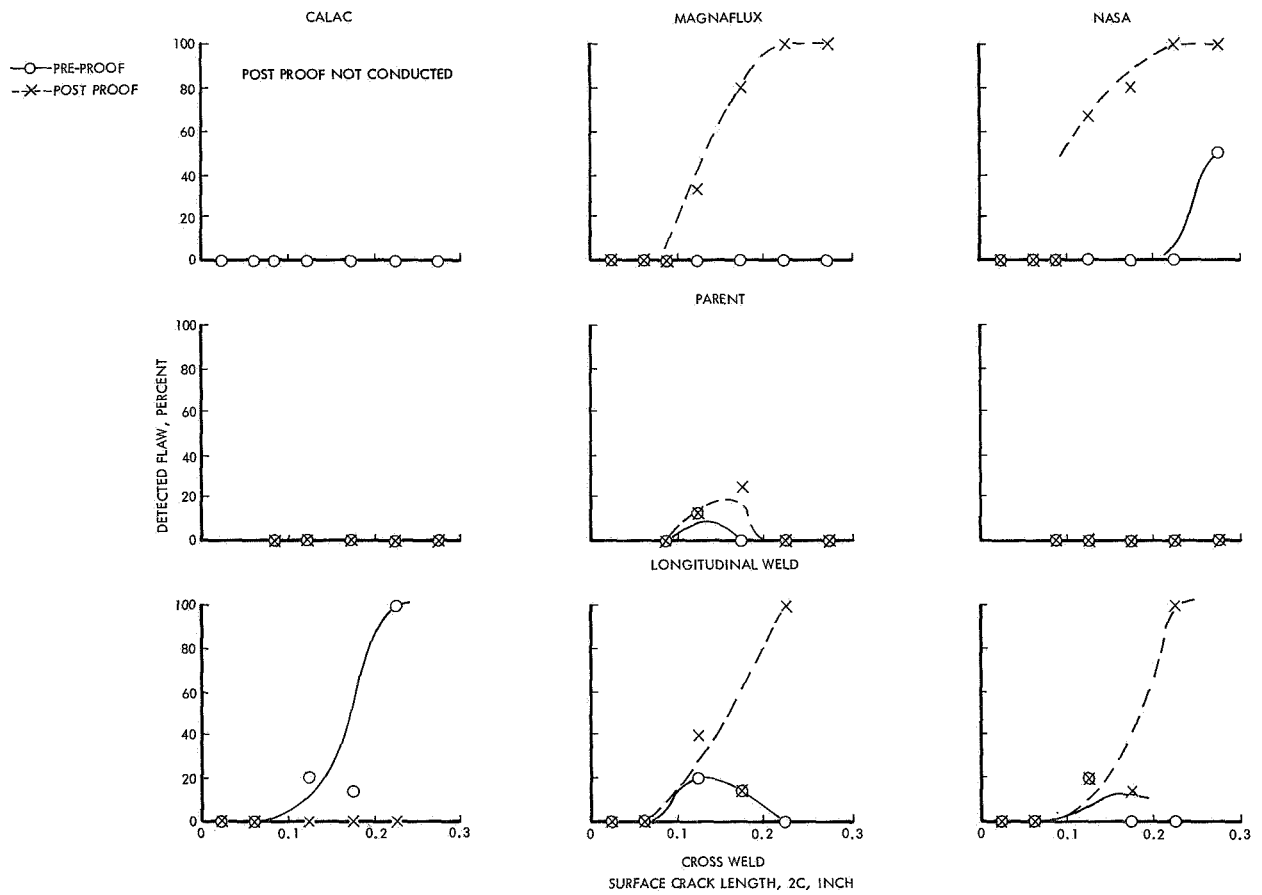
Figure 39. X-Ray Inspection Results by Investigating Laboratory
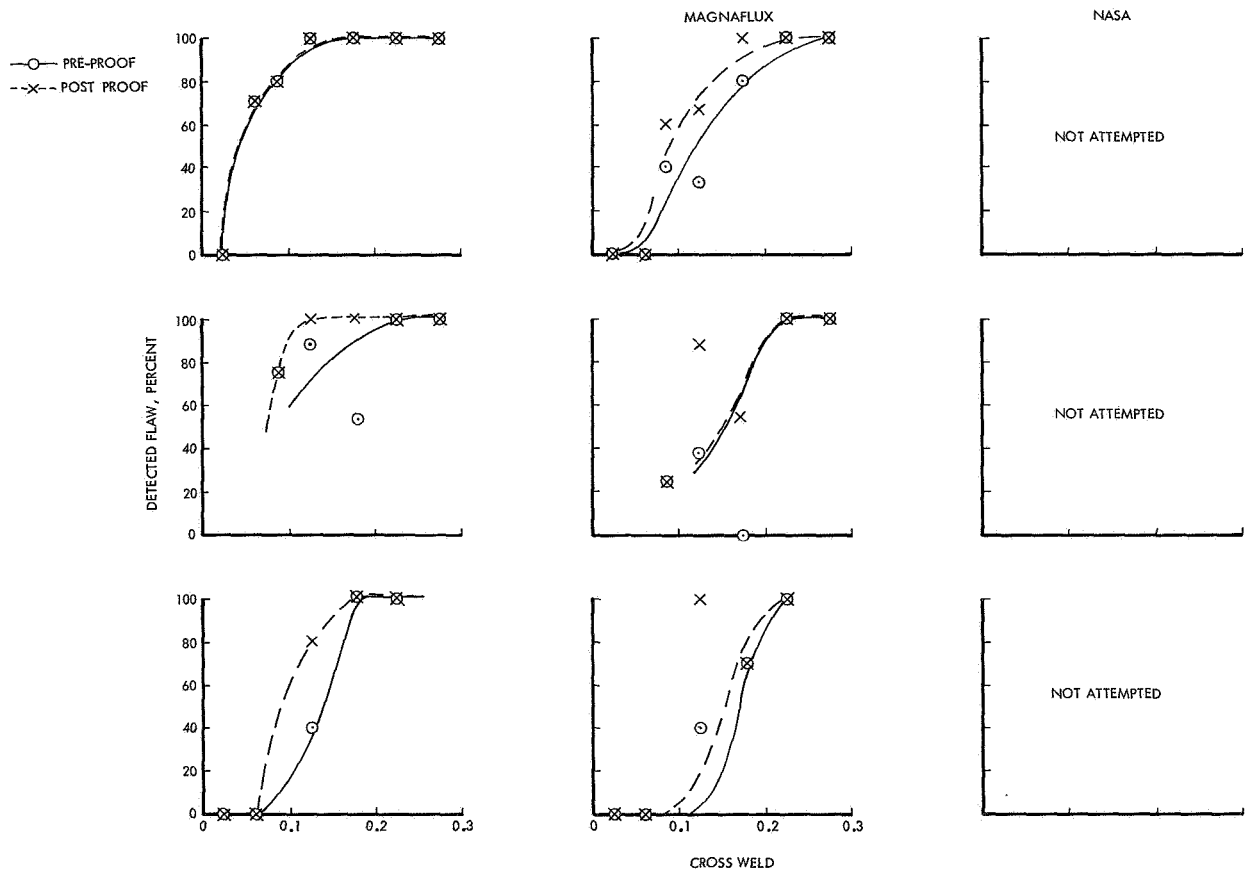
Figure 40. Eddy Current Inspection Results by Investigating Laboratory
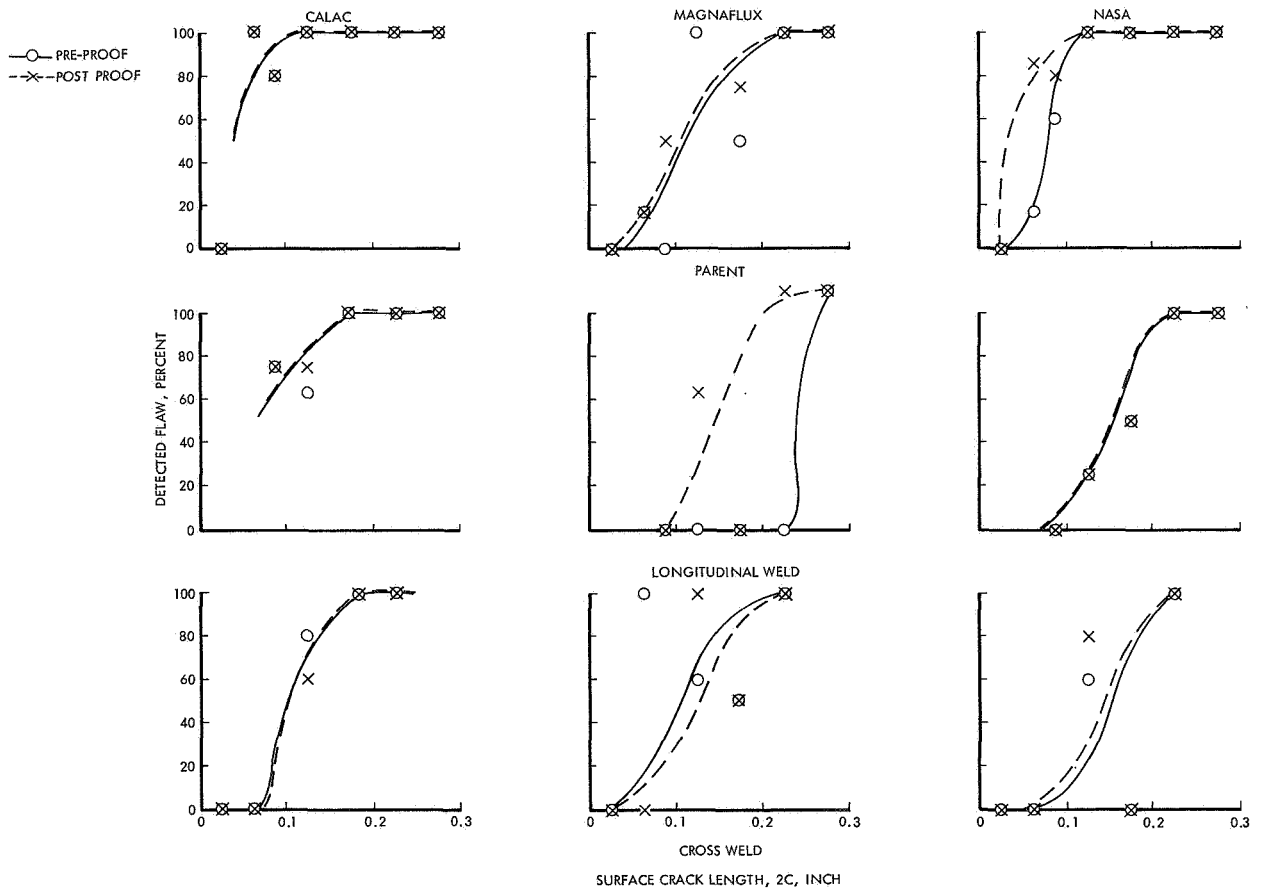
Figure 41.  Shear Wave Ultrasonic Inspection Results by Investigating Laboratory

94
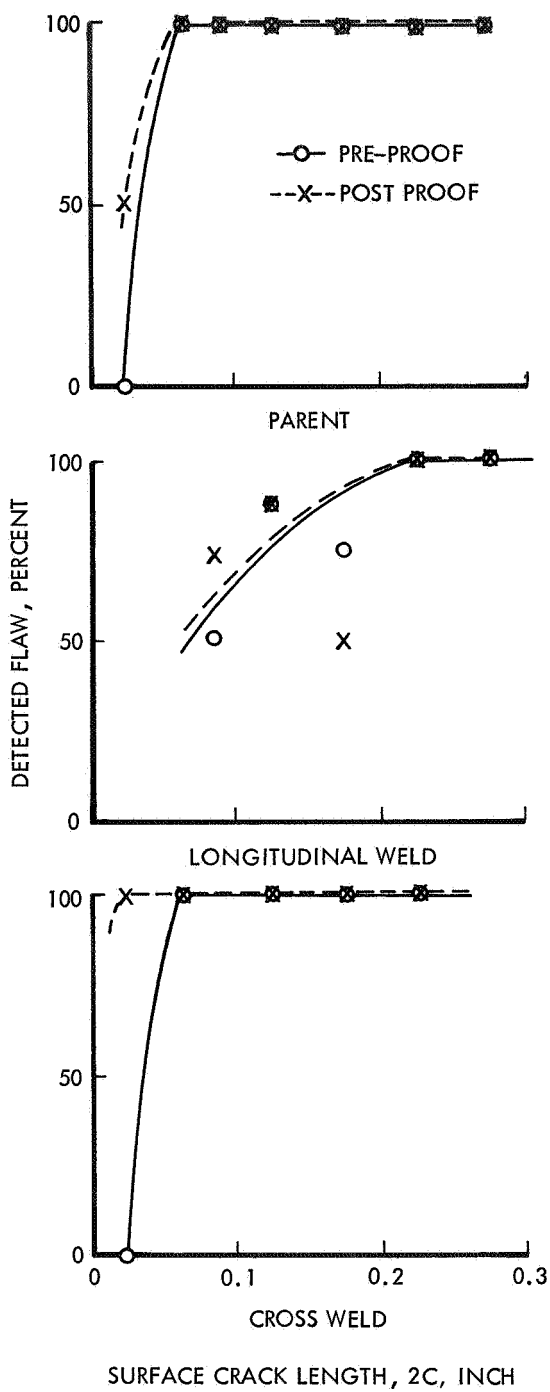
Figure 42. Surface Wave Inspection Results used by NASA/MSC

introduced by low stress fatigue from EDM notches. In addition, the
separation of detection and operator reporting accuracies was found to be
difficult at times. When the individual overlays of the specimens showing
the locations and estimated size of the detected defects were compared with
the master sheet showing the location of the prepared cracks, some mismatch
of location was occasionally noted. The criteria used for this study was
that the reported flaw location should be within approximately 1/2 inch
radius circle of the true location to be counted as a detection. However,
some judgment still was required when obvious cases of reporting errors
arose such as a single flaw of the approximately correct size being reported
at an erroneous location. Insufficient data were available from the riser
specimens for analysis.

The results shown in Figures 38 to 42 provide an opportunity to examine the
effectiveness of the various procedures used by the three laboratories.
The penetrant data show the Lockheed and NASA/MSC results to be generally
superior to the Magnaflux procedure. The X-ray results show similar results
for the three labs preproof results and for the two labs post proof results
(the Lockheed post proof results being ignored as will be subsequently
discussed). The eddy current results again show improved results for the
Lockheed procedure. The improved Lockheed results are not unexpected,
however, since more time was used in developing optimized inspection
procedures. This is again reflected in the shear wave ultrasonic results
where the Lockheed results are about the same as NASA/MSC and slightly
better than Magnaflux.

Figures 38 to 42 show that penetrant inspection generally detects smaller
flaws than the other inspection methods. Eddy current and shear wave ultra-
sonics are comparable while X-ray is least effective. The surface wave
ultrasonic technique used by NASA/MSC shows excellent detectability
approaching the level of detection shown by the penetrant results, but the
results of the method are limited to the one laboratory.

The influence of a prior proof stress cycle is seen to result in a generally improved detectability of cracks for the penetrant, shear and surface wave ultrasonic, and eddy current methods. The beneficial effect of the proof cycle is most apparent for the X-ray results where the Magnaflux and NASA/MSC results show a marked improvement. The lack of improvement in the post proof Lockheed X-ray results would appear to be due to operator variation or an unreported change in procedure since cracks detected before proof were not detected in the post proof examination.

The general improvement of crack detectability following a proof stress is believed due to the increased separation of the crack surfaces due to the residual effect of the larger plastic zone surrounding the crack produced by the high load proof cycle. A second possible reason for the increased detectability following proof could be the actual growth of the crack during proof. However, no evidence of such growth was reported by NASA/MSC following the breaking open of the flawed specimens.

7.2    Statistical Analysis

Two parameters were examined statistically, the accuracy of crack size estimation from NDI results, and the probability of detection of an existing crack. For the first examination, the accuracy of crack size estimation, the analysis was limited to the penetrant data since this was the only data where actual surface crack lengths were estimated, the results for the other methods being listed as the crack size relative to the available standard crack sizes.

A computer program was written in order to present graphically the results of nondestructive tests as a plot of estimated flaw size against the actual results determined by subsequent examination. The data points for each of seven regions of actual surface crack length were collected at the mean value of that region. Superimposed·upon the data points are the lines showing the mean and one and two standard deviation limits assuming that the data are distributed in each region on a log-normal curve.

The steps used to calculate these limits were as follows:

1.  Assume the arithmetic mean $\overline{Z}$ to be the actual value.
2.  Compute the normal standard deviation, $\sigma_Z$ from

$$\sigma_Z^2 = \frac{\Sigma(Z - \overline{Z})^2}{n} \qquad (20)$$

3.  The log-normal curve assumes that the natural logorithms of each $Z$ are distributed normally: $Y = \log_e Z$

4.  Compute the log-normal standard deviation $\sigma_y$ from:

$$\sigma_Y^2 = \log_e \left[ 1 + \left( \frac{\sigma_Z}{\overline{Z}} \right)^2 \right] \qquad (21)$$

5.  Determine the log-normal mean, $\overline{Y}$, from:

$$\overline{Y} = \log_e \overline{Z} - \frac{\sigma_Y^2}{2} \qquad (22)$$

6.  The $Z$ values for any specified $Y$ are computed from: $Z = e^Y$ and the values used to plot the curves were $Y = \overline{Y}$, $\overline{Y} \pm \sigma_Y$, $Y + \sigma_Y$ which should indicate the bounds containing 68 percent and 95 percent of the samples, respectively.

The results of this analysis as displayed by computer graphics showed that there was insufficient data to obtain meaningful statistical results for each case. As a result, all of the penetrant data was combined to provide a significantly large sample. The results are shown in Figure 43 for all penetrant results.

The second and most crucial parameter, from a design standpoint, is that of determining the probability of detecting a given size crack by a given NDI method. The following is a derivation of the expression used to determine the confidence limits and an estimate of the probability of detecting a flaw in a specimen by nondestructive testing. The assumption is that the
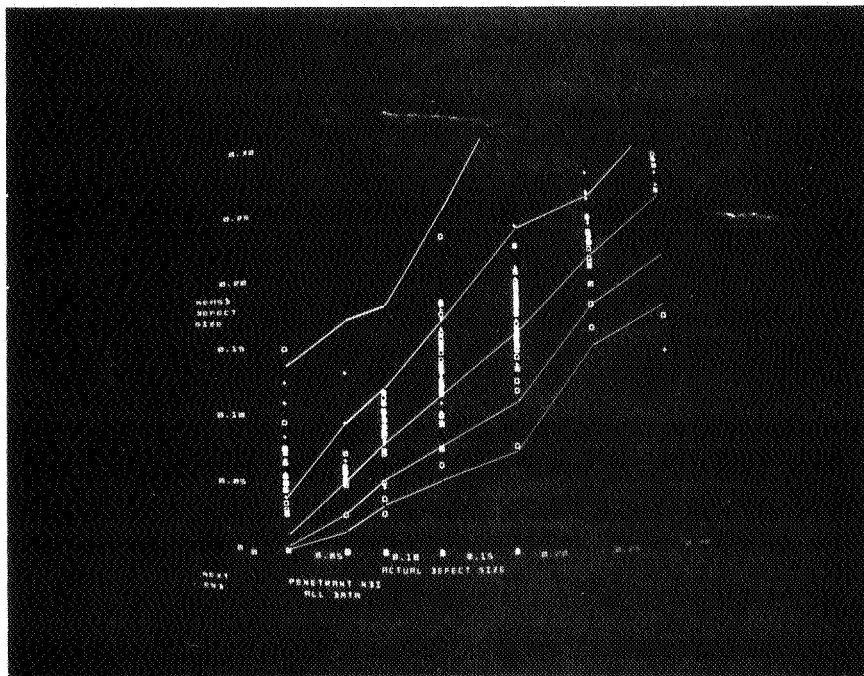
Figure 43. Flaw Size Estimation Accuracy from
Penetrant NDI Results, All Data

results of one experiment indicate that of n flaws, $S_n$ was detected. It is required to know with what confidence one can assume that the probability of detecting flaws, p, is $S_n/N$. Assume that S is distributed by the binomial distribution with mean np and standard deviation

$$\sqrt{n/P(1-p)} = \sqrt{npq} \tag{23}$$

Using De Moivre's theorem, we can say that the probability of S being bounded by a given interval is:

$$P\left\{hp + a\sqrt{npq} < S < np + \sigma\sqrt{npq}\right\} = \frac{1}{2n}\int_a^b e^{(-z^2/2)}dz \tag{24}$$

where a and b are real numbers with a < b if n is sufficiently large. To determine, for example, the 95 percent confidence interval for P, we find from tables of the normal distribution that

$$P\left\{-a < \frac{S - np}{\sqrt{npq}} < a\right\} = 0.95 \tag{25}$$

results in a = 1.96 and from this, we derive the expression

$$p^2(n + a^2) - p(2S + a^2) + S^2/N = 0 \tag{26}$$

The roots of this equation for given values of S, n and a give the required confidence limits. The equation was solved for each region of actual values for the following values of a:

| Confidence % | Value of a |
|---|---|
| 90 | 1.645 |
| 95 | 1.96 |
| 97.5 | 2.24 |

To obtain meaningful results from this analysis however, a relatively large data base is required. Due to the small number of specimens examined for each

condition, it was necessary to combine data in order to develop a significantly large data base for use in the analysis. While this procedure does obscure some of the variations due to differences in procedures, material, and thickness, it does provide a usable basis for comparing the "average" results for each of the four NDI methods examined.

The first study was to compare the pre- and post-proof results for each NDI method by combining the data for all thicknesses of the weld and parent material and from the three labs together. These results are shown in Figures 44 to 47. Again, however, the data bases are shown to be small enough that the confidence levels of interest (90 and 97.5 percent) were very low due to the small sample size. The one set of surface wave ultrasonics could not be analyzed due to the insufficient amount of data. Note that the effect of a limited amount of data even for the combined data results in the lower confidence level for the very large cracks where only a few cracks of that size were present. This is true even though there was a 100 percent detection reported.

Before attempting to rank the flaw detection limits of the various techniques, several observations must be made. First the basis for comparison must be decided. This includes both the crack parameter used and the detection limits required, i.e., the probability of detection or missing a flaw and the confidence levels of interest. Second, the variables and degree of legitimate data combining must be determined.

For example, Figures 44 to 47 present a statistical basis for the detection limits applicable to a structure of $0.045 \leq B \leq 0.16$ inch parent and $0.080 \leq B \leq 0.30$ inch welded material for each NDI method. However, this also requires an averaging together of the data from three laboratories using "optimum" but somewhat different procedures. While this may tend to compensate for operator variations not examined in this program, it will yield a conservative (larger) 100% detectable flaw size since it includes the worst as well as best procedure. If, however, the data is separated by laboratory, further
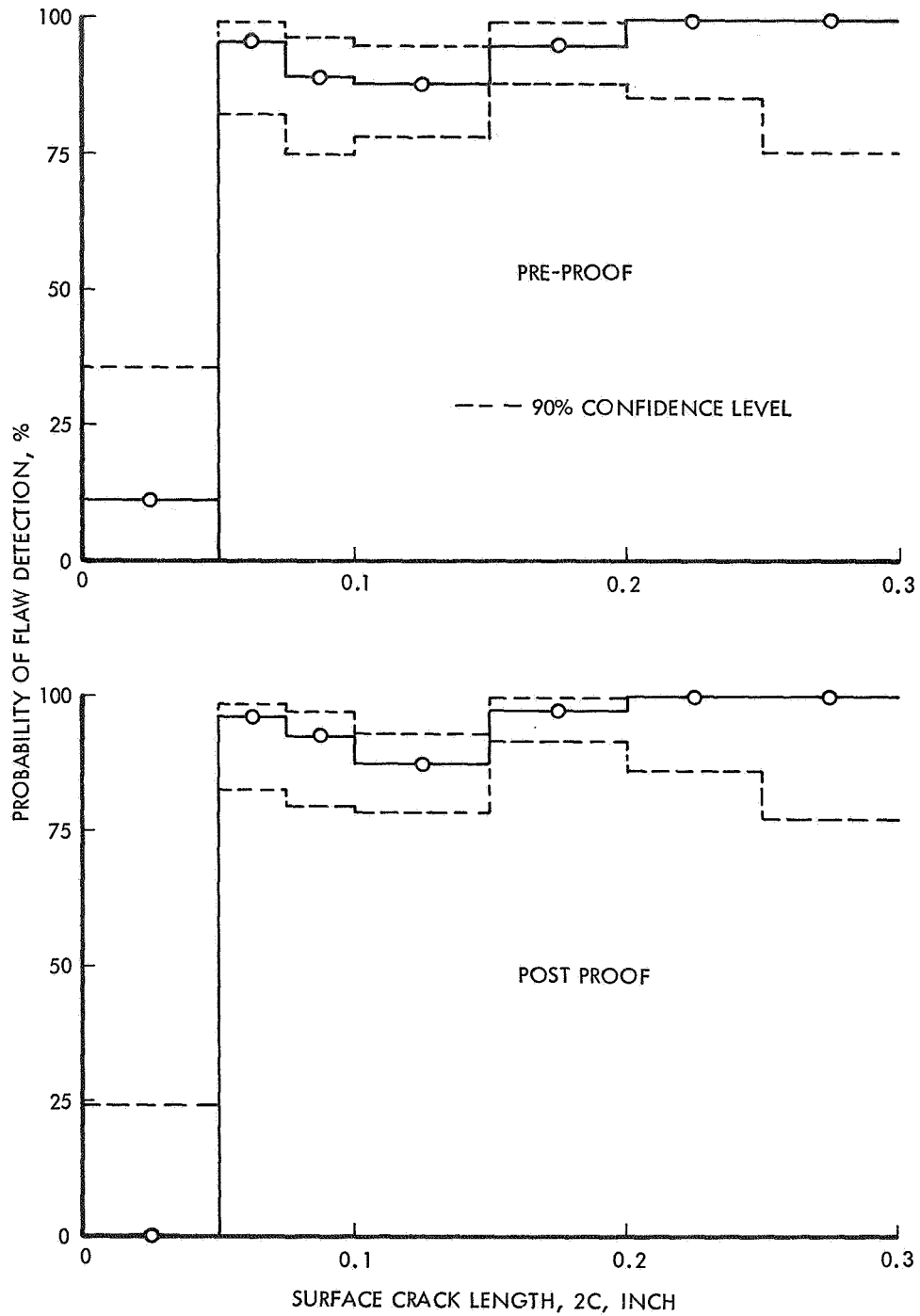
Figure 44. Pre-Proof and Post Proof Penetrant Inspection
Statistical Analysis Results (All Data)
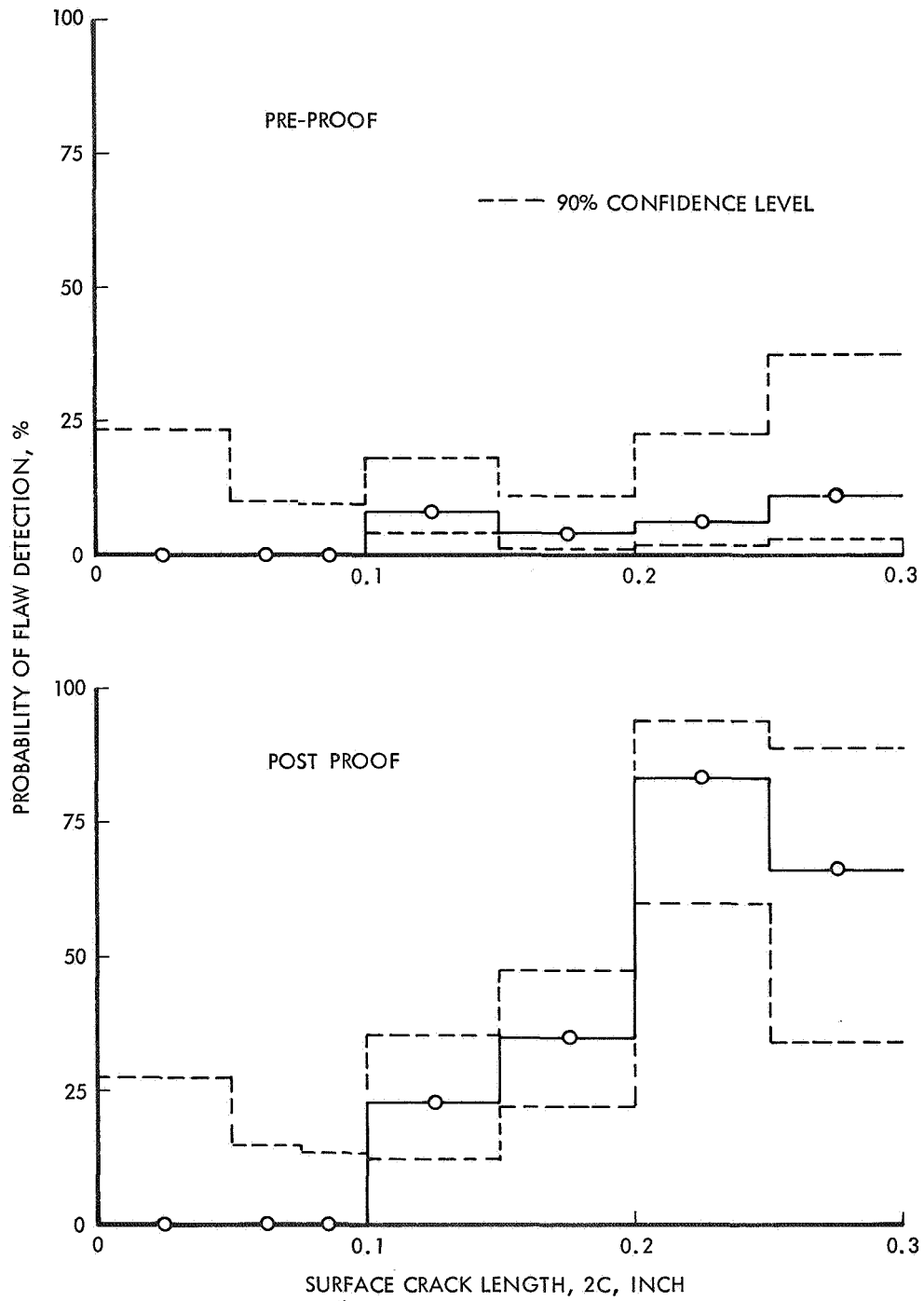
Figure 45.  Pre-Proof and Post Proof X-Ray Inspection Statistical
Analysis Results (All Data)

103
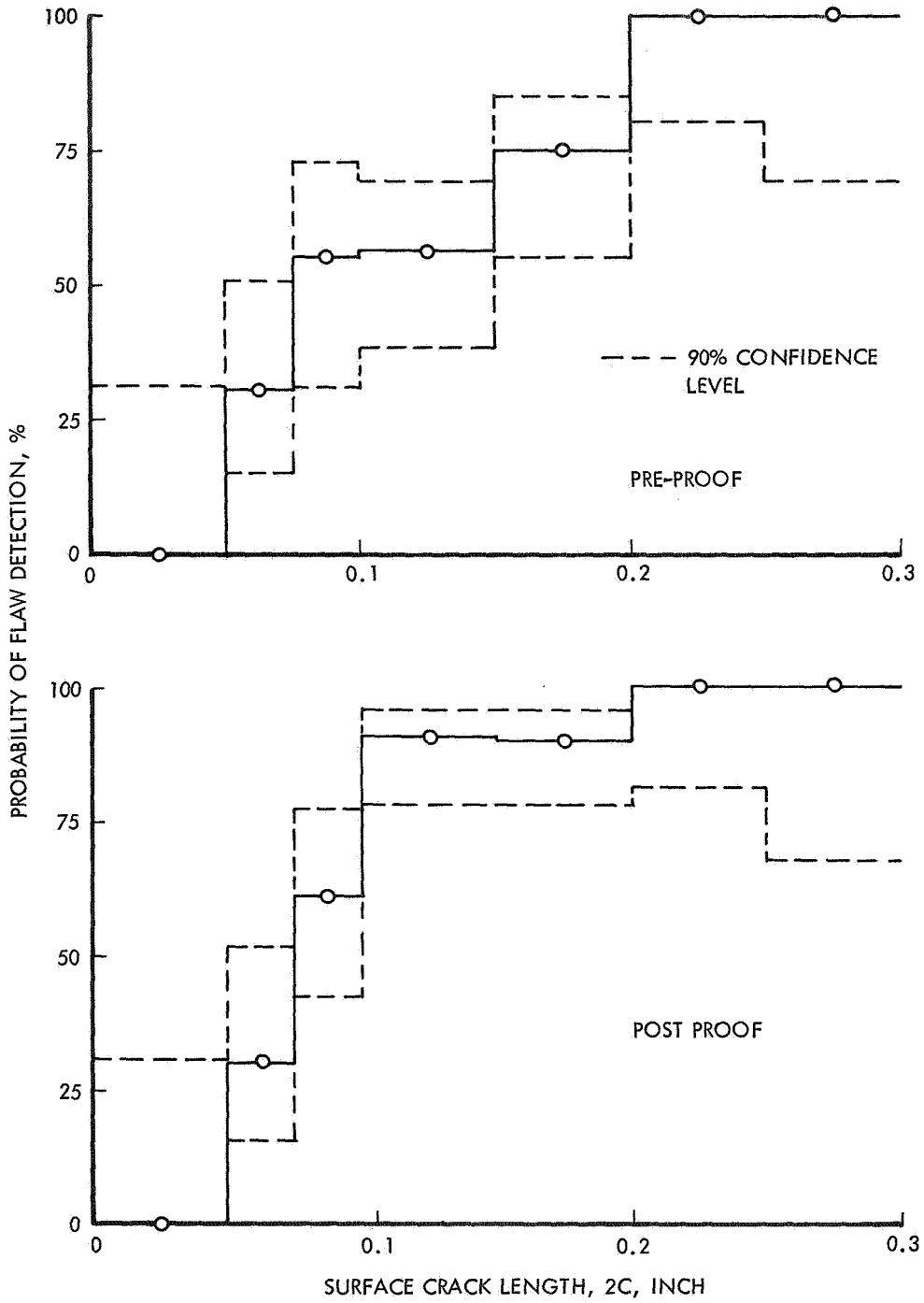
Figure 46. Pre-Proof and Post Proof Eddy Current Inspection
Statistical Analysis Results (All Data)

104
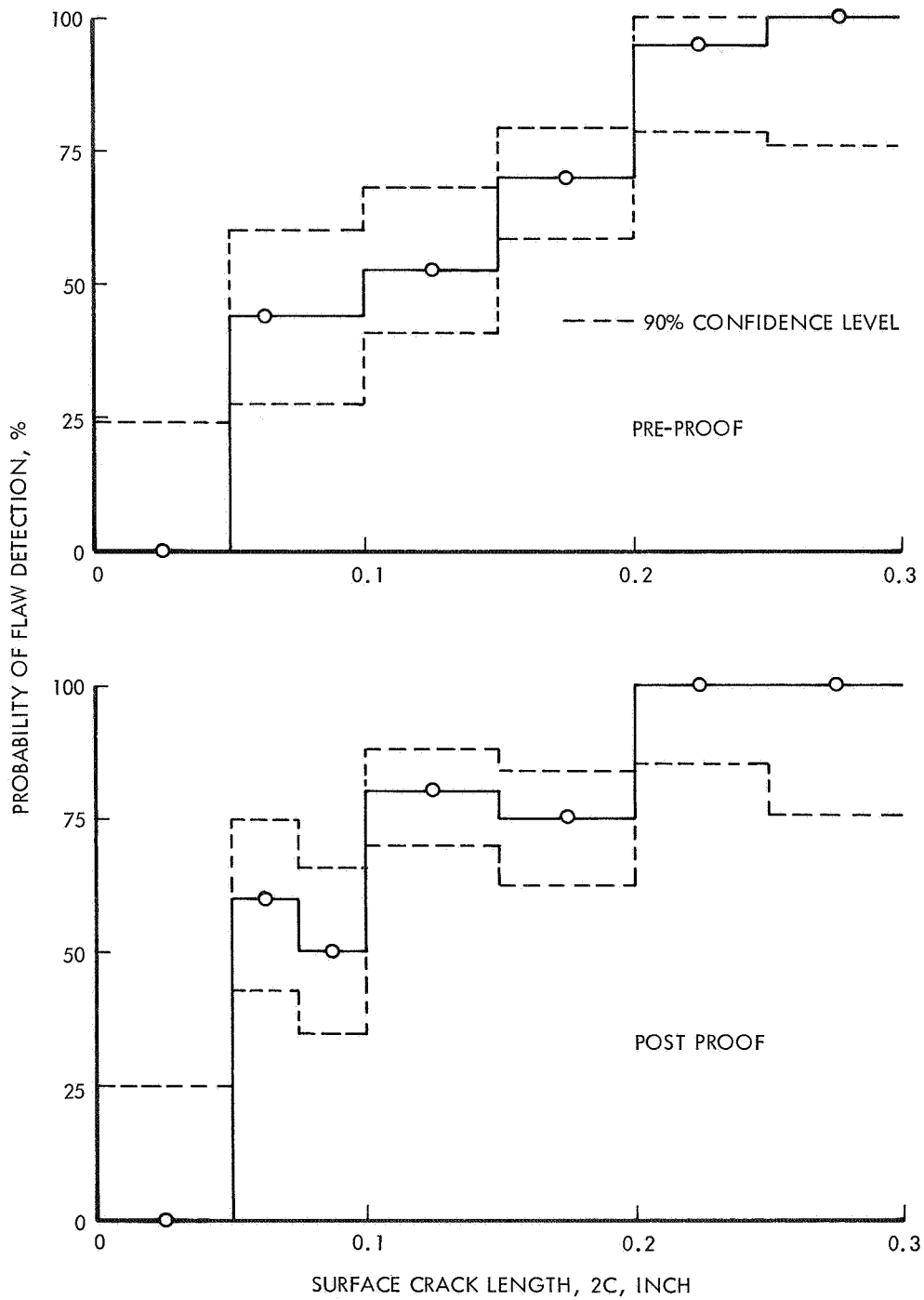
Figure 47. Pre-Proof and Post Proof Shear Wave Ultrasonic
Inspection Statistical Analysis Results (All Data)

shear wave ultrasonic and X-ray data separation becomes questionable since different gains, etc., were used for different thicknesses, parent and weld materials. However, the data base is much too small for such extensive separation of data.

For the purpose of this study, the combined data base was selected for the basis of comparison due to the limited data available for each thickness/material/laboratory combination. In essence this will yield detection limits and a ranking of the basic methods which would be applicable for all of the thickness/material conditions examined. For specific cases (i.e., thickness/material/laboratory) a smaller crack detection limit is indicated by the data but cannot be statistically verified with the small available data sample. The use of the combined data curves will thus provide conservative detection limits.

The following results indicate the tentative ranking of the various techniques and the minimum detectable surface crack length for the mean assumed probability of detection shown (no specific confidence level) based on the combined data.

| 100% Crack Detection | | 80% Crack Detection | |
|---|---|---|---|

### Pre-Proof

| 100% Crack Detection | | 80% Crack Detection | |
|---|---|---|---|
| 1. Surface Wave Ultrasonic / Penetrant / Eddy Current | $\geq$ 0.20 inch | 1. Penetrant | $\geq$ 0.05 inch |
| | | 2. Eddy Current / Shear Wave Ultrasonic / Surface Wave Ultrasonic | $\geq$ 0.20 inch |
| 2. Shear Wave Ultrasonic | $\geq$ 0.25 inch | | |
| 3. X-Ray | >>0.30 inch | 3. X-Ray | >>0.30 inch |

### Post Proof

| 100% Crack Detection | | 80% Crack Detection | |
|---|---|---|---|
| 1. Penetrant / Eddy Current / Shear Wave Ultrasonic / Surface Wave Ultrasonic | $\geq$ 0.20 inch | 1. Penetrant | $\geq$ 0.05 inch |
| | | 2. Eddy Current | $\geq$ 0.10 inch |
| | | 3. Surface Wave Ultrasonic / Shear Wave Ultrasonic | $\geq$ 0.20 inch |
| 2. X-Ray | >>0.30 inch | 4. X-Ray | >>0.30 inch |

106

Section 8


CONCLUDING DISCUSSION


As shown in the preceding sections, the use of Forman's equation to predict
the cycles-to-leak yields results which, while being generally conservative,
agrees with the trends in the data reasonably well. In general, however, the
predicted results are conservative. The source of this variation may lie
in the values used for $K_c$, since only estimated values were used. Another
source may be the use of the specific magnification factors selected. If
the elastic back surface corrections are set equal to unity, the predicted
lives typically increase as shown in Figure 48. However, while this shifts
the curve the right way, the data would indicate that a translation of the
curve rather than the translation plus slope change would provide a more
accurate expression. Thus, a further evaluation of appropriate $K_c$ values
and the constant C would seem warranted.


A comparison of the detectability limits from this program show a general
improvement in the crack size detection limits over earlier work by Packman
et al [13], particulary for the penetrant results. It should also be noted
that the work of Sattler [14] is not truly comparable since the flaw locations
were known. The statistically based detection limits are also found to be
somewhat larger than those generally given as the "detection limit" of a
typical NDI technique. This results from typical differences in definition
of "detection limit", a term sometimes used to define the smallest crack
that can "sometimes" be found as opposed to the FM/NDI definition that it is
the smallest crack that will "always" be detected to some statistical basis.


An integration of the cycles-to-leak results and the NDI capability can now
be made to estimate the feasibility of reliably obtaining a given design
life. If, for example, a design life of 1000 pressure cycles is desired,
the maximum initial flaw depths that can be tolerated as predicted by
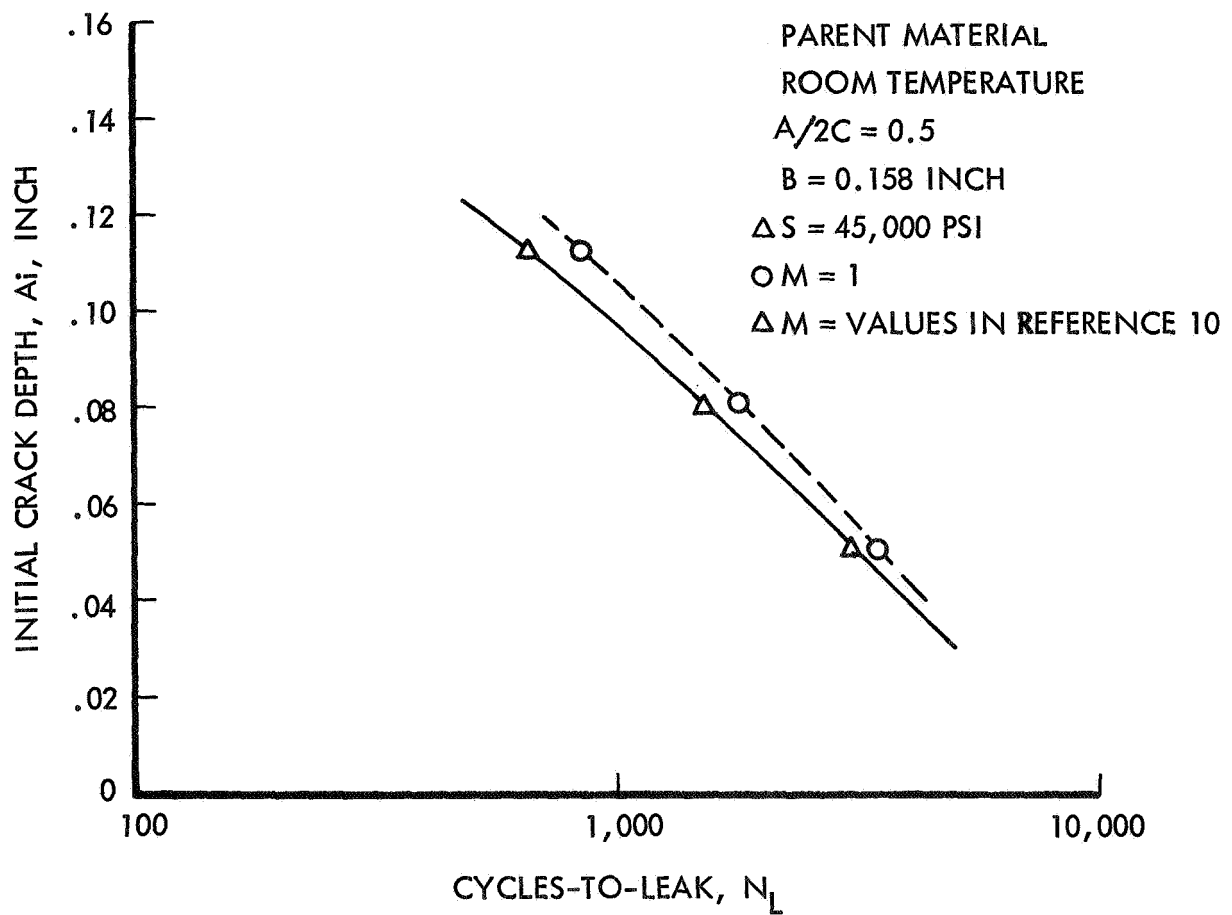
Figure 48. Effect of Back Surface Correction Factors on the
Cycles-To-Leak Predicted by Foreman's Equation

Forman's equation are summarized in Table 12 assuming a parent material stress cycle of 45,000 psi (R = 0) and a cross weld stress cycle of 20,000 psi (R = 0). The flaw depths, shown for A/2C ratios of 0.2 and 0.5, can then be converted to the corresponding surface crack length as shown. The problem now reduces to selecting the NDI procedures that will screen the given size flaw to the required confidence level in the material type and thickness in question. If the combined data penetrant results are used (2C $\geq$ 0.20 inch for 100 percent detection, $\geq$ 0.050 inch for 80 percent detection) we find that a 100 percent detection cannot be assured. If, however, we examine Figure 38 and consider the MSC penetrant results only, a crack with 2C $\geq$ 0.050 inch (no confidence level specified) would detect cracks large enough to cause failure in 1000 cycles. Thus, this procedure could be used to insure achieving the design life once this detection limit is verified statistically with additional tests.

In summary, the main conclusions that can be derived from the data in this report are as follows:

1. The Forman equation provides an adequate method of predicting the cycles-to-leak behavior of 2219-T87 parent and weld material, the results being typically conservative. The Hall equation, assuming Q constant, is not adequate and does not predict the observed trends in the cycles-to-leak data or the dA/dN data for 2219-T87 in the thickness examined.

2. A prior proof cycle does generally improve the detectability of cracks but may or may not improve the 100 percent detection limit for a given NDI method.

3. The combining of data that was required on this program to produce a sufficient data base for statistical analysis must be critically examined. In particular the development of a larger data base may well show the influence of such variables as thickness to be of significant importance for such procedures as ultrasonics and eddy current.

4. The ranking of the NDI procedures is influenced by the criteria used to evaluate the procedures.

# TABLE 13

## MAXIMUM INITIAL FLAW SIZE FOR
## 1000 CYCLE LIFE, R = 0, ROOM TEMPERATURE

| Calculated Initial Flaw Size, $(A/2C)_i$ | Sheet Thickness, B, Inch | | | | | |
|---|---|---|---|---|---|---|
| | Parent | | | Weld | | |
| | 0.04 | 0.08 | 0.16 | 0.08 | 0.16 | 0.30 |
| Calculated Initial Flaw Depth, $A_i$*, Inch | | | | | | |
| 0.2 | 0.024 | 0.042 | 0.063 | 0.054 | 0.096 | 0.146 |
| 0.5 | 0.032 | 0.056 | 0.098 | 0.075 | 0.143 | 0.250 |
| Associated Surface Crack Length, $2C_i$, Inch | | | | | | |
| 0.2 | 0.120 | 0.240 | 0.315 | 0.270 | 0.480 | 0.730 |
| 0.5 | 0.064 | 0.112 | 0.196 | 0.15 | 0.286 | 0.50 |

*Predicted using Forman's equation

Section 9

RECOMMENDATIONS

As a result of this program, several additional areas that require further study have emerged. Perhaps the area that potentially could have the largest impact is the determination of the effect of the prior proof cycle (which has been shown to be beneficial to NDI) on subsequent fatigue crack growth behavior. In particular the retardation effect of the prior proof cycle on the subsequent fatigue-crack propagation cycle may be a major effect that could change the predicted number of fatigue cycles to leak markedly. For this material it would be anticipated that the beneficial retardation effect of the residual plastic zone would offset any possible adverse crack growth effects during the proof cycle[22] and could increase the fatigue life dramatically.

A second area closely related to the effect of the prior proof cycle and its possible crack retardation effects is that of the fatigue-crack retardation under spectrum loading. Research on through cracked panels has shown that considerable variation in predicted fatigue-crack propagation rates can occur when linear cumulative damage concepts are used on spectrum data. However, virtually no work on spectrum effects and retardation effects on surface flaws has been conducted for 2219-T87.

A third area is that of the effect of plasticity and back surface magnification factors. The work in this program indicates that the use of elastic back surface magnification factors overcompensates when applied to fatigue-crack propagation of surface flaws. Additional study is required to identify whether or not these factors should be revised and consideration given to the possible relaxation at the crack tip due to the back surface rather than the magnification of the stress intensity parameter. In addition the effect of biaxial and complex loading modes on the fatigue-crack growth behavior should be evaluated for pressure vessel applications.

111

Finally, additional work is required to adequately standardize NDI procedures for use in establishing statistically significant inspection limits. More data are required to determine the validity of combining NDI data from various thickness and material tests. In addition, more work is required to examine the "human factors" that influence the reliability of a given procedure.

It is believed that additional study of these factors will be required to provide a high degree of structural integrity in spacecraft tankage structure.

# Section 10

## REFERENCES

1. G.R. Irwin, "Crack-Extension Force for a Part-Through Crack in a Plate," Journal of Applied Mechanics, V. 85, pp 651-654 (1962)

2. A.E. Green, I.N. Sneddon, "The Distribution of Stress in the Neighborhood of a Flat Elliptical Crack in an Elastic Solid," Proceedings of Cambridge Philosophical Society, V. 46, pp 159-164 (1950)

3. R.G. Forman, H.C. Kavanaugh, B. Stuckey, "Computer Analysis of Two-Dimensional Fatigue Flaw Growth Problems," NASA TM X-58086, (Feb. 1972)

4. A.S. Kobayashi, W.L. Moss, "Stress Intensity Magnification Fractures for Surface Flawed Tension Plate and Notched Round Bar," Proceedings of the Second International Conference on Fracture, Brighton, England, Paper No. 4 (April 1969)

5. R.W. Thresher, F.W. Smith, "Stress Intensity Factors for a Surface Crack in a Finite Solid,"ASME 71-APMW-6 (1971)

6. F.W. Smith, A.F. Emery, A.S. Kobayashi, "Stress Intensity Factors for Semi-Circular Cracks, Part II," Journal of Applied Mechanics, Trans. of ASME, V. 34, Series E, No. 4, pp 952-959 (December 1967)

7. A.S. Kobayashi, "On the Magnification Factors of Deep Surfaced Flaws," Structural Development Research Memorandum No. 16, The Boeing Company (December 1965)

8. F.W. Smith, "Stress Intensity Factors for a Semi-Elliptical Surface Flaw," Structural Development Research Memorandum No. 17, The Boeing Company (August 1966)

9. J.W. Masters, W.P. Haese, R.W. Finger, "Investigation of Deep Flaws in Thin Walled Tanks," NASA CR 72606 (December 1969)

10. R.C. Shah, A.S. Kobayashi, "Stress Intensity Factors for an Elliptical Crack Approaching the Surface of a Semi-Infinite Solid," submitted to International Journal of Fracture Mechanics, to be published

11. R.G. Forman, V.E. Kearney, R.M. Engle, "Numerical Analysis of Crack Propagation in Cyclic Loaded Structures," Journal of Basic Engineering Transactions of the ASME, pp 459-464 (September 1967)

12. L.R. Hall, "Plane Strain Cyclic Flaw Growth in 2014-T62 Aluminum and 6Al-4V (ELI) Titanium," NASA CR 72390

13. P.F. Packman, H.S. Pearson, G.B. Marchese, J.S. Owens, "The Applicability of a Fracture Mechanics-Nondestructive Testing Design Criterion," AFML TR-68-32 (1968)

14. F.J. Sattler, "Nondestructive Flaw Definition Techniques for Critical Defect Determination," NASA CR-72602 (Jan. 1970)

15. R.A. Cellitti, C.J. Carter, "Ultrasonic Measurement and Influence of Nonmetallic Inclusions on Fatigue and Engineering Behavior of Medium and High Strength Steels," Fatigue and Behavior of Steels, pp 288-304

16. W.M. Pless, B.L. Weil, W.H. Lewis, "Development, Fabrication, Testing, and Delivery of Advanced Filamentary Composite Nondestructive Test Standards," NAS 8-25679 (Nov. 1970)

17. Ultrasonic Testing of Materials, Edited and published by Dr. J. & H. Krautkramer, Cologne, Germany (1966)

18. D.M. Corbley, P.F. Packman, H.S. Pearson, "The Accuracy and Precision of Ultrasonic Shear Wave Flaw Measurement as a Function of Stress on the Flaw," Materials Evaluation, V. 28, p 103 (May 1970)

19. P.F. Packman, "$K_{Ic}$ and COD By Interferometry of Plastic Specimens," paper presented at Fall 1970 Meeting of ASTM Committee E-24, Philadelphia, Pennsylvania

20. Anonymous, "Development of the Ultrasonic Delta Technique for Aluminum Welds and Materials," NASA CR 61952, Automation Industries, Inc., (May 15, 1968)

21. R.G. Forman, "Fatigue Flaw Growth Behavior of 2219-T87 Aluminum at Cryogenic, Room, and Elevated Temperatures," Materials Technology Branch Report 71-ES5-1 (Sept. 1971)

22. W.L. Engstrom, "Determination of Design Allowable Properties - Fracture of 2219-T87 Aluminum Alloy," NASA CR 115388 (March 1972)

23. R.G. Forman, Private Communication

APPENDIX I

CYCLES-TO-LEAK DATA

| SPECIMEN NUMBER | THICKNESS B, INCH | INITIAL SURFACE CRACK LENGTH $2C_I$, INCH | INITIAL CRACK DEPTH $A_I$, INCH | STRESS RATIO R | MAXIMUM STRESS S, KSI | CYCLES TO LEAK $N_L$ | FINAL SURFACE CRACK LENGTH $2C_F$, INCH | FINAL CRACK DEPTH $A_F$, INCH |
|---|---|---|---|---|---|---|---|---|
| | | | 0.080-INCH THICK PARENT MATERIAL | | | | | |
| A-1-B26 | .082 | .078 | .021 | 0 | 45 | 4,884 | .200 | .082 |
| A-1-B25 | .081 | .109 | .034 | 0 | 45 | 3,109 | .207 | .081 |
| A-1-B30 | .082 | .158 | .046 | 0 | 45 | 1,414 | .253 | .082 |
| A-1-B15 | .082 | .102 | .034 | 0 | 39 | 4,824 | .212 | .082 |
| A-1-B10 | .082 | .109 | .037 | 0 | 39 | 3,377 | .213 | .082 |
| A-1-B14 | .082 | .131 | .036 | 0 | 39 | 3,022 | .221 | .082 |
| A-1-B36 | .082 | .087 | .024 | 0 | 28 | 15,090 | .199 | .082 |
| A-1-B13 | .082 | .111 | .044 | 0 | 28 | 10,465 | .202 | .082 |
| A-1-B31 | .080 | .141 | .042 | 0 | 28 | 8,721 | .218 | .080 |
| A-1-B22 | .081 | .085 | .026 | 0 | 45 | 5,349 | .179 | .081 |
| A-1-B33 | .081 | .120 | .040 | 0 | 45 | 2,882 | .256 | .081 |
| A-1-B23 | .080 | .160 | .046 | 0 | 45 | 1,701 | .267 | .080 |
| A-1-B6 | .082 | .076 | .013 | 0 | 39 | 5,000DNL | .112 | .050 |
| A-1-B18 | .082 | .132 | .039 | 0 | 39 | 2,898 | .221 | .082 |
| A-1-B12 | .082 | .283 | .051 | 0 | 39 | 795 | .334 | .082 |
| A-1-B9 | .080 | .039 | .019 | 0 | 28 | 20,000DNL | .063 | .030 |
| A-1-B19 | .079 | .140 | .032 | 0 | 28 | 8,773 | .209 | .079 |
| A-1-B32 | .080 | .157 | .041 | 0 | 28 | 6,413 | .222 | .080 |
| | | | 0.160-INCH THICK PARENT MATERIAL | | | | | |
| C1-24 | .157 | .251 | .104 | 0 | 45 | 886 | .450 | .157 |
| C1-11 | .156 | .180 | .084 | 0 | 45 | 1,941 | .450 | .156 |
| C1-23 | .155 | .112 | .055 | 0 | 45 | 5,175 | .405 | .155 |
| C1-12 | .160 | .258 | .111 | 0 | 39 | 1,383 | .401 | .160 |
| C1-2 | .158 | .159 | .080 | 0 | 39 | 3,258 | .432 | .158 |
| C1-14 | .158 | .125 | .055 | 0 | 39 | 5,701 | .407 | .158 |
| C1-5 | .160 | .276 | .123 | 0 | 28 | 3,028 | .377 | .160 |
| C1-3 | .158 | .247 | .110 | 0 | 28 | 4,169 | .390 | .158 |
| C1-1 | .160 | .194 | .091 | 0 | 28 | 6,334 | .330 | .160 |
| C1-15 | .156 | .274 | .133 | 0.5 | 45 | 2,166 | .455 | .156 |
| C1-25 | .156 | .161 | .080 | 0.5 | 45 | 10,181 | .500 | .156 |
| C1-32 | .158 | .286 | .135 | 0.5 | 28 | 8,164 | .380 | .158 |
| C1-29 | .157 | .180 | .085 | 0.5 | 28 | 20,000DNL* | .253 | .105 |
| C1-27 | .158 | .350 | .138 | 0 | 45 | 60 | .403 | .158 |
| C1-20 | .155 | .268 | .074 | 0 | 45 | 1,348 | .520 | .155 |
| C1-16 | .155 | .140 | .046 | 0 | 45 | 4,008 | .480 | .155 |
| F1-37 | .157 | .317 | .110 | 0 | 39 | 2,340 | .410 | .157 |
| C1-17 | .157 | .239 | .070 | 0 | 39 | 4,213 | .482 | .157 |
| C1-35 | .158 | .100 | .020 | 0 | 39 | 18,305** | .420 | .158 |
| C1-38 | .157 | .310 | .135 | 0 | 28 | 1,732 | .379 | .157 |
| C1-6 | .158 | .400 | .110 | 0 | 28 | 3,745 | .520 | .158 |
| C1-21 | .159 | .247 | .073 | 0 | 28 | 7,567 | .457 | .159 |
| F1-31 | .157 | .401 | .089 | 0 | 45 | 609 | .565 | .157 |
| F1-19 | .159 | .302 | .081 | 0 | 45 | 978 | .532 | .159 |
| C1-22 | .156 | .213 | .052 | 0 | 45 | 2,481 | .496 | .156 |
| F1-26 | .159 | .465 | .093 | 0 | 39 | 904 | .573 | .159 |
| C1-28 | .158 | .305 | .071 | 0 | 39 | 2,001 | .540 | .158 |
| C1-36 | .158 | .223 | .062 | 0 | 39 | 3,433 | .433 | .158 |
| C1-8 | .156 | .566 | .101 | 0 | 28 | 1,703 | .705 | .156 |
| F1-4 | .157 | .377 | .090 | 0 | 28 | 3,655 | .501 | .157 |
| C1-7 | .159 | .289 | .078 | 0 | 28 | 6,066 | .485 | .159 |
| F1-33 | .157 | .455 | .093 | 0.5 | 45 | 1,592 | .587 | .157 |
| C1-30 | .156 | .382 | .072 | 0.5 | 45 | 6,682 | .685 | .156 |
| C1-34 | .157 | .320 | .118 | 0.5 | 28 | 7,344 | .408 | .157 |
| C1-10 | .159 | .421 | .088 | 0.5 | 28 | 14,757 | .561 | .159 |

*DNL - Did Not Leak

**Crack Not Completely Out of EDM

# TABLE I-1. RESULTS OF ROOM TEMPERATURE CYCLES-TO-LEAK TESTS FOR PARENT 2219-T87 (CONTINUED)

| SPECIMEN NUMBER | THICKNESS B, INCH | INITIAL SURFACE CRACK LENGTH $2C_I$, INCH | INITIAL CRACK DEPTH $A_I$, INCH | STRESS RATIO R | MAXIMUM STRESS S, KSI | CYCLES TO LEAK $N_L$ | FINAL SURFACE CRACK LENGTH $2C_F$, INCH | FINAL CRACK DEPTH $A_F$, INCH |
|---|---|---|---|---|---|---|---|---|
| | | | 0.040-INCH THICK PARENT MATERIAL | | | | | |
| B-1-5 | .042 | .038 | .016 | 0 | 45 | 5,687DNL* | .085 | .040 |
| B-1-47 | .040 | .037 | .022 | 0 | 45 | 4,555 | .086 | .040 |
| B-1-3 | .042 | .056 | .029 | 0 | 45 | 1,452 | .083 | .042 |
| B-1-8 | .043 | -- | -- | 0 | 39 | Buckled First Cycle | | |
| B-1-6 | .040 | .033 | .012 | 0 | 39 | 5,041DNL | .079 | .030 |
| B-1-4 | .040 | .066 | .029 | 0 | 39 | 3,634 | .187 | .040 |
| B-1-7 | .043 | .027 | .013 | 0 | 28 | 5,000DNL | .030 | .015 |
| B-1-10 | .042 | .045 | .023 | 0 | 28 | 5,025DNL | .058 | .031 |
| B-1-9 | .042 | .080 | .038 | 0 | 28 | 993 | .087 | .041 |
| B-1-11 | .041 | .044 | .023 | 0.5 | 45 | 5,000DNL | .059 | .035 |
| B-1-13 | .041 | .069 | .030 | 0.5 | 45 | 3,878 | .087 | .041 |
| B-1-31 | .042 | .043 | .022 | 0.5 | 28 | 20,000DNL | .039 | .026 |
| B-1-14 | .042 | .061 | .027 | 0.5 | 28 | 5,000DNL | .063 | .028 |
| B-1-48 | .041 | .044 | .019 | 0 | 45 | 5,027 | .105 | .041 |
| B-1-44 | .040 | .049 | .014 | 0 | 45 | 3,288 | .106 | .040 |
| B-1-26 | .041 | .065 | .020 | 0 | 45 | 1,645 | .111 | .041 |
| B-1-45 | .041 | .032 | .010 | 0 | 39 | 11,754 | .096 | .041 |
| B-1-22 | .042 | .057 | .016 | 0 | 39 | 11,594 | .108 | .042 |
| B-1-16 | .042 | .077 | .022 | 0 | 39 | 2,709 | .125 | .042 |
| B-1-49 | .041 | .044 | .021 | 0 | 28 | 20,000DNL | .068 | .031 |
| B-1-40 | .041 | .051 | .019 | 0 | 28 | 12,038 | .102 | .041 |
| B-1-27 | .041 | .071 | .020 | 0 | 28 | 11,480 | .091 | .041 |
| B-1-46 | .041 | .036 | .020 | 0 | 45 | 5,671 | .092 | .041 |
| B-1-29 | .040 | .052 | .018 | 0 | 45 | 4,479 | .109 | .040 |
| B-1-21 | .041 | .068 | .027 | 0 | 45 | 2,008 | .110 | .041 |
| B-1-53 | .040 | .041 | .016 | 0 | 39 | 9,643 | .107 | .040 |
| B-1-15 | .042 | .068 | .022 | 0 | 39 | 3,590 | .108 | .042 |
| B-1-20 | .042 | .078 | .019 | 0 | 39 | 2,988 | .117 | .042 |
| B-1-19 | .042 | .085 | .020 | 0 | 28 | 18,826 | .113 | .042 |
| B-1-50 | .040 | .099 | .028 | 0 | 28 | 4,909 | .127 | .040 |
| B-1-43 | .042 | .118 | .032 | 0 | 28 | 3,357 | .172 | .042 |
| B-1-28 | .041 | .051 | .021 | 0.5 | 45 | 20,000DNL | .080 | .035 |
| B-1-18 | .041 | .049 | .028 | 0.5 | 45 | 6,685 | .135 | .041 |
| B-1-51 | .041 | .061 | .016 | 0.5 | 28 | 20,000DNL | .092 | .026 |
| B-1-41 | .042 | .108 | .028 | 0.5 | 28 | 20,000DNL | .132 | .038 |
| | | | 0.080-INCH THICK PARENT MATERIAL | | | | | |
| A-1-B24 | .080 | .037 | .021 | 0 | 45 | 7,123 | .179 | .080 |
| A-1-B27 | .081 | .073 | .038 | 0 | 45 | 3,412 | .181 | .081 |
| A-1-B35 | .082 | .103 | .055 | 0 | 45 | 1,508 | .184 | .082 |
| A-1-B7 | .082 | .035 | .025 | 0 | 39 | 12,526 | .182 | .082 |
| A-1-B34 | .083 | .065 | .037 | 0 | 39 | 6,980 | .183 | .083 |
| A-1-B5 | .081 | .110 | .049 | 0 | 39 | 2,111 | .172 | .081 |
| A-1-B20 | .080 | .033 | .019 | 0 | 28 | 20,000DNL | .068 | .033 |
| A-1-B3 | .081 | .064 | .034 | 0 | 28 | 17,773 | .178 | .081 |
| A-1-B21 | .080 | .102 | .050 | 0 | 28 | 6,460 | .176 | .080 |

# TABLE I-2. RESULTS FOR CROSS WELDED 2219-T87 ALUMINUM CYCLES-TO-LEAK

| SPECIMAN NUMBER | THICKNESS, B, INCH | INITIAL SURFACE CRACK LENGTH, $2c_i$, INCH | INITIAL CRACK DEPTH $A_i$, INCH | STRESS RATIO R | MAXIMUM STRESS, S, KSI | CYCLES-TO-LEAK $N_L$ | FINAL SURFACE CRACK LENGTH, $2c_f$, INCH | FINAL CRACK DEPTH, $A_f$, INCH |
|---|---|---|---|---|---|---|---|---|
| A-5-6-U | .074 | .141 | .070 | 0 | 20 | 810 | .154 | .074 |
| A-5-6-T | .073 | .134 | .065 | 0 | 20 | 2,261 | .146 | .073 |
| A-11-12-C | .067 | .110 | .052 | 0 | 20 | 6,400 | .169 | .067 |
| A-1-2-Q | .072 | .125 | .052 | 0 | 20 | 11,528 | .208 | .072 |
| A-5-6-W | .075 | .116 | .067 | 0 | 17.5 | 4,800 | .139 | .075 |
| A-5-6-R | .072 | .150 | .067 | 0 | 17.5 | 6,178 | .167 | .072 |
| A-5-6-V | .075 | .109 | .058 | 0 | 17.5 | 9,153 | .129 | .075 |
| A-11-12-H | .074 | .122 | .052 | 0 | 17.5 | 20,000 DNL | .147 | .060 |
| A-9-10P | .068 | .170 | .061 | 0.5 | 20 | 6,804 | .193 | .068 |
| A-11-12N | .070 | .153 | .059 | 0.5 | 20 | 20,000 DNL | .180 | .067 |
| A-11-12K | .076 | .170 | .075 | 0.5 | 17.5 | 1 | .170 | .076 |
| A-9-10-Y | .083 | .180 | .075 | 0 | 20 | 371 | .188 | .083 |
| A-11-12-E | .069 | .148 | .062 | 0 | 20 | 475 | .162 | .069 |
| A-9-10-S | .076 | .164 | .063 | 0 | 20 | 2,922 | .194 | .076 |
| A-1-2-Z | .081 | .158 | .061 | 0 | 20 | 8,900 | .191 | .081 |
| A-7-8-L | .072 | .164 | .072 | 0 | 17.5 | 1 | .164 | .072 |
| A-3-4-X | .077 | .142 | .063 | 0 | 17.5 | 7,400 | .176 | .077 |
| A-9-10-M | .069 | .162 | .060 | 0 | 17.5 | 11,482 | .184 | .069 |
| A-3-4-J | .068 | .142 | .051 | 0 | 17.5 | 20,000 DNL | .147 | .065 |
| A-3-4-aa | .076 | .192 | .074 | 0 | 20 | 10 | .192 | .074 |
| A-3-4-cc | .078 | .166 | .058 | 0 | 20 | 6,186 | .209 | .078 |
| A-3-4-bb | .079 | .167 | .045 | 0 | 20 | 17,101 | .204 | .079 |
| A-11-12-D | .066 | .098 | .030 | 0 | 20 | 20,000 DNL | .138 | .046 |
| A-1-2-ii | .080 | .170 | .050 | 0 | 17.5 | 6,146 | .222 | .080 |
| A-1-2-gg | .079 | .200 | .047 | 0 | 17.5 | 14,635 | .206 | .079 |
| A-1-2-ee | .079 | .204 | .046 | 0 | 17.5 | 19,364 | .230 | .079 |
| A-7-8-dd | .074 | .177 | .051 | 0 | 17.5 | 20,000 DNL | .200 | .072 |
| A-1-2kk | .079 | .210 | .043 | 0.5 | 17.5 | 20,000 DNL | .220 | .049 |
| A-1-2jj | .079 | .150 | .056 | 0.5 | 17.5 | 20,000 DNL | .155 | .060 |
| 0.16 INCH THICK, CROSS WELD RESULTS | | | | | | | | |
| D-4 | .153 | .319 | .131 | 0 | 20 | 1,542 | .391 | .153 |
| D-3 | .153 | .247 | .100 | 0 | 20 | 4,157 | .437 | .153 |
| D-1 | .158 | .149 | .068 | 0 | 20 | 17,361 | .398 | .158 |
| D-25 | .141 | .322 | .117 | 0 | 17.5 | 2,781 | .397 | .141 |
| D-8 | .155 | .269 | .112 | 0 | 17.5 | 5,703 | .403 | .155 |
| D-22 | .151 | .329 | .116 | 0 | 17.5 | 6,647 | .422 | .151 |
| D-24 | .141 | .342 | .124 | 0 | 20 | 1,252 | .413 | .141 |
| D-16 | .153 | .277 | .109 | 0 | 20 | 2,514 | .392 | .153 |
| D-17 | .144 | .197 | .077 | 0 | 20 | 6,157 | .375 | .144 |
| D-10 | .155 | .448 | .144 | 0 | 17.5 | 334 | .464 | .155 |
| D-19 | .154 | .285 | .100 | 0 | 17.5 | 12,427 | .404 | .154 |
| D-18 | .155 | .217 | .072 | 0 | 17.5 | 20,000 DNL* | .612 | .144 |

# TABLE I-2. RESULTS FOR CROSS WELDED 2219-T87 ALUMINUM CYCLES-TO-LEAK (CONTINUED)

| SPECIMEN NUMBER | THICKNESS B, INCH | INITIAL SURFACE CRACK DEPTH $2c_i$, INCH | INITIAL CRACK DEPTH $A_i$, INCH | STRESS RATIO R | MAXIMUM STRESS S, KSI | CYCLES-TO-LEAK $N_L$ | FINAL SURFACE CRACK LENGTH $2c_f$, INCH | FINAL CRACK DEPTH $A_f$, INCH |
|---|---|---|---|---|---|---|---|---|
| | | | 0.16 INCH THICK, CROSS WELD RESULTS | | | | | |
| D-2 | .146 | .412 | .096 | 0 | 20 | 1,137 | .505 | .146 |
| D-9 | .146 | .348 | .085 | 0 | 20 | 7,444 | .475 | .146 |
| D-7 | .147 | .229 | .054 | 0 | 20 | 11,593 | .441 | .147 |
| D-5 | .154 | .459 | .100 | 0 | 17.5 | 2,287 | .549 | .154 |
| D-6 | .145 | .350 | .080 | 0 | 17.5 | 4,421 | .457 | .145 |
| D-13 | .160 | .273 | .070 | 0 | 17.5 | 17,366 | .471 | .160 |
| | | | 0.30 INCH THICK CROSS-WELD | | | | | |
| C-2 | .290 | .580 | .249 | 0 | 20 | 532 | .745 | .290 |
| C-1 | .291 | .462 | .201 | 0 | 20 | 2,807 | .816 | .291 |
| C-5 | .307 | .380 | .188 | 0 | 20 | 5,840 | .740 | .307 |
| C-3 | .302 | .570 | .255 | 0 | 17.5 | 1,200 | .746 | .302 |
| C-4 | .298 | .590 | .236 | 0 | 17.5 | 3,028 | .822 | .298 |
| C-13 | .305 | .462 | .219 | 0 | 17.5 | 4,966 | .653 | .305 |
| C-15 | .300 | .614 | .265 | 0.5 | 20 | 3,514 | .690 | .300 |
| C-14 | .295 | .565 | .238 | 0.5 | 20 | 6,700 | .755 | .295 |
| C-16 | .287 | .642 | .292 | 0.5 | 17.5 | 19 | .660 | .287 |
| C-17 | .297 | .559 | .240 | 0.5 | 17.5 | 19,773 | .777 | .297 |
| C-6 | .302 | .492 | .200 | 0 | 20 | 1,559 | .675 | .302 |
| C-7 | .296 | .442 | .187 | 0 | 20 | 1,914 | .683 | .296 |
| C-8 | .298 | .415 | .181 | 0 | 20 | 2,288 | .681 | .300 |
| C-12 | .300 | .584 | .215 | 0 | 17.5 | 3,985 | .753 | .300 |
| C-11 | .300 | .532 | .206 | 0 | 17.5 | 4,845 | .805 | .300 |
| C-10 | .287 | .455 | .175 | 0 | 17.5 | 5,653 | .615 | .287 |
| C-19 | .297 | .987 | .169 | 0 | 20 | 697 | 1.067 | .297 |
| C-9 | .286 | .846 | .173 | 0 | 20 | 757 | 1.069 | .286 |
| C-20 | .298 | .594 | .134 | 0 | 20 | 4,378 | 0.935 | .297 |
| C-21 | .296 | .774 | .162 | 0 | 17.5 | 1,748 | .971 | .296 |
| C-22 | .288 | .826 | .158 | 0 | 17.5 | 2,359 | 1.070 | .288 |
| C-18 | .300 | .672 | .220 | 0 | 17.5 | 2,974 | .907 | .300 |
| C-25 | .294 | .781 | .167 | 0.5 | 20 | 7,792 | 0.978 | .294 |
| C-23 | .302 | .860 | .167 | 0.5 | 20 | 10,823 | 1.024 | .302 |
| C-26 | .297 | .963 | .264 | 0.5 | 17.5 | 350 | 1.017 | .297 |
| C-24 | .300 | .975 | .168 | 0.5 | 17.5 | 10,960 | 1.211 | .300 |

DNL - DID NOT LEAK

## TABLE I-3. RESULTS OF ROOM TEMPERATURE CYCLE-TO-LEAK TESTS FOR LONGITUDINAL WELD 2219-T87

| SPECIMEN NUMBER | THICKNESS B, INCH | INITIAL SURFACE CRACK LENGTH $2c_I$, INCH | INITIAL CRACK DEPTH $A_I$, INCH | STRESS RATIO R | MAXIMUM STRESS S, KSI | CYCLES TO LEAK N | FINAL SURFACE CRACK LENGTH $2c_F$, INCH | FINAL CRACK DEPTH $A_F$, INCH |
|---|---|---|---|---|---|---|---|---|
| 0.080 INCH THICK, LONGITUDINAL WELD, FLAW AT WELD CENTER |
| B-2 | 0.080 | 0.141 | 0.067 | 0 | 20 | 5,883 | 0.195 | 0.080 |
| B-3 | 0.081 | 0.129 | 0.060 | 0 | 20 | 20,000DNL | 0.146 | 0.065 |
| B-4 | 0.079 | 0.156 | 0.070 | 0 | 17.5 | 6,720 | 0.180 | 0.079 |
| B-5 | 0.080 | 0.142 | 0.065 | 0 | 17.5 | 20,000DNL | 0.156 | 0.071 |
| B-10 | 0.079 | 0.262 | 0.054 | 0 | 20 | 2,993 | 0.288 | 0.079 |
| B-7 | 0.080 | 0.232 | 0.050 | 0 | 20 | 6,432 | 0.273 | 0.080 |
| B-15 | 0.080 | 0.185 | 0.039 | 0 | 17.5 | 20,000DNL | 0.258 | 0.048 |
| B-17 | 0.080 | 0.177 | 0.040 | 0 | 17.5 | 20,000DNL | 0.177 | 0.043 |
| 0.080 INCH THICK, LONGITUDINAL WELD, FLAW AT WELD EDGE |
| B-9 | 0.081 | 0.158 | 0.078 | 0 | 20 | 116 | 0.163 | 0.081 |
| B-11 | 0.081 | 0.104 | 0.054 | 0 | 20 | 20,000DNL | 0.127 | 0.065 |
| B-8 | 0.083 | 0.167 | 0.078 | 0 | 17.5 | 366 | 0.179 | 0.083 |
| B-14 | 0.081 | 0.157 | 0.067 | 0 | 17.5 | 7,562 | 0.201 | 0.081 |
| B-13 | 0.080 | 0.194 | 0.060 | 0 | 20 | 2,874 | 0.225 | 0.080 |
| B-16 | 0.082 | 0.235 | 0.045 | 0 | 20 | 4,723 | 0.283 | 0.082 |
| B-20 | 0.081 | 0.260 | 0.080 | 0 | 17.5 | 1 | 0.260 | 0.081 |
| B-19 | 0.081 | 0.199 | 0.065 | 0 | 17.5 | 3,979 | 0.271 | 0.081 |
| 0.16 INCH THICK, LONGITUDINAL WELD, FLAW AT WELD CENTER |
| F-7 | 0.157 | 0.306 | 0.144 | 0 | 20 | 2,470 | 0.349 | 0.157 |
| F-16 | 0.157 | 0.253 | 0.126 | 0 | 20 | 20,000DNL | 0.266 | 0.140 |
| F-15 | 0.158 | 0.322 | 0.157 | 0 | 17.5 | 2,260 | 0.335 | 0.158 |
| F-14 | 0.158 | 0.253 | 0.129 | 0 | 17.5 | 20,000DNL | 0.266 | 0.137 |
| F-4 | 0.159 | 0.471 | 0.106 | 0 | 20 | 2,966 | 0.529 | 0.159 |
| F-2 | 0.159 | 0.351 | 0.094 | 0 | 20 | 7,437 | 0.431 | 0.159 |
| F-8 | 0.160 | 0.487 | 0.095 | 0 | 17.5 | 3,422 | 0.550 | 0.160 |
| F-5 | 0.163 | 0.379 | 0.086 | 0 | 17.5 | 13,580 | 0.452 | 0.163 |
| 0.16 INCH THICK, LONGITUDINAL WELD, FLAW AT WELD EDGE |
| F-12 | 0.159 | 0.305 | 0.133 | 0 | 20 | 2,246 | 0.365 | 0.159 |
| F-13 | 0.160 | 0.254 | 0.130 | 0 | 20 | 3,309** | 0.315 | 0.153 |
| F-11 | 0.163 | 0.367 | 0.162 | 0 | 17.5 | 23 | 0.368 | 0.163 |
| F-10 | 0.159 | 0.298 | 0.112 | 0 | 17.5 | 12,217 | 0.400 | 0.159 |
| F-1 | 0.159 | 0.512 | 0.104 | 0 | 20 | 1,872 | 0.571 | 0.159 |
| F-3 | 0.161 | 0.391 | 0.092 | 0 | 20 | 4,872 | 0.490 | 0.161 |
| F-9 | 0.156 | 0.483 | 0.100 | 0 | 17.5 | 3,648 | 0.549 | 0.156 |
| F-6 | 0.159 | 0.433 | 0.090 | 0 | 17.5 | 5,548 | 0.544 | 0.159 |
| 0.30 INCH THICK LONGITUDINAL WELD, FLAW AT WELD CENTERLINE |
| L-2 | 0.300 | 0.548 | 0.231 | 0 | 20 | 3,182 | 0.678 | 0.300 |
| L-1 | 0.298 | 0.420 | 0.185 | 0 | 20 | 8,770 | 0.633 | 0.298 |
| L-4 | 0.304 | 0.601 | 0.271 | 0 | 17.5 | 2,852 | 0.691 | 0.304 |
| L-3 | 0.299 | 0.501 | 0.218 | 0 | 17.5 | 12,344 | 0.702 | 0.299 |

TABLE I-3. RESULTS OF ROOM TEMPERATURE CYCLE-TO-LEAK TESTS FOR LONGITUDINAL WELD 2219-T87 (CONTINUED)

| SPECIMEN NUMBER | THICKNESS B, INCH | INITIAL SURFACE CRACK LENGTH $2C_I$, INCH | INITIAL CRACK DEPTH $A_I$, INCH | STRESS RATIO R | MAXIMUM TO LEAK N | CYCLES TO LEAK N | FINAL SURFACE CRACK LENGTH $2C_F$, INCH | FINAL CRACK DEPTH $A_F$, INCH |
|---|---|---|---|---|---|---|---|---|
| | | | 0.30 INCH THICK LONGITUDINAL WELD, FLAW AT WELD CENTERLINE | | | | | |
| L-10 | 0.307 | 0.971 | 0.175 | 0 | 20 | 2,274 | 1.113 | 0.307 |
| L-7 | 0.307 | 0.751 | 0.166 | 0 | 20 | 4,141 | 0.863 | 0.307 |
| L-12 | 0.296 | 1.000 | 0.280 | 0 | 17.5 | 6 | 1.040 | 0.296 |
| L-16 | 0.296 | 0.701 | 0.162 | 0 | 17.5 | 8,244 | 0.954 | 0.296 |
| | | | 0.30 INCH THICK LONGITUDINAL WELD, FLAW AT WELD EDGE | | | | | |
| L-6 | 0.298 | 0.554 | 0.246 | 0 | 20 | 1,881 | 0.709 | 0.298 |
| L-5 | 0.300 | 0.507 | 0.218 | 0 | 20 | 2,972 | 0.667 | 0.300 |
| L-8 | 0.300 | 0.555 | 0.255 | 0 | 17.5 | 2,416 | 0.648 | 0.300 |
| L-9 | 0.299 | 0.475 | 0.228 | 0 | 17.5 | 15,932 | 0.702 | 0.299 |
| L-15 | 0.302 | 1.002 | 0.218* | 0 | 20 | 3,652 | 1.150 | 0.302 |
| L-14 | 0.298 | 0.792 | 0.133 | 0 | 20 | 5,936 | 0.968 | 0.298 |
| L-17 | 0.305 | 0.885 | 0.174 | 0 | 17.5 | 4,231 | 1.078 | 0.305 |
| L-13 | 0.300 | 0.577 | 0.168 | 0 | 17.5 | 12,676 | 0.883 | 0.300 |

*DNL - Did Not Leak
**Machine Malfunction

## TABLE I-4. CYCLES-TO-LEAK RESULTS FOR PARENT AND CROSS WELD 2219-T8 AT 300°

| MATERIAL CONDITION | SPECIMEN NUMBER | THICKNESS INCH | INITIAL SURFACE CRACK LENGTH, $2c_i$, INCH | INITIAL CRACK DEPTH, $A_i$, INCH | STRESS RATIO, R | STRESS KSI | CYCLES-TO-LEAK, $N_L$ | FINAL SURFACE CRACK LENGTH, $2c_f$, INCH | FINAL CRACK DEPTH, $A_f$, INCH |
|---|---|---|---|---|---|---|---|---|---|
| Parent | HP1 | .042 | .060 | .033 | 0 | 36 | 2,461 | .098 | thru |
| | HP3 | .042 | .051 | .024 | 0 | 36 | 4,253 | .123 | thru |
| | HP4 | .043 | .063 | .033 | 0 | 23 | 12,238 | .129 | thru |
| | HP2 | .042 | .063 | .033 | 0 | 23 | 17,195 | .128 | thru |
| Parent | HP5 | .042 | .096 | .027 | 0 | 36 | 1.891 | .143 | thru |
| | HP15 | .042 | .106 | .038 | 0 | 23 | 2,553 | .129 | thru |
| | HP9 | .042 | .094 | .032 | 0 | 36 | 1,932 | .151 | thru |
| | HP16 | .041 | .101 | .026 | 0 | 23 | 4,448 | .156 | thru |
| Parent | HP7 | .157 | .375 | .133 | 0 | 36 | 183 | .447 | thru |
| | HP11 | .156 | .236 | .108 | 0 | 36 | 1,379 | .410 | thru |
| | HP14 | .159 | .310 | .136 | 0 | 23 | 5,668 | .503 | thru |
| | HP13 | .159 | .292 | .132 | 0 | 23 | 8,408 | .479 | thru |
| Parent | HP6 | .158 | .504 | .101 | 0 | 36 | 513 | .732 | thru |
| | HP10 | .156 | .294 | .070 | 0 | 36 | 2,037 | .710 | thru |
| | HP12 | .158 | .546 | .094 | 0 | 23 | 3,936 | .732 | thru |
| | HP8 | .158 | .658 | .240 | 0 | 23 | 4,655 | .861 | thru |
| Cross Weld | HC11 | .082 | .131 | .069 | 0 | 17.5 | 2,383 | .178 | thru |
| | HC10 | .080 | .131 | .046 | 0 | 17.5 | 12,173 | .208 | thru |
| | HC12 | .070 | .170 | .070 | 0 | 15 | 2 | .170 | thru |
| | HC16 | .081 | .112 | .048 | 0 | 15 | 20,000 | .180 | .074 |
| Cross Weld | HC15 | .071 | .190 | .040 | 0 | 17.5 | 2,863 | .217 | thru |
| | HC14 | .080 | .138 | .039 | 0 | 17.5 | 9,659 | .209 | thru |
| | HC13 | .076 | .208 | .062 | 0 | 15 | 3,401 | .248 | thru |
| | HC17 | Void | | | | | | | |
| Cross Weld | HC2 | .290 | .547 | .270 | 0 | 15 | 560 | .665 | thru |
| | HC1 | .296 | .531 | .219 | 0 | 17.5 | 2,587 | .836 | thru |
| | HC6 | .294 | .631 | .238 | 0 | 15 | 1,133 | .693 | thru |
| | HC7 | Void | | | | | | | |
| Cross Weld | HC5 | .303 | 1.432 | .204 | 0 | 17.5 | 300 | 1.486 | thru |
| | HC4 | .303 | 1.183 | .195 | 0 | 15 | 667 | 1.322 | thru |
| | HC8 | .300 | .651 | .241 | 0 | 15 | 2,357 | .853 | thru |

APPENDIX II

NDI FIAW DETECTION DATA

# TABLE II-1. NDI FLAW DETECTION RESULTS FOR SPECIMENS CONTAINING UNKNOWN CRACKS

I - LOCKHEED CALIFORNIA COMPANY
II - MAGNAFLUX
III - NASA/MSC

X - DETECTED
X - POSSIBLE FLAW REPORTED
O - NOT DETECTED

\* NOT CONDUCTED

| SPECIMEN | NOMINAL THICKNESS $B_1$ INCH | MEASURED CRACK SIZE $2c_1$ INCH | MEASURED CRACK SIZE $A_1$ INCH | PENETRANT (2c REPORTED) PREPROOF I | PREPROOF II | PREPROOF III | POSTPROOF I | POSTPROOF II | POSTPROOF III | X-RAY PREPROOF I | PREPROOF II | PREPROOF III | POSTPROOF I | POSTPROOF II | POSTPROOF III | EDDY CURRENT PREPROOF I | PREPROOF II | POSTPROOF I | POSTPROOF II | SHEAR WAVE PREPROOF I | PREPROOF II | PREPROOF III | POSTPROOF I | POSTPROOF II | POSTPROOF III | SURFACE WAVE PREPROOF III | POSTPROOF III |
|---|---|---|---|---|---|---|---|---|---|---|---|---|---|---|---|---|---|---|---|---|---|---|---|---|---|---|---|
| | | | | | | | P A R E N T   S P E C I M E N S | | | | | | | | | | | | | | | | | | | | |
| 1 | .040 | .077 | .023 | .090 | .094 | X | .090 | .094 | X | 0 | 0 | 0 | * | 0 | 0 | X | X | X | X | X | X | X | X | * | X | X | X |
| | | .102 | .028 | .100 | .110 | X | .130 | .110 | X | 0 | 0 | 0 | * | 0 | X | X | O | X | O | X | X | X | X | * | X | X | X |
| | | .092 | .025 | .100 | .110 | X | .100 | .110 | X | 0 | 0 | 0 | * | 0 | 0 | X | X | X | X | X | X | O | X | * | X | X | X |
| | | .076 | .013 | 0 | 0 | X | 0 | 0 | X | 0 | 0 | 0 | * | 0 | 0 | 0 | 0 | 0 | 0 | O | O | O | O | * | O | O | O |
| 2 | .040 | .055 | .015 | .050 | 0 | X | .050 | 0 | X | 0 | 0 | 0 | * | 0 | 0 | X | X | X | X | X | X | O | X | * | O | O | O |
| | | .166 | Through | .175T | .19T | X | .20T | .14T | X | 0 | 0 | 0 | * | X | X | X | X | X | X | X | X | X | X | * | X | X | X |
| A | .040 | None | -- | -- | -- | -- | -- | -- | -- | -- | -- | -- | -- | -- | -- | -- | -- | -- | -- | -- | -- | -- | -- | -- | -- | -- | -- |
| 24 | .080 | .056 | .020 | .050 | .062 | X | .060 | .094 | X | 0 | 0 | 0 | * | 0 | 0 | O | O | X | O | X | X | X | O | X | X | X | X |
| | | .051 | .024 | .060 | .062 | X | .050 | .062 | X | 0 | 0 | 0 | * | 0 | 0 | O | X | O | O | O | X | O | X | O | X | O | X |
| | | .064 | .019 | .075 | .062 | X | .060 | .062 | X | 0 | 0 | 0 | * | X | X | X | O | O | O | X | X | X | X | X | X | X | X |
| | | .229 | Through | .230T | .232T | X | .250T | .250T | X | 0 | 0 | X | * | X | X | X | X | X | X | X | X | X | X | X | X | X | X |
| | | .265 | Through | .300T | .280T | X | .300T | .310T | X | 0 | 0 | 0 | * | 0 | 0 | X | X | X | X | X | X | O | X | O | X | X | X |
| | | .058 | .021 | .075 | .062 | X | .060 | .062 | X | 0 | 0 | 0 | * | 0 | 0 | O | O | O | O | X | O | O | X | O | O | O | O |
| 23 | .080 | .093 | .037 | .070 | .094 | X | .100 | .094 | X | 0 | 0 | 0 | * | 0 | 0 | X | X | X | X | X | X | X | X | X | O | O | X |
| | | .171 | .056 | .175 | .187 | X | .200 | .187 | X | 0 | 0 | 0 | * | X | X | X | O | X | X | X | X | X | X | X | X | X | X |
| | | .193 | .068 | .200 | .200 | X | .220 | .200 | X | 0 | 0 | 0 | * | X | X | X | X | X | X | X | X | X | X | X | X | X | X |
| | | .039 | .011 | 0 | 0 | X | 0 | 0 | X | 0 | 0 | 0 | * | 0 | 0 | O | O | O | X | O | O | O | X | O | O | O | O |
| | | .027 | .013 | 0 | 0 | O | 0 | 0 | O | 0 | 0 | 0 | * | 0 | 0 | O | O | O | X | O | O | O | X | O | O | O | X |
| 3 | .160 | .151 | .062 | .140 | .156 | X | .170 | .187 | X | 0 | 0 | 0 | * | X | X | X | X | X | X | X | X | X | X | X | O | X | X |
| | | .147 | .068 | .110 | .125 | X | .170 | .187 | X | 0 | 0 | 0 | * | X | X | O | O | X | X | X | X | X | X | X | X | X | X |
| | | .233 | .098 | .210 | X | X | .260 | .250 | X | 0 | 0 | 0 | * | X | X | X | X | X | X | X | X | X | X | X | X | X | X |
| | | .242 | .099 | .250 | .235 | X | .260 | .280 | X | 0 | 0 | 0 | * | X | X | X | X | X | X | X | X | X | X | X | X | X | X |
| | | .212 | .082 | .210 | .156 | X | .250 | .265 | X | 0 | 0 | 0 | * | X | X | X | X | X | X | X | X | X | X | X | X | X | X |
| 4 | .160 | .073 | .028 | .060 | .062 | X | .070 | .078 | X | 0 | 0 | 0 | * | 0 | 0 | X | X | X | X | O | O | O | O | O | X | O | O |
| | | .070 | .026 | .075 | .062 | X | .070 | .090 | X | 0 | 0 | 0 | * | X | X | X | X | X | X | X | X | X | X | O | X | X | O |
| | | .094 | .039 | .100 | .078 | X | .100 | .110 | X | 0 | 0 | 0 | * | X | X | X | X | X | X | X | X | X | X | O | X | X | X |
| | | .140 | .053 | .150 | .156 | X | .150 | .156 | X | 0 | 0 | 0 | * | X | X | X | X | X | X | X | X | X | X | O | X | X | X |
| | | .175 | .071 | .200 | .172 | X | .200 | .187 | X | 0 | 0 | 0 | * | O | O | X | O | X | O | X | O | O | X | O | X | X | X |
| | | .253 | .103 | .275 | .250 | X | .250 | .260 | X | 0 | 0 | 0 | * | X | X | X | X | X | X | X | X | X | X | X | X | X | X |
| | | | | | | | P A R E N T   S P E C I M E N S   W I T H   R I S E R S | | | | | | | | | | | | | | | | | | | | |
| E | .080 | .175 | .063 | .150 | .187 | X | Failed Thru Flaw | Failed Thru Flaw | X | 0 | 0 | 0 | Failed Thru Flaw | X | X | Failed-Flaw | X | Failed-Flaw | X | * | O | X | Failed Thru Flaw | Failed Thru Flaw | X | X | Failed |
| | | .081 | .029 | .070 | .062 | X | .075 | .062 | O | 0 | 0 | 0 | * | O | O | * | O | * | O | * | O | O | * | O | O | X | O |
| | | .128 | .019 | 0 | 0 | O | .125 | .187 | X | 0 | 0 | 0 | * | X | X | * | O | * | O | * | O | X | O | O | X | X | X |

I - LOCKHEED CALIFORNIA COMPANY
II - MAGNAFLUX
III - NASA/MSC

X - DETECTED
X - POSSIBLE FLAW REPORTED
O - NOT DETECTED

| SPECIMEN | NOMINAL THICKNESS $B_1$ INCH | MEASURED CRACK SIZE $2C_1$ INCH | MEASURED CRACK SIZE $A_1$ INCH | PENETRANT (2C REPORTED) PREPROOF I | PREPROOF II | PREPROOF III | POSTPROOF I | POSTPROOF II | POSTPROOF III |
|---|---|---|---|---|---|---|---|---|---|
| F | .160 | .202 | .039 | 0 | X | X | .250 | .187 | X |
| | | .070 | .010 | 0 | 0 | 0 | .060 | 0 | X |
| | | .090 | .019 | 0 | 0 | X | .090 | .062 | X |
| | | .229 | .097 | 0 | 0 | 0 | 0 | .235 | X |
| | | | CROSS WELD SPECIMENS | | | | | | |
| 11 | .160 | .114 | .027 | .150 | .141 | X | .125 | .172 | X |
| | | .199 | .045 | .200 | .250 | X | .250 | .250 | X |
| | | .101 | .022 | 0 | .016 | X | .100 | .062 | X |
| 10 | .160 | .028 | .008 | .015 | 0 | 0 | .030 | .031 | O |
| | | .037 | .016 | .025 | 0 | 0 | .050 | .031 | O |
| | | .112 | .030 | .100 | .125 | X | .125 | .125 | X |
| | | .114 | .045 | .125 | .141 | X | .125 | .125 | X |
| | | .201 | .080 | .200 | .220 | X | .250 | .220 | X |
| 21 | .30 | .141 | .018 | .200 | 0 | X | .125 | 0 | X |
| | | .071 | .011 | .100 | .062 | X | .062 | .062 | X |
| | | .176 | .042 | .200 | .187 | X | .375 | .187 | X |
| | | .178 | .036 | .200 | .125 | X | .375 | .187 | X |
| 20 | .30 | .197 | .059 | .200 | .141 | X | .375 | .187 | X |
| | | .179 | .044 | .200 | 0 | X | .375 | .187 | X |
| | | .195 | .051 | .200 | .172 | X | .375 | .265 | X |
| | | .196 | .068 | .200 | .220 | X | .375 | .220 | X |
| | | | LONGITUDINAL WELD SPECIMENS | | | | | | |
| 14 | .080 | .155 | .051 | .120 | .141 | X | .150 | 0 | X |
| | | .105 | .038 | .100 | Porosity | X | .150 | 0 | X |
| | | .128 | .045 | .100 | .094 | X | .150 | .016 | X |
| | | .132 | .050 | .120 | .156 | X | .120 | 0 | X |
| | | .129 | .041 | 0 | 0 | X | .100 | .016 | X |
| 15 | .080 | .120 | .018 | .150 | .125 | X | .140 | 0 | X |
| | | .123 | .052 | .150 | .125 | X | .140 | .141 | X |
| | | .080 | .020 | Porosity | Porosity | X | Porosity | Porosity | X |

*   NOT CONDUCTED
**  BACK SURFACE OF WELD CURVED INWARD

## TABLE II-1. NDI FLAW DETECTION RESULTS FOR SPECIMENS CONTAINING UNKNOWN CRACKS (CONTINUED)

I - LOCKHEED CALIFORNIA COMPANY
II - MAGNAFLUX
III - NASA/MSC

X - DETECTED
X - POSSIBLE FLAW REPORTED
O - NOT DETECTED

| SPECIMEN | NOMINAL THICKNESS $B_1$ INCH | MEASURED CRACK SIZE $2C_1$ INCH | MEASURED CRACK SIZE $A_1$ INCH | PENETRANT (2C REPORTED) PREPROOF I | II | III | POSTPROOF I | II | III | X-RAY PREPROOF I | II | III | POSTPROOF I | II | III | EDDY CURRENT PREPROOF I | II | POSTPROOF I | II | SHEAR WAVE ULTRASONICS PREPROOF I | II | III | POSTPROOF I | II | III | SURFACE WAVE ULTRASONICS PREPROOF III | POSTPROOF III |
|---|---|---|---|---|---|---|---|---|---|---|---|---|---|---|---|---|---|---|---|---|---|---|---|---|---|---|---|
| 17 | .160 | .175 | .068 | .200 | .187 | X | .200 | .187 | X | O | O | O | O | O | O | X | X | X | X | X | O | X | X | O | X | X | X |
|  |  | .080 | .031 | .100 | 0 | X | .100 | .079 | X | O | O | O | O | O | O | X | O | X | X | X | O | O | X | O | O | X | X |
| 16 | .160 | .084 | .020 | .100 | .110 | X | .090 | 0 | X | O | O | O | O | O | O | O | O | X | O | X | O | O | X | X | O | O | O |
|  |  | .114 | .034 | .150 | .125 | X | .125 | 0 | X | O | O | O | O | O | O | X | X | X | X | X | O | X | X | O | X | X | O |
|  |  | .250 | .082 | .275 | .250 | X | .250 | .250 | X | O | O | O | O | O | O | X | X | X | O | X | X | X | X | X | X | X | X |
|  |  | .081 | .028 | .025 | .031 | X | .100 | .078 | X | O | O | O | O | O | O | X | O | X | X | X | O | O | X | O | O | O | O |
| 18 | .300 | .093 | .017 | .030 | .031 | X | .030 | .031 | X | O | O | O | O | O | O | O | O | O | O | O | O | O | O | O | O | O | O |
|  |  | .201 | .080 | .200 | .171 | X | .225 | .219 | X | O | O | O | O | O | O | X | X | X | X | X | O | X | X | O | X | X | X |
| 19 | .300 | .143 | .038 | .150 | .156 | X | .180 | 0 | X | O | O | O | O | O | O | O | O | X | X | O | O | O | O | O | O | O | O |
|  |  | .162 | .036 | .150 | 0 | X | .180 | .156 | X | O | O | O | O | X | O | X | X | O | O | X | X | X | X | X | O | O | O |
|  |  | .172 | .045 | .150 | .062 | X | .150 | .156 | X | O | O | O | O | O | O | O | O | X | X | O | O | O | O | O | O | O | O |
| 68 | .300 | None |  | -- | -- | -- | -- | -- | -- | -- | -- | -- | -- | -- | -- | -- | -- | -- | -- | -- | -- | -- | -- | -- | -- | -- | -- |

\* NOT CONDUCTED

\*\* BACK SURFACE OF WELD CURVED INWARD

FIGURE II-1.   DISTRIBUTION OF CRACK SIZES OF ALL SPECIMENS